PACIFIC EARTHQUAKE ENGINEERING RESEARCH CENTER

A Modal Pushover Analysis Procedure to Estimate Seismic Demands for Buildings:
Theory and Preliminary Evaluation

Anil K. Chopra
University of California
Berkeley

Rakesh K. Goel
California Polytechnic State University
San Luis Obispo

A report on research conducted under grant no. CMS-9812531
from the National Science Foundation:
U.S.-Japan Cooperative Research in Urban Earthquake Disaster Mitigation

PEER 2001/03
JAN. 2001

A Modal Pushover Analysis Procedure to Estimate Seismic Demands for Buildings:

Theory and Preliminary Evaluation

Anil K. Chopra
University of California
Berkeley

Rakesh K. Goel
California Polytechnic State University
San Luis Obispo

A report on research conducted under Grant No. CMS-9812531 from the National Science Foundation: U.S.-Japan Cooperative Research in Urban Earthquake Disaster Mitigation

PEER Report 2001/03
Pacific Earthquake Engineering Research Center
College of Engineering
University of California Berkeley

January 2001

ABSTRACT

The principal objective of this investigation is to develop a pushover analysis procedure based on structural dynamics theory, which retains the conceptual simplicity and computational attractiveness of current procedures with invariant force distribution, but provides superior accuracy in estimating seismic demands on buildings.

The standard response spectrum analysis (RSA) for elastic buildings is reformulated as a Modal Pushover Analysis (MPA). The peak response of the elastic structure due to its nth vibration mode can be exactly determined by pushover analysis of the structure subjected to lateral forces distributed over the height of the building according to $\mathbf{s}_n^* = \mathbf{m}\boldsymbol{\phi}_n$, where m is the mass matrix and $\boldsymbol{\phi}_n$ its nth-mode, and the structure is pushed to the roof displacement determined from the peak deformation D_n of the nth-mode elastic SDF system. Combining these peak modal responses by modal combination rule leads to the MPA procedure.

The MPA procedure is extended to estimate the seismic demands for inelastic systems: First, a pushover analysis determines the peak response r_{no} of the inelastic MDF system to individual modal terms, $\mathbf{p}_{\mathrm{eff},n}(t) = -\mathbf{s}_n \ddot{u}_g(t)$, in the modal expansion of the effective earthquake forces, $\mathbf{p}_{\mathrm{eff},n}(t) = -\mathbf{m}\,\iota\,\ddot{u}_g(t)$. The base shear-roof displacement $(V_{bn} - u_m)$ curve is developed from a pushover analysis for force distribution $\mathbf{s}_n^*$. This pushover curve is idealized as bilinear and converted to the force-deformation relation for the nth-"mode" inelastic SDF system. The peak deformation of this SDF system is used to determine the roof displacement, at which the seismic response, r_{no}, is determined by pushover analysis. Second, the total demand, r_o, is determined by combining the $r_{no}\,(n = 1, 2, \ldots)$ according to an appropriate modal combination rule.

Comparing the peak inelastic response of a 9-story SAC building determined by the approximate MPA procedure with rigorous nonlinear response history analysis (RHA) demonstrates that the approximate procedure provides good estimates of floor displacements and story drifts, and identifies locations of most plastic hinges; plastic hinge rotations are less accurate. The results presented for El Centro ground motion scaled by factors varying from 0.25 to 3.0, show that MPA estimates the response of buildings responding well into the inelastic

range to a similar degree of accuracy when compared to standard RSA for estimating peak response of elastic systems. Thus the MPA procedure is accurate enough for practical application in building evaluation and design.

Comparing the earthquake-induced demands for the selected 9-story building determined by pushover analysis using three force distributions in FEMA-273, MPA, and nonlinear RHA, it is demonstrated that the FEMA force distributions greatly underestimate the story drift demands, and the MPA procedure is more accurate than all the FEMA force distributions methods in estimating seismic demands. However, all pushover analysis procedures considered do not seem to compute to acceptable accuracy local response quantities, such as hinge plastic rotations. Thus the present trend of comparing computed hinge plastic rotations against rotation limits established in FEMA-273 to judge structural performance does not seem prudent. Instead, structural performance evaluation should be based on story drifts known to be closely related to damage and can be estimated to a higher degree of accuracy by pushover analyses.

ACKNOWLEDGMENT

This research investigation is funded by the National Science Foundation under Grant CMS-9812531, a part of the U.S.-Japan Cooperative Research in Urban Earthquake Disaster Mitigation. This financial support is gratefully acknowledged.

CONTENTS

ABSTRACT .... **iii**

ACKNOWLEDGMENT .... **v**

TABLE OF CONTENTS .... **vii**

1. INTRODUCTION **1**

2. ONE-STORY SYSTEMS **3**

2.1 Equation of Motion 3
2.2 System and Excitation Considered 5
2.3 Response History Analysis 6
2.4 Pushover Analysis 6

3. ELASTIC MULTISTORY BUILDINGS **9**

3.1 Modal Response History Analysis 9
3.2 Modal Response Spectrum Analysis 12
3.3 Modal Pushover Analysis 12
3.4 Comparative Evaluation of Analysis Procedures 13
3.4.1 System and Excitation Considered 13
3.4.2 Response History Analysis 16
3.4.3 Modal Pushover Analysis 22

4. INELASTIC MULTISTORY BUILDINGS **27**

4.1 Response History Analysis 27
4.2 Uncoupled Modal Response History Analysis 28
4.2.1 Underlying Assumptions and Accuracy 33
4.2.2 Properties of *n*th-"mode" Inelastic SDF System 34
4.2.3 Summary 36
4.3 Modal Pushover Analysis 36
4.3.1 Summary 37
4.4 Comparative Evaluation of Analysis Procedures 38
4.4.1 Uncoupled Modal Response History Analysis 38
4.4.2 Modal Pushover Analysis 41
4.4.3 Modal Pushover Analysis with Gravity Loads 48

5. COMPARISON OF MODAL AND FEMA PUSHOVER ANALYSES **55**

5.1 FEMA-273 Pushover Analysis 55
5.2 Comparative Evaluation 55

6. CONCLUSIONS **65**

REFERENCES **69**

APPENDICES

A: UNCOUPLED MODAL RESPONSE HISTORY ANALYSIS **71**

B: MODAL PUSHOVER ANALYSIS **81**

C: FEMA FORCE DISTRIBUTION CALCULATION **85**

1 Introduction

Estimating seismic demands at low performance levels, such as life safety and collapse prevention, requires explicit consideration of inelastic behavior of the structure. While nonlinear response history analysis (RHA) is the most rigorous procedure to compute seismic demands, current structural engineering practice uses the nonlinear static procedure (NSP) or pushover analysis in FEMA-273 [Building Seismic Safety Council, 1997]. The seismic demands are computed by nonlinear static analysis of the structure subjected to monotonically increasing lateral forces with an invariant height-wise distribution until a predetermined target displacement is reached. Both the force distribution and target displacement are based on the assumption that the response is controlled by the fundamental mode and that the mode shape remains unchanged after the structure yields.

Obviously, after the structure yields both assumptions are approximate, but investigations [Saiidi and Sozen, 1981; Miranda, 1991; Lawson et al., 1994; Fajfar and Fischinger, 1988; Krawinkler and Seneviratna, 1998; Kim and D'Amore, 1999; Maison and Bonowitz, 1999; Gupta and Krawinkler, 1999, 2000; Skokan and Hart, 2000] have led to good estimates of seismic demands. However, such satisfactory predictions of seismic demands are mostly restricted to low- and medium-rise structures in which inelastic action is distributed throughout the height of the structure [Krawinkler and Seneviratna, 1998; Gupta and Krawinkler, 1999].

None of the invariant force distributions can account for the contributions of higher modes to response, or for a redistribution of inertia forces because of structural yielding and the associated changes in the vibration properties of the structure. To overcome these limitations, several researchers have proposed adaptive force distributions that attempt to follow more closely the time-variant distributions of inertia forces [Fajfar and Fischinger, 1988; Bracci et al., 1997; Gupta and Kunnath, 2000]. While these adaptive force distributions may provide better estimates of seismic demands [Gupta and Kunnath, 2000], they are conceptually complicated and computationally demanding for routine application in structural engineering practice. Attempts have also been made to consider more than the fundamental vibration mode in pushover analysis [Paret et al., 1996; Sasaki et al., 1998; Gupta and Kunnath, 2000; Kunnath and Gupta, 2000; Matsumori et al., 2000].

The principal objective of this investigation is to develop an improved pushover analysis procedure based on structural dynamics theory that retains the conceptual simplicity and computational attractiveness of the procedure with invariant force distribution, but provides superior accuracy in estimating seismic demands on buildings. First, we show that pushover analysis of a one-story system predicts perfectly peak seismic demands. Next we develop a modal pushover analysis (MPA) procedure for linearly elastic buildings and demonstrate that it is equivalent to the well-known response spectrum analysis (RSA) procedure. The MPA procedure is then extended to inelastic buildings, the underlying assumptions and approximations are identified, and the errors in the procedure relative to a rigorous nonlinear RHA are documented. Finally, the seismic demands determined by pushover analysis using three force distributions in FEMA-273 are compared against the MPA and nonlinear RHA procedures.

2 One-Story Systems

2.1 EQUATION OF MOTION

Consider the idealized one-story structure shown in Fig. 2.1a. It consists of a mass *m* (or weight *w*) concentrated at the roof level, a massless frame that provides stiffness to the system, and a linear viscous damper with damping coefficient *c*. The hysteretic relation between the lateral force f_s and lateral displacement u of the mass relative to the base of the frame is denoted by $f_s\left(u, \operatorname{sign} \dot{u}\right)$.

This lateral-force displacement relation is idealized as shown in Fig. 2.1b. It is the familiar bilinear hysteretic relationship. On initial loading, this system is linearly elastic with stiffness *k* as long as the force does not exceed f_y, the yield strength. Yielding begins when the force reaches f_y and the deformation reaches u_y, the yield deformation. During yielding the stiffness of the frame is αk, where $0<\alpha<<1$. The yield strength is the same in the two directions of deformation. Unloading from a maximum deformation takes place along a path parallel to the initial elastic branch. Similarly, reloading from a minimum deformation takes place along a path parallel to the initial elastic branch. The yield strength is related to f_o, the strength required for the structure to remain elastic during the ground motion, through the yield strength reduction factor, R_y, defined by

$$R_y = \frac{f_o}{f_y} \tag{2.1}$$

The governing equation for this inelastic system subjected to horizontal ground acceleration $\ddot{u}_g\left(t\right)$ is

$$m\ddot{u} + c\dot{u} + f_s\left(u, \operatorname{sign} \dot{u}\right) = -m\ddot{u}_g\left(t\right) \tag{2.2}$$

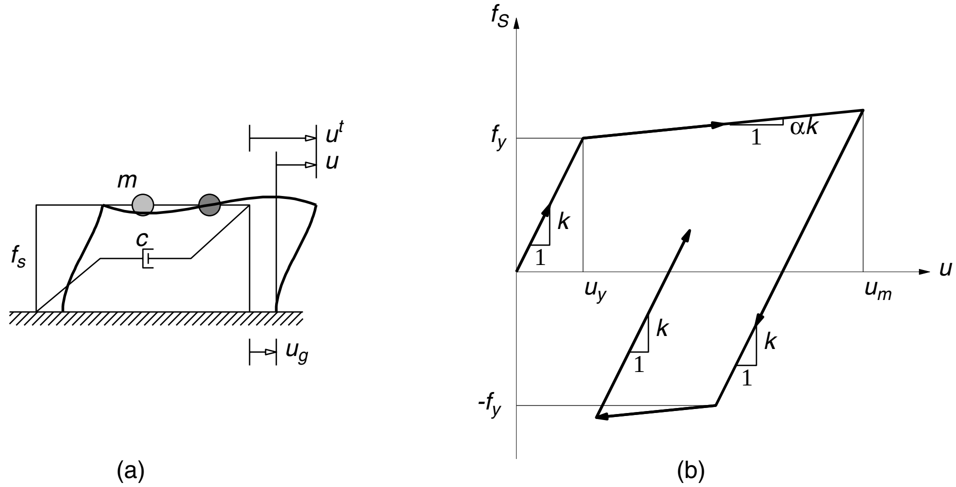

Fig. 2.1. (a) Idealized one-story structure; and (b) bilinear hysteretic force-deformation relation

For a given excitation $\ddot{u}_g(t)$, the deformation $u(t)$ depends on three systems parameters: ω_n, ζ, and u_y, in addition to the form of the force-deformation relation. This becomes evident if Eq. (2.1) is divided by m to obtain

$$\ddot{u} + 2\zeta\omega_n \dot{u} + \omega_n^2 u_y \tilde{f}_s(u, \text{sign}\,\dot{u}) = -\ddot{u}_g(t) \tag{2.3}$$

where

$$\omega_n = \sqrt{\frac{k}{m}} \qquad \zeta = \frac{c}{2m\omega_n} \qquad \tilde{f}_s = \frac{f_s}{f_y} \tag{2.4}$$

and ω_n is the natural vibration frequency, $T_n = 2\pi/\omega_n$ is the natural vibration period, and ζ is the damping ratio of the system vibrating within its linear elastic range (i.e., $u \le u_y$).

The peak, or absolute (without regard to algebraic sign) maximum, deformation is denoted by u_m, and the ductility factor is

$$\mu = \frac{u_m}{u_y} \tag{2.5}$$

For a given $\ddot{u}_g(t)$, μ depends on three system parameters: ω_n, ζ_y, and R_y [Chopra, 2001; Section 7.3].

2.2 SYSTEM AND EXCITATION CONSIDERED

Consider the one-story system in Fig. 2.2: the dimensions and flexural rigidity of the structural elements are noted, with $T_n = 0.5\,\text{sec}$ and $\zeta = 5\%$ subjected to the north-south component of the El Centro (1940) ground motion (Fig. 6.1.4 in Chopra, 2001) and scaled up by a factor of 2. For this system and excitation, $f_o/w = 1.84$. The yield strength of the inelastic system, based on $R_y = 8$, is $f_y/w = (f_o/w) \div 8 = 0.2311$, and $f_y = 39.26\,\text{kN (8.826 kips)}$ for $w = 169.9\,\text{kN (38.2 kips)}$.

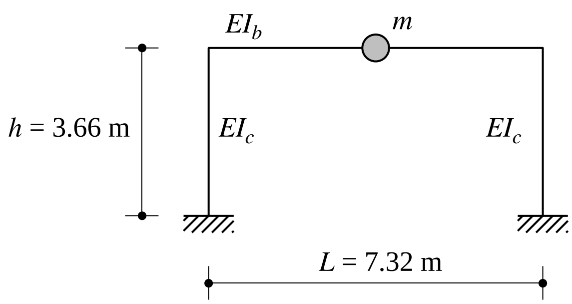

Fig. 2.2. One-story, one-bay frame

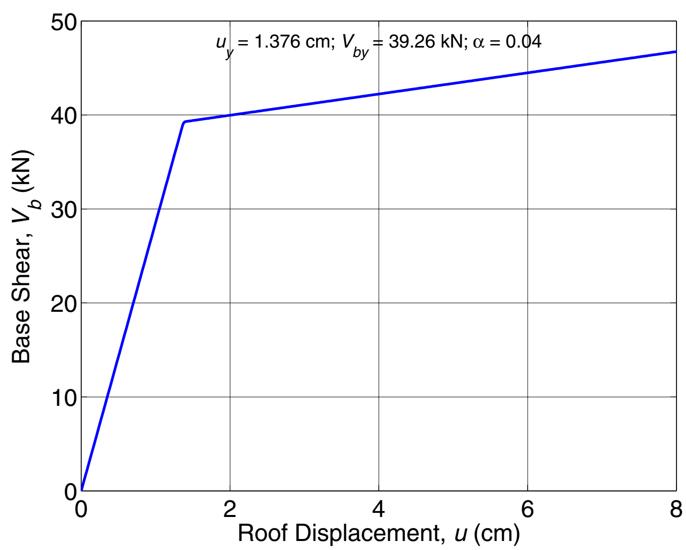

Fig. 2.3. Pushover curve for structure shown in Fig. 2.2

The yield moments in the beam and columns are defined as the bending moments due to the lateral force f_y. Implementing this analysis with $I_c = 6.077 \times 10^7 \text{mm}^4$ (146 in.^{4}), $I_b = 3.134 \times 10^7 \text{mm}^4$ (75.3 in.^{4}), and $E = 2 \times 10^8$ kPa (29×10^3 ksi) gives yield moments of 21.65 kN-m (191.6 kip-in.) and 50.18 kN-m (444.1 kip-in.) for the beam and columns, respectively. The yielding stiffness of each structural element is defined as 3% of its initial stiffness. A static pushover analysis of this one-story system leads to the force-displacement relationship shown in Fig. 2.3. This pushover curve turns out to be bilinear because the beam and the columns are designed to yield simultaneously when f_s reaches f_y.

2.3 RESPONSE HISTORY ANALYSIS

Figure 2.4 shows the earthquake response of the system described in the preceding section determined by response history analysis (RHA). It is organized in five parts: (a) shows the deformation $u(t)$; (b) shows the lateral force $f_s(t)$ or base shear $V_b(t)$ normalized relative to the weight; (c) shows the joint rotation $\theta(t)$; (d) shows the rotation $\theta_p(t)$ of the plastic hinges at the beam ends; and (e) shows the force-deformation relation. The peak values of the various response quantities are as follows: $u_m = 7.36$ cm, $\theta_m = 0.0217$ rad, and $\theta_{pm} = 0.017$ rad. The system is excited well beyond the yield deformation, as apparent in Fig. 2.4e; the ductility factor $\mu = 5.35$.

2.4 PUSHOVER ANALYSIS

Static analysis of the one-story nonlinear system subjected to lateral force that increases in small increments is implemented until the lateral displacement reaches $u_m = 7.36$ cm, the peak value determined from RHA. The resulting pushover curve is shown in Fig. 2.4f, wherein the hysteretic force-deformation history of Fig. 2.4e—determined from RHA—is superimposed. Observe that the pushover curve matches the initial loading path of the hysteretic system. Determined from pushover analysis at the exact peak deformation, the joint rotation and beam hinge rotation are identical to values θ_m and θ_{pm} determined from RHA. However, pushover analysis cannot provide any cumulative measure of response; e.g., the energy dissipated in yielding during the ground motion, or the cumulative rotation at a plastic hinge. This represents an inherent limitation of pushover analyses.

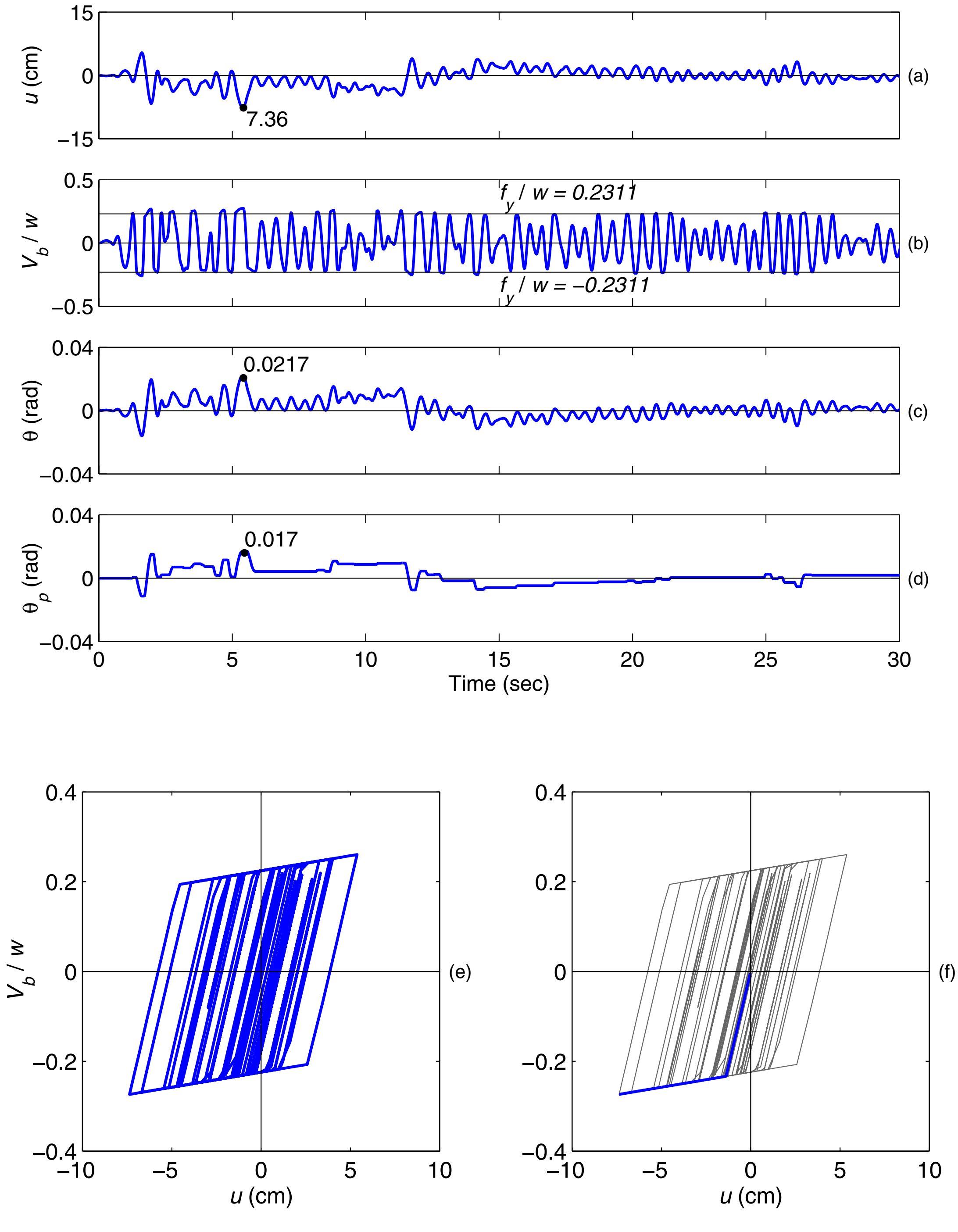

Fig. 2.4. Response of one-story system to El Centro ground motion: (a) deformation; (b) base shear; (c) joint rotation; (d) plastic hinge rotation; (e) force-deformation relation; and (f) pushover curve

3 Elastic Multistory Buildings

3.1 MODAL RESPONSE HISTORY ANALYSIS

The differential equations governing the response of a multistory building to horizontal earthquake ground motion $\ddot{u}_g(t)$ are as follows:

$$\mathbf{m}\ddot{\mathbf{u}} + \mathbf{c}\dot{\mathbf{u}} + \mathbf{k}\mathbf{u} = -\mathbf{m}\boldsymbol{\iota}\, \ddot{u}_g(t) \tag{3.1}$$

where $\mathbf{u}$ is the vector of N lateral floor displacements relative to the ground, $\mathbf{m}$, $\mathbf{c}$, and $\mathbf{k}$ are the mass, classical damping, and lateral stiffness matrices of the system; each element of the influence vector $\boldsymbol{\iota}$ is equal to unity.

The right side of Eq. (3.1) can be interpreted as effective earthquake forces:

$$\mathbf{p}_{\text{eff}}(t) = -\mathbf{m}\boldsymbol{\iota}\, \ddot{u}_g(t) \tag{3.2}$$

The spatial distribution of these "forces" over the height of the building is defined by the vector $\mathbf{s} = \mathbf{m}\boldsymbol{\iota}$ and their time variation by $\ddot{u}_g(t)$. This force distribution can be expanded as a summation of modal inertia force distributions $\mathbf{s}_n$ [Chopra, 2001: Section 13.12]:

$$\mathbf{m}\boldsymbol{\iota} = \sum_{n=1}^{N} \mathbf{s}_n = \sum_{n=1}^{N} \Gamma_n \mathbf{m}\boldsymbol{\phi}_n \tag{3.3}$$

where $\boldsymbol{\phi}_n$ is the nth natural vibration mode of the structure, and

$$\mathbf{p}_{\text{eff}}(t) = \sum_{n=1}^{N} \mathbf{p}_{\text{eff},n}(t) = \sum_{n=1}^{N} -\mathbf{s}_n \ddot{u}_g(t) \tag{3.4}$$

The effective earthquake forces can then be expressed as

$$\mathbf{p}_{\text{eff}}(t) = \sum_{n=1}^{N} \mathbf{p}_{\text{eff},n}(t) = \sum_{n=1}^{N} -\mathbf{s}_n \ddot{u}_g(t) \tag{3.5}$$

The contribution of the nth mode to $\mathbf{s}$ and to $\mathbf{p}_{\text{eff}}(t)$ are:

$$\mathbf{s}_n = \Gamma_n \mathbf{m} \boldsymbol{\phi}_n \qquad\qquad \mathbf{p}_{\text{eff},n}(t) = -\mathbf{s}_n \ddot{u}_g(t) \tag{3.6}$$

respectively.

Next, we will outline that the response of the MDF system to $\mathbf{p}_{\text{eff},n}(t)$ is entirely in the nth-mode, with no contribution from other modes. The equations governing the response of the system are

$$\mathbf{m}\ddot{\mathbf{u}} + \mathbf{c}\dot{\mathbf{u}} + \mathbf{k}\mathbf{u} = -\mathbf{s}_n \ddot{u}_g(t) \tag{3.7}$$

By utilizing the orthogonality property of modes, it can be demonstrated that none of the modes other than the nth mode contribute to the response. Then the floor displacements are

$$\mathbf{u}_n(t) = \boldsymbol{\phi}_n q_n(t) \tag{3.8}$$

where the modal coordinate $q_n(t)$ is governed by

$$\ddot{q}_n + 2\zeta_n \omega_n \dot{q}_n + \omega_n^2 q_n = -\Gamma_n \ddot{u}_g(t) \tag{3.9}$$

in which ω_n is the natural vibration frequency and ζ_n is the damping ratio for the nth mode. The solution $q_n(t)$ can readily be obtained by comparing Eq. (3.9) to the equation of motion for the nth-mode elastic SDF system, an SDF system with vibration properties—natural frequency ω_n and damping ratio ζ_n—of the nth-mode of the MDF system, subjected to $\ddot{u}_g(t)$:

$$\ddot{D}_n + 2\zeta_n \omega_n \dot{D}_n + \omega_n^2 D_n = -\ddot{u}_g(t) \tag{3.10}$$

Comparing Eqs. (3.9) and (3.10) gives

$$q_n(t) = \Gamma_n D_n(t) \tag{3.11}$$

and substituting in Eq. (3.8) gives the floor displacements

$$\mathbf{u}_n(t) = \Gamma_n \boldsymbol{\phi}_n D_n(t) \tag{3.12}$$

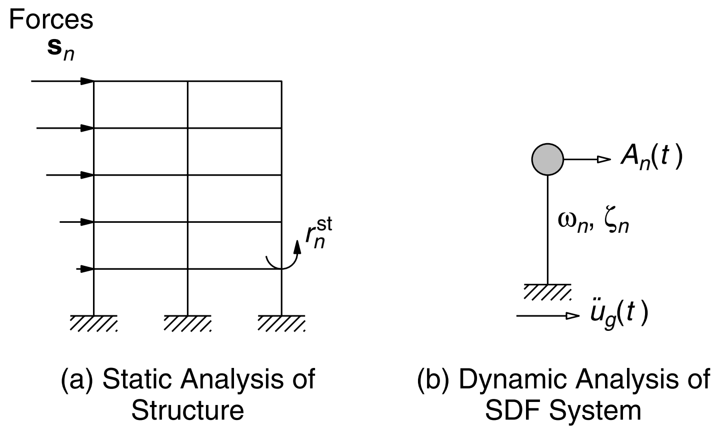

Fig. 3.1. Conceptual explanation of modal response history analysis of elastic MDF systems

Any response quantity $r(t)$—story drifts, internal element forces, etc.—can be expressed by

$$r_n(t) = r_n^{\mathrm{st}} A_n(t) \tag{3.13}$$

where r_n^{st} denotes the modal static response, the static value of r due to external forces $\mathbf{s}_n$, and

$$A_n(t) = \omega_n^2 D_n(t) \tag{3.14}$$

is the pseudo-acceleration response of the nth-mode SDF system [Chopra, 2001; Section 13.1]. The two analyses leading to r_n^{st} and $A_n(t)$ are shown schematically in Fig. 3.1.

Equations (3.12) and (3.13) represent the response of the MDF system to $\mathbf{p}_{\mathrm{eff},n}(t)$. Therefore, the response of the system to the total excitation $\mathbf{p}_{\mathrm{eff}}(t)$ is

$$\mathbf{u}(t) = \sum_{n=1}^{N} \mathbf{u}_n(t) = \sum_{n=1}^{N} \Gamma_n \phi_n D_n(t) \tag{3.15}$$

$$r(t) = \sum_{n=1}^{N} r_n(t) = \sum_{n=1}^{N} r_n^{\mathrm{st}} A_n(t) \tag{3.16}$$

This is the classical modal RHA procedure wherein Eq. (3.9) is the standard modal equation governing $q_n(t)$, Eqs. (3.12) and (3.13) define the contribution of the nth-mode to the response, and Eqs. (3.15) and (3.16) reflect combining the response contributions of all modes. However, these standard equations have been derived in an unconventional way. In contrast to the classical derivation found in textbooks (e.g., Chopra, 2001; Sections 12.4 and 13.1.3), we used the modal expansion of the spatial distribution of the effective earthquake forces. This concept provides a rational basis for the modal pushover analysis procedure developed later.

3.2 MODAL RESPONSE SPECTRUM ANALYSIS

The peak value r_o of the total response $r(t)$ can be estimated directly from the response spectrum for the ground motion without carrying out the response history analysis (RHA) implied in Eqs. (3.9)-(3.16). In such a response spectrum analysis (RSA), the peak value r_{no} of the nth-mode contribution $r_n(t)$ to response $r(t)$ is determined from

$$r_{no} = r_n^{\mathrm{st}} A_n \tag{3.17}$$

where A_n is the ordinate $A(T_n, \zeta_n)$ of the pseudo-acceleration response (or design) spectrum for the nth-mode SDF system, and $T_n = 2\pi/\omega_n$ is the natural vibration period of the nth-mode of the MDF system.

The peak modal responses are combined according to the Square-Root-of-Sum-of-Squares (SRSS) or the Complete Quadratic Combination (CQC) rules. The SRSS rule, which is valid for structures with well-separated natural frequencies such as multistory buildings with symmetric plan, provides an estimate of the peak value of the total response:

$$r_o \approx \left(\sum_{n=1}^{N} r_{no}^2 \right)^{1/2} \tag{3.18}$$

3.3 MODAL PUSHOVER ANALYSIS

To develop a pushover analysis procedure consistent with RSA, we note that static analysis of the structure subjected to lateral forces

$$\mathbf{f}_{no} = \Gamma_n \mathbf{m} \boldsymbol{\phi}_n A_n \tag{3.19}$$

will provide the same value of r_{no}, the peak nth-mode response as in Eq. (3.17) [Chopra, 2001; Section 13.8.1]. Alternatively, this response value can be obtained by static analysis of the structure subjected to lateral forces distributed over the building height according to

$$\mathbf{s}_n^* = \mathbf{m}\boldsymbol{\phi}_n \tag{3.20}$$

and the structure is pushed to the roof displacement, u_{rno} , the peak value of the roof displacement due to the nth-mode, which from Eq. (3.12) is

$$u_{rno} = \Gamma_n \phi_{rn} D_n \pi \tag{3.21}$$

where $D_n = A_n / \omega_n^2$. Obviously D_n and A_n are available from the response (or design) spectrum.

The peak modal responses, r_{no}, each determined by one pushover analysis, can be combined according to Eq. (3.18) to obtain an estimate of the peak value r_o of the total response. This modal pushover analysis (MPA) for linearly elastic systems is equivalent to the well-known RSA procedure (Section 3.2).

3.4 COMPARATIVE EVALUATION OF ANALYSIS PROCEDURES

3.4.1 System and Excitation Considered

The 9-story structure, shown in Fig. 3.2, was designed by Brandow & Johnston Associates[1] for the SAC[2] Phase II Steel Project. Although not actually constructed, this structure meets seismic code and represents typical medium-rise buildings designed for the Los Angeles, California, region.

A benchmark structure for the SAC project, this building is 45.73 m (150 ft) × 45.73 m (150 ft) in plan, and 37.19 m (122 ft) in elevation. The bays are 9.15 m (30 ft) on center, in both directions, with five bays each in the north-south (N-S) and east-west (E-W) directions. The building's lateral load-resisting system is composed of steel perimeter moment-resisting frames (MRFS) with simple framing on the farthest south E-W frame. The interior bays of the structure contain simple framing with composite floors. The columns are 345 MPa (50 ksi) steel wide-flange sections. The levels of the 9-story building are numbered with respect to the ground level (see Fig. 3.2), with the ninth level being the roof. The building has a basement level, denoted B-1. Typical floor-to-floor heights (for analysis purposes measured from center-of-beam to center-

[1] Brandow & Johnston Associates, Consulting Structural Engineers, 1660 W. Third St., Los Angeles, CA 90017.
[2] SAC is a joint venture of three non-profit organizations: The Structural Engineers Association of California (SEAOC), the Applied Technology Council (ATC), and California Universities for Research in Earthquake Engineering (CUREE). SAC Steel Project Technical Office, 1301 S. 46th Street, Richmond, CA 94804-4698.

of-beam) are 3.96 m (13 ft). The floor-to-floor height of the basement level is 3.65 m (12 ft) and for the first floor is 5.49 m (18 ft).

The column lines employ two-tier construction, i.e., monolithic column pieces are connected every two levels beginning with the first level. Column splices, which are seismic (tension) splices to carry bending and uplift forces, are located on the first, third, fifth, and seventh levels at 1.83 m (6 ft) above the center-line of the beam to column joint. The column bases are modeled as pinned and secured to the ground (at the B-1 level). Concrete foundation walls and surrounding soil are assumed to restrain the structure at the ground level from horizontal displacement.

The floor system is composed of 248 MPa (36 ksi) steel wide-flange beams in acting composite action with the floor slab. Each frame resists one half of the seismic mass associated with the entire structure. The seismic mass of the structure is due to various components of the structure, including the steel framing, floor slabs, ceiling/flooring, mechanical/electrical, partitions, roofing and a penthouse located on the roof. The seismic mass of the ground level is 9.65×10^5 kg (66.0 kips-sec^2/ft), for the first level is 1.01×10^6 kg (69.0 kips-sec^2/ft), for the second through eighth levels is 9.89×10^5 kg (67.7 kips-sec^2/ft), and for the ninth level is 1.07×10^6 kg (73.2 kips-sec^2/ft). The seismic mass of the above ground levels of the entire structure is 9.00×10^6 kg (616 kips- sec^2/ft). The 9-story N-S MRF is depicted in Fig. 3.2.

The building is modeled in DRAIN-2DX [Allahabadi and Powell, 1988] using the M1 model developed by Krawinkler and Gupta [1998]. This model is based on centerline dimensions of the bare frame in which beams and columns extend from centerline to centerline. The strength, dimension, and shear distortion of panel zones are neglected but large deformation (P-Δ) effects are included. The simple model adopted here is sufficient for the objectives of this study; if desired more complex models, such as those described in Gupta and Krawinkler [1999] can be used.

The first three vibration modes and periods of the building for linearly elastic vibration are shown in Fig. 3.3; the vibration periods are 2.27, 0.85, and 0.49 sec, respectively. The force distributions, $\mathbf{s}_n^*$ [Eq. (3.20)], for the first three modes are shown in Fig. 3.4. These force distributions will be used in the pushover analysis to be presented later.

To ensure that this structure remains elastic, we select a weak ground motion: the north-south component of the El Centro (1940) ground motion scaled down by a factor of 4.

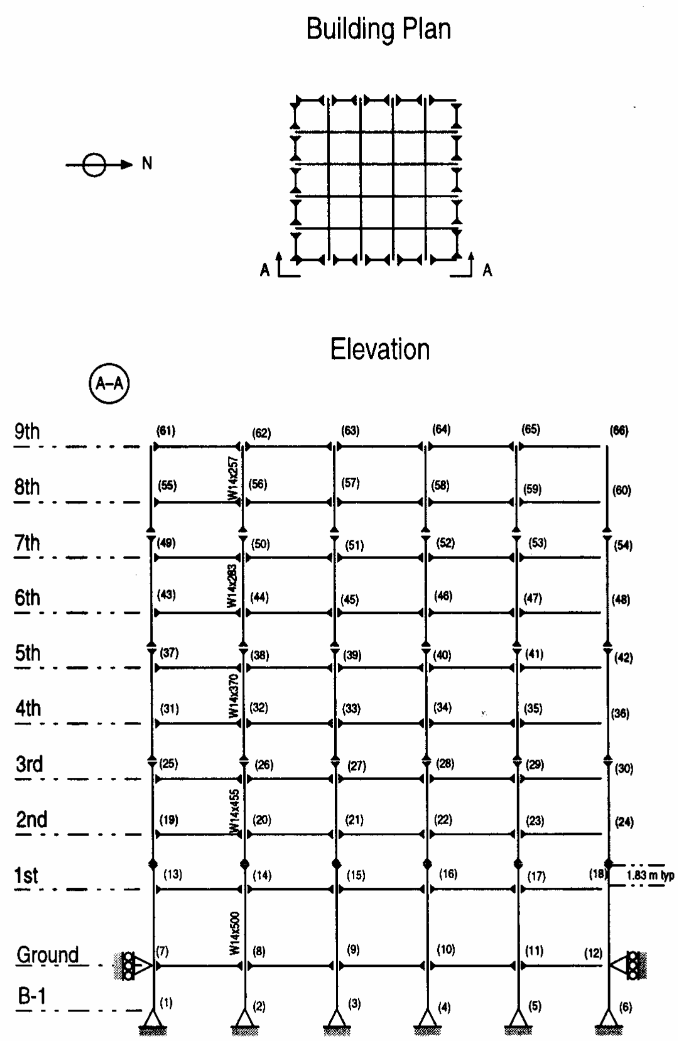

NOTES

Beams (248 MPa):

Ground– 2nd level	W36x160;
3rd – 6th level	W36x135;
7th level	W30x99;
8th level	W27x84;
9th level	W24x68.

Columns (345 MPa):
- column sizes change at splices
- corner columns and interior columns the same, respectively, throughout elevation;

Restraints:
- columns pinned at base;
- structure laterally restrained at 1st level.

Splices:
- denoted with ⫩;
- are at 1.83 m (6 ft) w.r.t. beam-to-column joint

Connections:
- ⊣ ⊢ indicates a moment resisting connection.
- – – indicates a simple (hinged) connection.

Dimensions:
- all measurements are center line;

basement level height	3.65 m (12′-0″);
Ground level height	5.49 m (18′-0″);
1st – 8th level heights	3.96 m (13′-0″);
bay widths (all)	9.15 m (30′-0″).

Seismic Mass:
- including steel framing, for both N-S MRFs;

Ground level	9.65×10^5 kg;
1st level	1.01×10^6 kg;
2nd – 8th level	9.89×10^5 kg;
9th level	1.07×10^6 kg;
entire structure (above ground)	9.00×10^6 kg.

Fig. 3.2. Nine-story building [adapted from Ohtori et al., 2000]

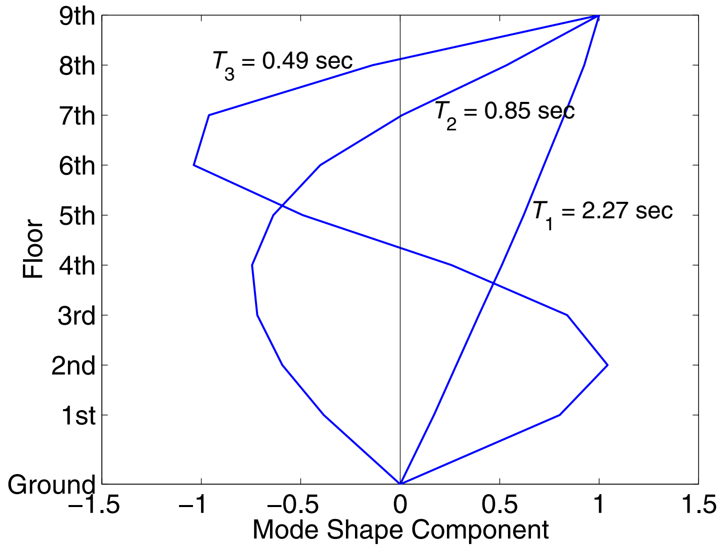

Fig. 3.3. First three natural-vibration periods and modes of the 9-story building

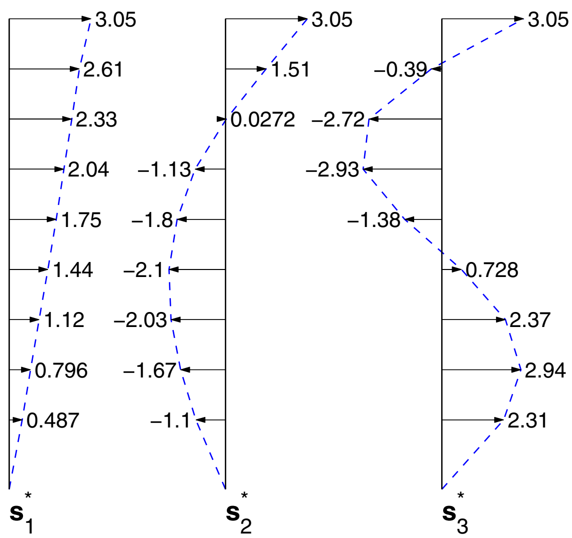

Fig. 3.4. Force distributions $\mathbf{s}_n^* = \mathbf{m}\phi_n$, $n = 1$, 2, and 3

3.4.2 Response History Analysis

The structural response due to individual vibration modes, $n =$ 1, 2, and 3, determined by RHA [Eqs. (3.12) and (3.13)], is shown in Figs. 3.5, 3.6, and 3.7, respectively. Each figure is organized in four parts: (a) shows the roof displacement $u_{rn}(t)$; (b) shows the base shear $V_{bn}(t)$

normalized relative to the weight W of the building; (c) shows the joint rotation $\theta_n(t)$ of an external joint at the roof level; and (d) shows the $V_{bn} - u_{rn}$ relation. The linear relationship between the base shear and roof displacement for each mode implies that the structure did not yield. The peak values of the various response quantities are noted in these figures; in particular, the peak roof displacement due to each of three modes is $u_{r1o} = 9.12$ cm, $u_{r2o} = 2.23$ cm, and $u_{r3o} = 0.422$ cm, respectively. The peak values of displacements of all floors, drifts in all stories, and rotations of external joints with moment connections are presented in Tables 3.1, 3.2, and 3.3, respectively.

Combining the modal response histories for all modes gives the total response [Eqs. (3.15) and (3.16)]; the results for the roof displacement and top-story drift are shown in Fig. 3.8. The same method was used to determine the peak values of many response quantities, which are listed in Tables 3.1, 3.2, and 3.3. Also included are the combined response due to one, two, and three vibration modes, the exact response considering all modes, and the percentage errors due to truncation of higher modal contributions. As expected, errors generally decrease as response contributions of more modes are included. For a fixed number of modes included, errors are smallest in floor displacements, larger in story drifts, and even larger in joint rotations, consistent with the increasing significance of the higher mode response among these three sets of response quantities. This is illustrated in Fig. 3.8, where the second and third modal responses are a larger percentage of the top story drift compared to roof displacement.

The peak values of floor displacements and story drifts determined by RHA, including one, two, three, or all modes, are presented in Fig. 3.9. It is apparent that the first mode alone is inadequate, especially in estimating the story drifts, but three modes—perhaps even two modes—are sufficient. The errors due to truncating the contributions of vibration modes beyond the third mode are negligible, with the first three modes provide essentially the exact response.

Table 3.1. Peak values of floor displacements (as % of building height = 37.14 m[3]) from RHA for 0.25 × El Centro ground motion

Floor	Displacement /Height (%)							Error (%)		
	Modal Response			Combined (RHA)			RHA (all modes)			
	Mode 1	Mode 2	Mode 3	1 Mode	2 Modes	3 Modes		1 Mode	2 Modes	3 Modes
1st	0.042	0.023	-0.009	0.042	0.060	0.054	0.055	-23.9	9.7	-1.6
2nd	0.069	0.035	-0.012	0.069	0.097	0.089	0.090	-23.4	7.6	-1.3
3rd	0.097	0.043	-0.010	0.097	0.130	0.124	0.124	-22.1	4.6	-0.6
4th	0.125	0.045	-0.003	0.125	0.159	0.157	0.156	-19.9	1.5	0.2
5th	0.152	0.038	0.006	0.152	0.179	0.183	0.181	-16.0	-1.1	0.9
6th	0.177	0.024	0.012	0.177	0.192	0.199	0.197	-10.1	-2.3	1.2
7th	0.202	-0.001	0.011	0.202	0.202	0.205	0.203	-0.5	-0.6	1.0
8th	0.227	-0.032	0.002	0.227	0.226	0.225	0.226	0.4	0.0	-0.4
9th	0.245	-0.060	-0.011	0.245	0.258	0.265	0.264	-7.2	-2.4	0.3

Table 3.2. Peak values of story drift ratios (as % of story height) from RHA for 0.25 × El Centro ground motion

Story	Drift Ratio (%)							Error (%)		
	Modal Response			Combined (RHA)			RHA (all modes)			
	Mode 1	Mode 2	Mode 3	1 Mode	2 Modes	3 Modes		1 Mode	2 Modes	3 Modes
1st	0.282	0.156	-0.062	0.282	0.406	0.364	0.370	-23.9	9.7	-1.6
2nd	0.259	0.117	-0.026	0.259	0.350	0.333	0.336	-22.7	4.4	-0.8
3rd	0.260	0.071	0.022	0.260	0.311	0.325	0.321	-19.1	-3.3	1.1
4th	0.266	0.015	0.062	0.266	0.275	0.311	0.300	-11.2	-8.4	3.6
5th	0.253	-0.060	0.080	0.253	0.265	0.263	0.266	-4.9	-0.4	-1.1
6th	0.235	-0.133	0.058	0.235	0.307	0.303	0.310	-24.4	-1.0	-2.2
7th	0.237	-0.231	-0.008	0.237	0.399	0.400	0.407	-41.7	-2.1	-1.8
8th	0.229	-0.295	-0.088	0.229	0.453	0.475	0.466	-50.8	-2.8	1.9
9th	0.173	-0.261	-0.121	0.173	0.378	0.413	0.401	-56.9	-5.8	3.1

Table 3.3. Peak values of joint rotations (radians) from RHA for 0.25 × El Centro ground motion

Floor	Joint Rotation (rad)							Error (%)		
	Modal Response			Combined (RHA)			RHA (all modes)			
	Mode 1	Mode 2	Mode 3	1 Mode	2 Modes	3 Modes		1 Mode	2 Modes	3 Modes
1st	2.03E-03	-1.03E-03	3.28E-04	2.03E-03	2.56E-03	2.50E-03	2.65E-03	-23.2	-3.4	-5.8
2nd	1.88E-03	-6.78E-04	1.66E-05	1.88E-03	2.14E-03	2.13E-03	2.38E-03	-20.9	-10.1	-10.4
3rd	2.09E-03	-3.42E-04	-3.26E-04	2.09E-03	2.11E-03	2.33E-03	2.47E-03	-15.5	-14.9	-6.0
4th	1.89E-03	1.74E-04	-5.11E-04	1.89E-03	1.99E-03	2.09E-03	1.94E-03	-2.8	2.6	7.3
5th	1.76E-03	6.91E-04	-5.01E-04	1.76E-03	2.29E-03	2.00E-03	2.08E-03	-15.3	9.9	-3.7
6th	1.63E-03	1.22E-03	-2.01E-04	1.63E-03	2.64E-03	2.50E-03	2.44E-03	-33.0	8.1	2.6
7th	2.00E-03	2.24E-03	3.74E-04	2.00E-03	3.90E-03	4.15E-03	3.73E-03	-46.4	4.7	11.3
8th	1.74E-03	2.44E-03	9.13E-04	1.74E-03	3.85E-03	4.45E-03	3.72E-03	-53.2	3.2	19.5
9th	1.31E-03	1.99E-03	9.38E-04	1.31E-03	3.03E-03	3.65E-03	3.09E-03	-57.7	-2.0	18.1

[3] Building height is measured from the ground floor to the 9th floor.

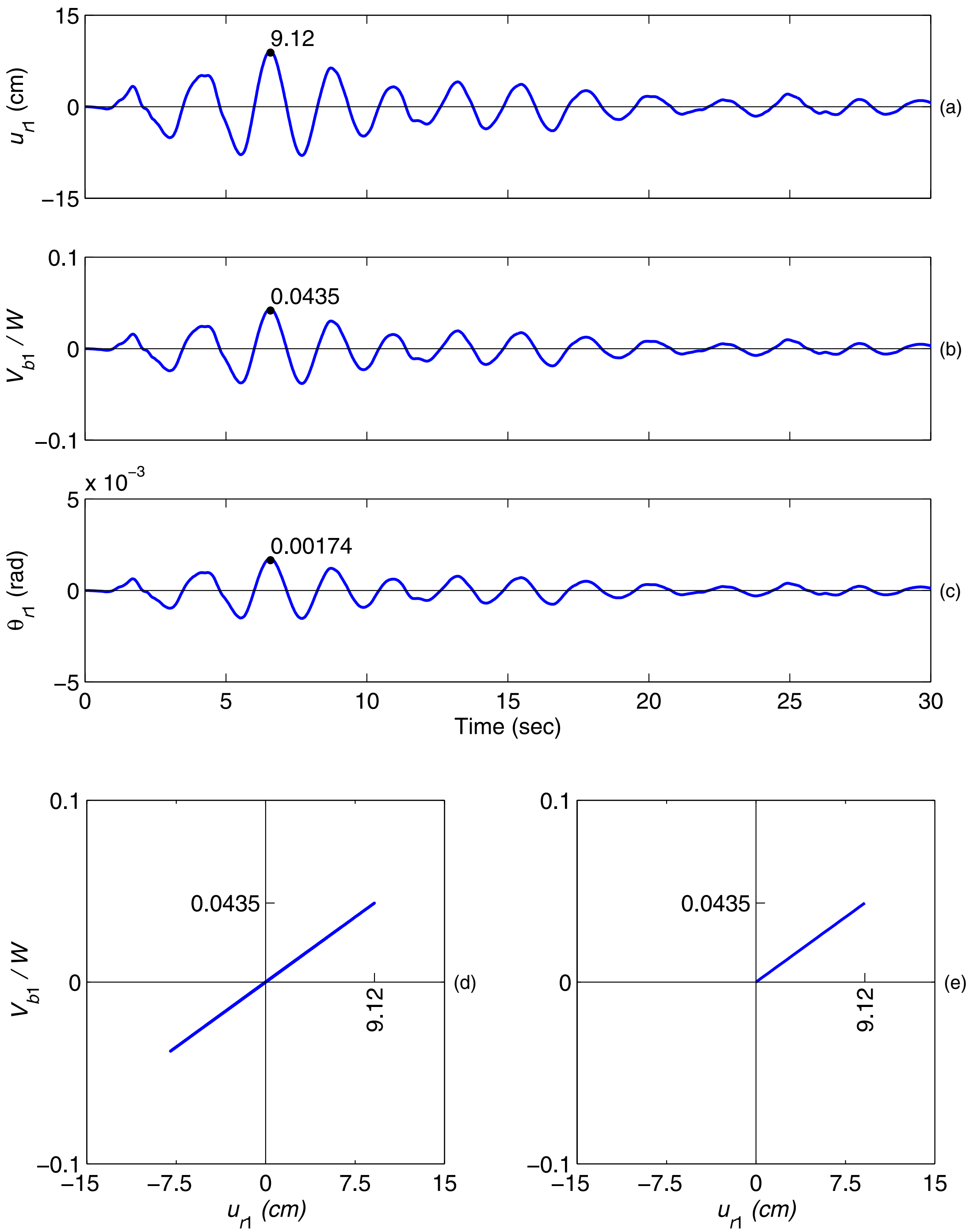

Fig. 3.5. Response due to first mode: (a) roof displacement; (b) base shear; (c) joint rotation; (d) force-deformation history; and (e) pushover curve. Excitation is 0.25 × El Centro ground motion

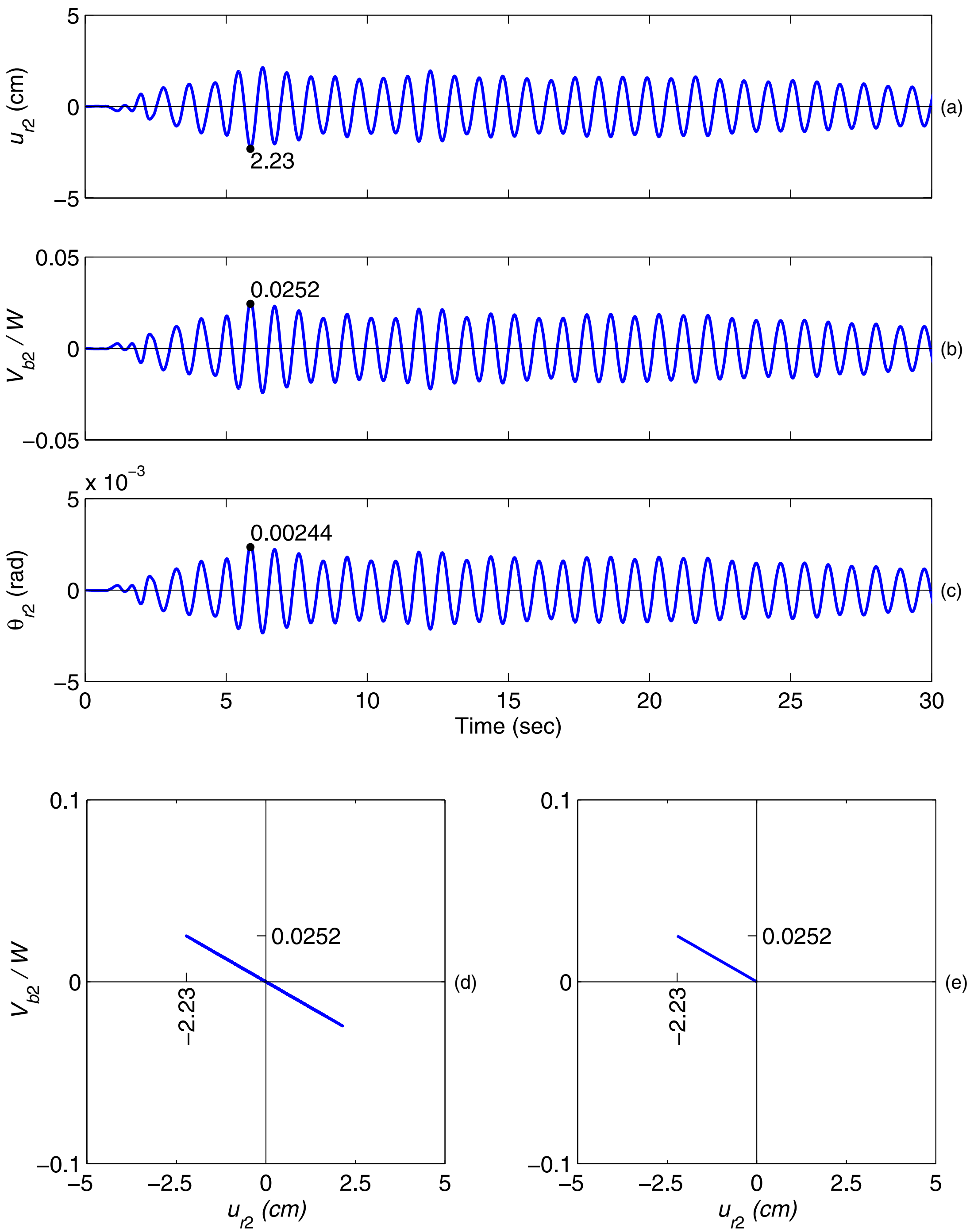

Fig. 3.6. Response due to second mode: (a) roof displacement; (b) base shear; (c) joint rotation; (d) force-deformation history; and (e) pushover curve. Excitation is 0.25 × El Centro ground motion

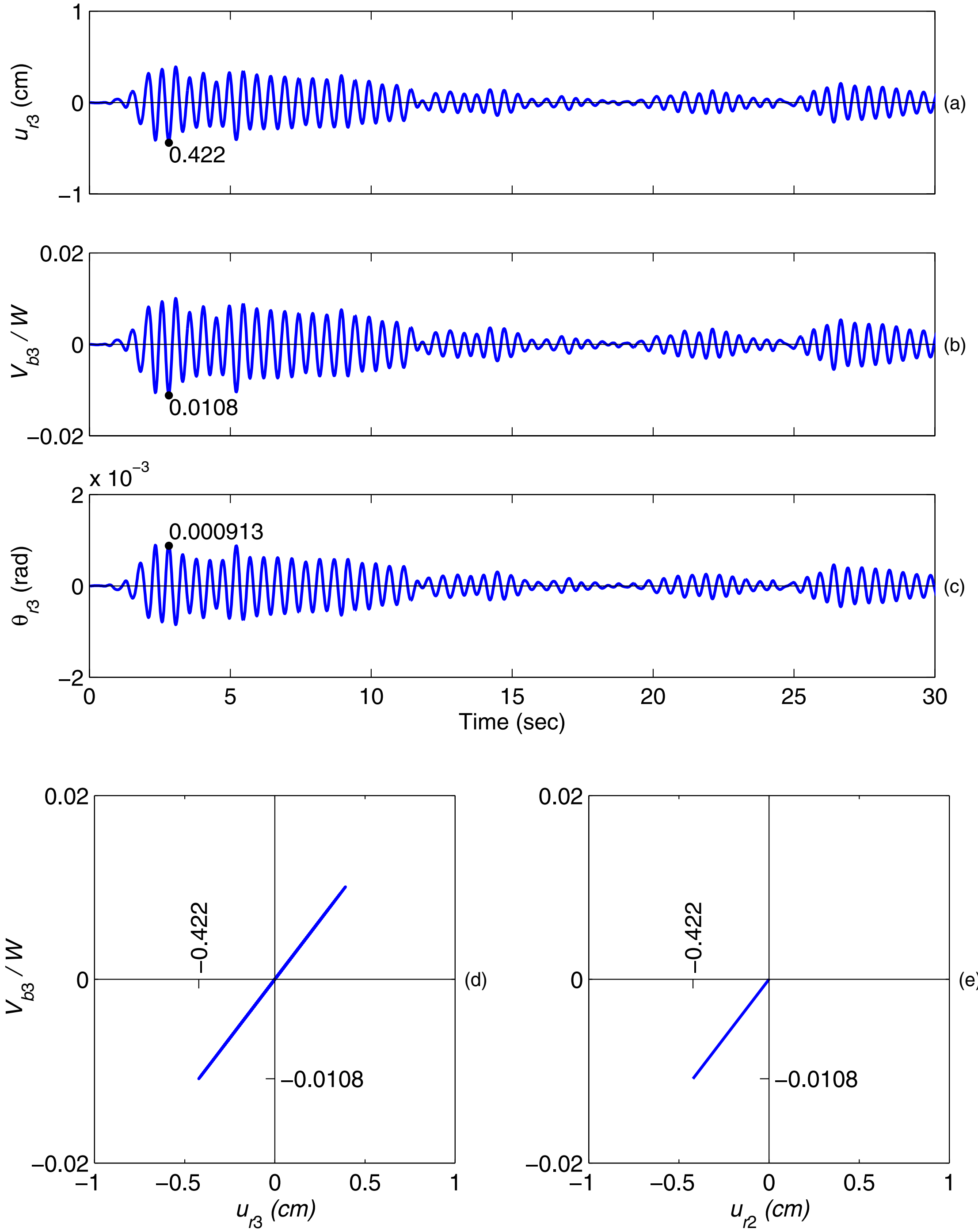

Fig. 3.7. Response due to third mode: (a) roof displacement; (b) base shear; (c) joint rotation; (d) force-deformation history; and (e) pushover curve. Excitation is 0.25 × El Centro ground motion

3.4.3 Modal Pushover Analysis

Implementing MPA for the fundamental vibration mode, i.e., pushing the structure using the force distribution of Eq. (3.20) with $n = 1$ (Fig. 3.4) to roof displacement $u_{r1o} = 9.12$ cm, the value determined by RHA (Fig. 3.8) leads to the pushover curve shown in Fig. 3.5e. This pushover curve is consistent with the relationship between the base shear and roof displacement determined by RHA (Fig. 3.5d). As suggested by Eq. (3.12), the floor displacements are proportional to the mode shape $\boldsymbol{\phi}_1$ because the structure remains elastic. The floor displacements, story drifts, and external joint rotations computed by pushover analysis are presented in Tables 3.4, 3.5, and 3.6, respectively. These values of the response quantities are identical to the peak response values determined from RHA (Tables 3.1, 3.2, and 3.3), except for the algebraic sign associated with Γ_1 and minor round-off errors, confirming that MPA gives the exact values of the individual modal responses.

Implementing pushover analysis for the second and third modes, i.e., pushing the structure, using the force distribution of Eq. (3.20) with $n = 2$ and 3 up to roof displacements $u_{r2o} = 2.23$ cm, and $u_{r3o} = 0.422$ cm, respectively, leads to the pushover curves shown in Figs. 3.6e and 3.7e and to the floor displacements, story drifts, and external joint rotations in Tables 3.4, 3.5, and 3.6. As for the first mode, these pushover curves are consistent with the $V_b - u_r$ relations determined by RHA (Figs. 3.6d and 3.7d), and the computed response values are identical to the peak response values determined from RHA (Tables 3.1, 3.2, and 3.3). Observe that the target roof displacement in each pushover analysis is identical to its exact value determined by RHA. In practical application, this value would be determined directly from the response (or design) spectrum, which would provide the D_n value to be substituted in Eq. (3.21).

Figure 3.10 and Tables 3.4, 3.5, and 3.6 present estimates of the combined response according to Eq. (3.18), considering one, two, or three vibration modes, respectively, and the errors in these estimates relative to the exact response from RHA considering all modes. For a fixed number of modes included considered, the errors in the MPA results are generally larger than in RHA (Fig. 3.9 and Tables 3.1 through 3.3), although both analyses led to identical peak values of the individual modal responses. In RHA the errors arise only from truncating the responses due to higher modes, and it is apparent in the example considered that three modes provide most of the response (Fig. 3.9), implying that the modal truncation errors are small if at least three modes are included. Additional errors are introduced in pushover analysis due to the approximation inherent in modal combination rules.

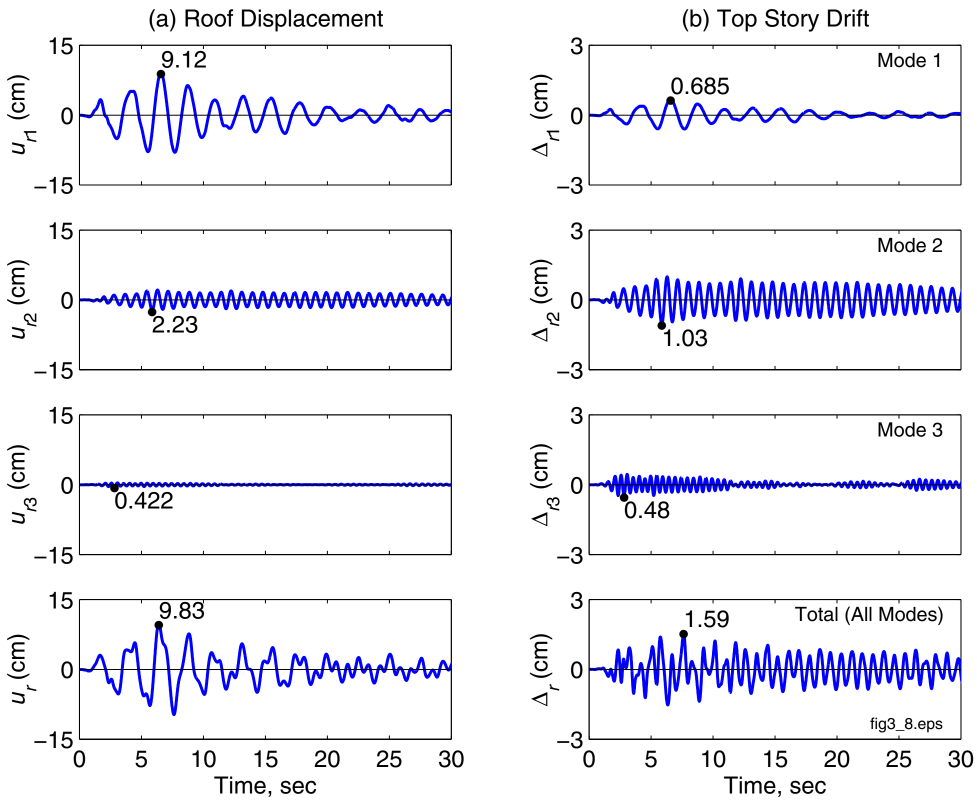

Fig. 3.8. Response histories of roof displacement and top-story drift from RHA for 0.25 × El Centro ground motion: first three modal responses and total (all modes) response

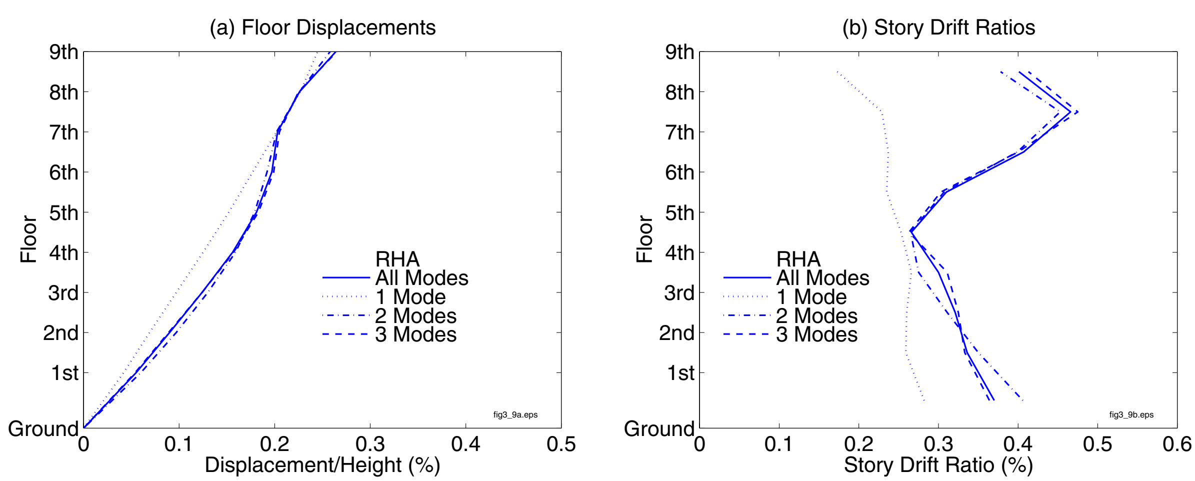

Fig. 3.9. Heightwise variation of floor displacements and story drifts from RHA for 0.25 × El Centro ground motion

Table 3.4. Peak values of floor displacements (as % of building height = 37.14 m) from MPA for 0.25 × El Centro ground motion

Floor	Displacement /Height (%)							Error (%)		
	Modal Response			Combined (MPA)			RHA (All Modes)	Modal Response		
	Mode 1	Mode 2	Mode 3	1 Mode	2 Modes	3 Modes		1 Mode	2 Modes	3 Modes
1st	0.042	-0.023	0.009	0.042	0.048	0.048	0.055	-23.8	-12.9	-11.3
2nd	0.069	-0.036	0.012	0.069	0.078	0.079	0.090	-23.4	-13.9	-12.9
3rd	0.097	-0.043	0.010	0.097	0.106	0.106	0.124	-22.1	-14.8	-14.4
4th	0.125	-0.045	0.003	0.125	0.133	0.133	0.156	-19.9	-14.9	-14.9
5th	0.152	-0.038	-0.006	0.152	0.157	0.157	0.181	-16.0	-13.4	-13.4
6th	0.177	-0.024	-0.012	0.177	0.179	0.179	0.197	-10.1	-9.2	-9.0
7th	0.203	0.001	-0.011	0.203	0.203	0.203	0.203	-0.4	-0.4	-0.3
8th	0.227	0.032	-0.002	0.227	0.229	0.229	0.226	0.4	1.4	1.4
9th	0.245	0.060	0.011	0.245	0.253	0.253	0.264	-7.2	-4.4	-4.3

Table 3.5. Peak values of story drift ratios (as % of story height) from MPA for 0.25 × El Centro ground motion

Story	Drift Ratio (%)							Error (%)		
	Modal Response			Combined (MPA)			RHA (all modes)			
	Mode 1	Mode 2	Mode 3	1 Mode	2 Modes	3 Modes		1 Mode	2 Modes	3 Modes
1st	-0.282	0.156	-0.062	0.282	0.322	0.328	0.370	-23.8	-12.9	-11.3
2nd	-0.259	0.117	-0.026	0.259	0.285	0.286	0.336	-22.7	-15.2	-14.8
3rd	-0.260	0.071	0.022	0.260	0.270	0.270	0.321	-19.1	-16.1	-15.9
4th	-0.267	0.015	0.062	0.267	0.267	0.274	0.300	-11.2	-11.0	-8.7
5th	-0.253	-0.060	0.080	0.253	0.260	0.272	0.266	-4.9	-2.3	2.2
6th	-0.235	-0.133	0.058	0.235	0.270	0.276	0.310	-24.3	-13.1	-11.0
7th	-0.237	-0.231	-0.008	0.237	0.331	0.332	0.407	-41.7	-18.6	-18.6
8th	-0.230	-0.296	-0.088	0.230	0.374	0.385	0.466	-50.8	-19.7	-17.6
9th	-0.173	-0.261	-0.121	0.173	0.313	0.336	0.401	-56.9	-21.9	-16.2

Table 3.6. Peak values of joint rotation (radians) from MPA for 0.25 × El Centro ground motion

Floor	Joint Rotation (rad)							Error (%)		
	Modal Response			Combined (MPA)			RHA (all modes)			
	Mode 1	Mode 2	Mode 3	1 Mode	2 Modes	3 Modes		1 Mode	2 Modes	3 Modes
1st	-2.03E-03	1.03E-03	-3.42E-04	2.03E-03	2.28E-03	2.31E-03	2.65E-03	-23.2	-13.9	-12.9
2nd	-1.89E-03	6.80E-04	-1.73E-05	1.89E-03	2.00E-03	2.00E-03	2.38E-03	-20.9	-15.9	-15.9
3rd	-2.09E-03	3.43E-04	3.40E-04	2.09E-03	2.12E-03	2.15E-03	2.47E-03	-15.4	-14.3	-13.2
4th	-1.89E-03	-1.74E-04	5.33E-04	1.89E-03	1.90E-03	1.97E-03	1.94E-03	-2.8	-2.3	1.4
5th	-1.76E-03	-6.92E-04	5.22E-04	1.76E-03	1.89E-03	1.96E-03	2.08E-03	-15.3	-9.0	-5.6
6th	-1.63E-03	-1.22E-03	2.09E-04	1.63E-03	2.04E-03	2.05E-03	2.44E-03	-33.0	-16.3	-15.9
7th	-2.00E-03	-2.24E-03	-3.90E-04	2.00E-03	3.00E-03	3.03E-03	3.73E-03	-46.4	-19.4	-18.7
8th	-1.74E-03	-2.44E-03	-9.53E-04	1.74E-03	3.00E-03	3.15E-03	3.72E-03	-53.2	-19.4	-15.5
9th	-1.31E-03	-1.99E-03	-9.78E-04	1.31E-03	2.38E-03	2.57E-03	3.09E-03	-57.7	-22.9	-16.7

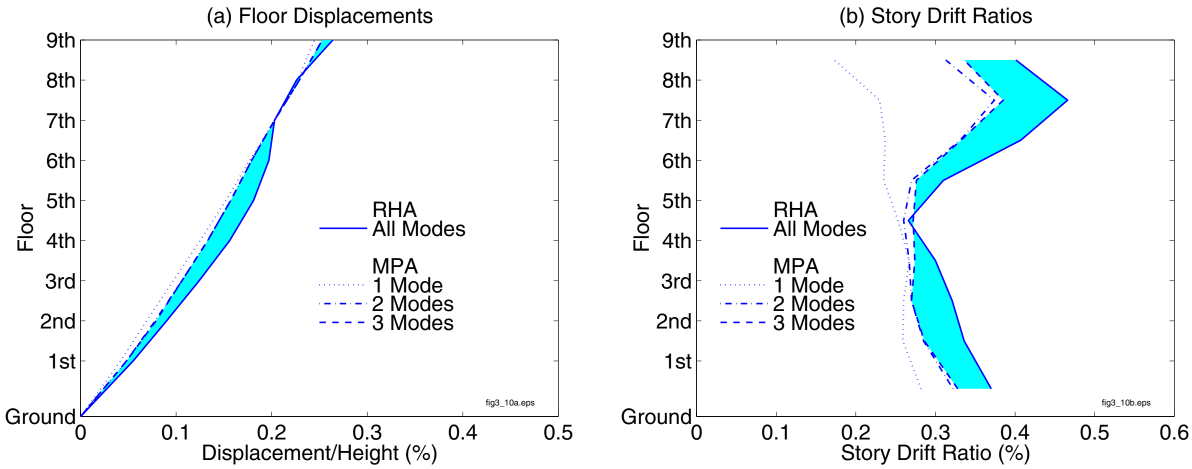

Fig. 3.10. Heightwise variation of floor displacements and story drifts from MPA for 0.25 × El Centro ground motion; shading indicates modal combination error

4 Inelastic Multistory Buildings

4.1 RESPONSE HISTORY ANALYSIS

For each structural element of a building, the initial loading curve is idealized as bilinear, and the unloading and reloading curves differ from the initial loading branch. Thus, the relations between lateral forces $\mathbf{f}_s$ at the N floor levels and the lateral displacements $\mathbf{u}$ are not single valued, but depend on the history of the displacements:

$$\mathbf{f}_s = \mathbf{f}_s\left(\mathbf{u}, \text{sign}\ \dot{\mathbf{u}}\right) \tag{4.1}$$

With this generalization for inelastic systems, Eq. (3.1) becomes

$$\mathbf{m}\ddot{\mathbf{u}} + \mathbf{c}\dot{\mathbf{u}} + \mathbf{f}_s\left(\mathbf{u}, \text{sign}\ \dot{\mathbf{u}}\right) = -\mathbf{m}\,\boldsymbol{\iota}\,\ddot{u}_g\left(t\right) \tag{4.2}$$

The standard approach is to solve directly these coupled equations, leading to the “exact” nonlinear response history analysis (RHA).

Although classical modal analysis (Section 3.1) is not valid for inelastic systems, it is useful for later reference to transform Eq. (4.2) to the modal coordinates of the corresponding linear system. Each structural element of this elastic system is defined to have the same stiffness as the initial stiffness of the structural element of the inelastic system. Both systems have the same mass and damping. Therefore, the natural vibration periods and modes of the corresponding linear system are the same as the vibration properties of the inelastic system undergoing small oscillations (within the linear range).

Expanding the displacements of the inelastic system in terms of the natural vibration modes of the corresponding linear system we get

$$\mathbf{u}\left(t\right) = \sum_{n=1}^{N} \boldsymbol{\phi}_n q_n\left(t\right) \tag{4.3}$$

Substituting Eq. (4.3) in Eq. (4.2), premultiplying by $\boldsymbol{\phi}_n^T$, and using the mass- and classical damping-orthogonality property of modes gives

$$\ddot{q}_n + 2\zeta_n \omega_n \dot{q}_n + \frac{F_{sn}}{M_n} = -\Gamma_n \ddot{u}_g(t) \qquad n = 1, 2, \ldots N \tag{4.4}$$

where the only term that differs from Eq. (3.9) involves

$$F_{sn} = F_{sn}(\mathbf{q}_n, \operatorname{sign} \dot{\mathbf{q}}_n) = \boldsymbol{\phi}_n^T \mathbf{f}_s(\mathbf{u}_n, \operatorname{sign} \dot{\mathbf{u}}_n) \tag{4.5}$$

This resisting force depends on all modal coordinates $q_n(t)$, implying coupling of modal coordinates because of yielding of the structure.

Equation (4.4) represents N equations in the modal coordinates $\mathbf{q}_n$. Unlike Eq. (3.9) for linearly elastic systems, these equations are coupled for inelastic systems. Simultaneously solving these coupled equations and using Eq. (4.3) will, in principle, give the same results for $\mathbf{u}(t)$ as obtained directly from Eq. (4.2). However, Eq. (4.4) is rarely solved because it offers no particular advantage over Eq. (4.2).

4.2 UNCOUPLED MODAL RESPONSE HISTORY ANALYSIS

Neglecting the coupling of the N equations in modal coordinates [Eq. (4.4)] leads to the uncoupled modal response history analysis (UMRHA) procedure. This approximate RHA procedure is the preliminary step in developing a modal pushover analysis procedure for inelastic systems.

The spatial distribution $\mathbf{s}$ of the effective earthquake forces is expanded into the modal contributions $\mathbf{s}_n$ according to Eq. (3.3), where $\boldsymbol{\phi}_n$ are now the modes of the corresponding linear system. The equations governing the response of the inelastic system to $\mathbf{p}_{\text{eff},n}(t)$ given by Eq. (3.6b) are

$$\mathbf{m}\ddot{\mathbf{u}} + \mathbf{c}\dot{\mathbf{u}} + \mathbf{f}_s(\mathbf{u}, \operatorname{sign} \dot{\mathbf{u}}) = -\mathbf{s}_n \ddot{u}_g(t) \tag{4.6}$$

The solution of Eq. (4.6) for inelastic systems will no longer be described by Eq. (3.8) because $q_r(t)$ will generally be nonzero for "modes" other than the nth "mode," implying that other "modes" will also contribute to the solution. For linear systems, however, $q_r(t) = 0$ for all

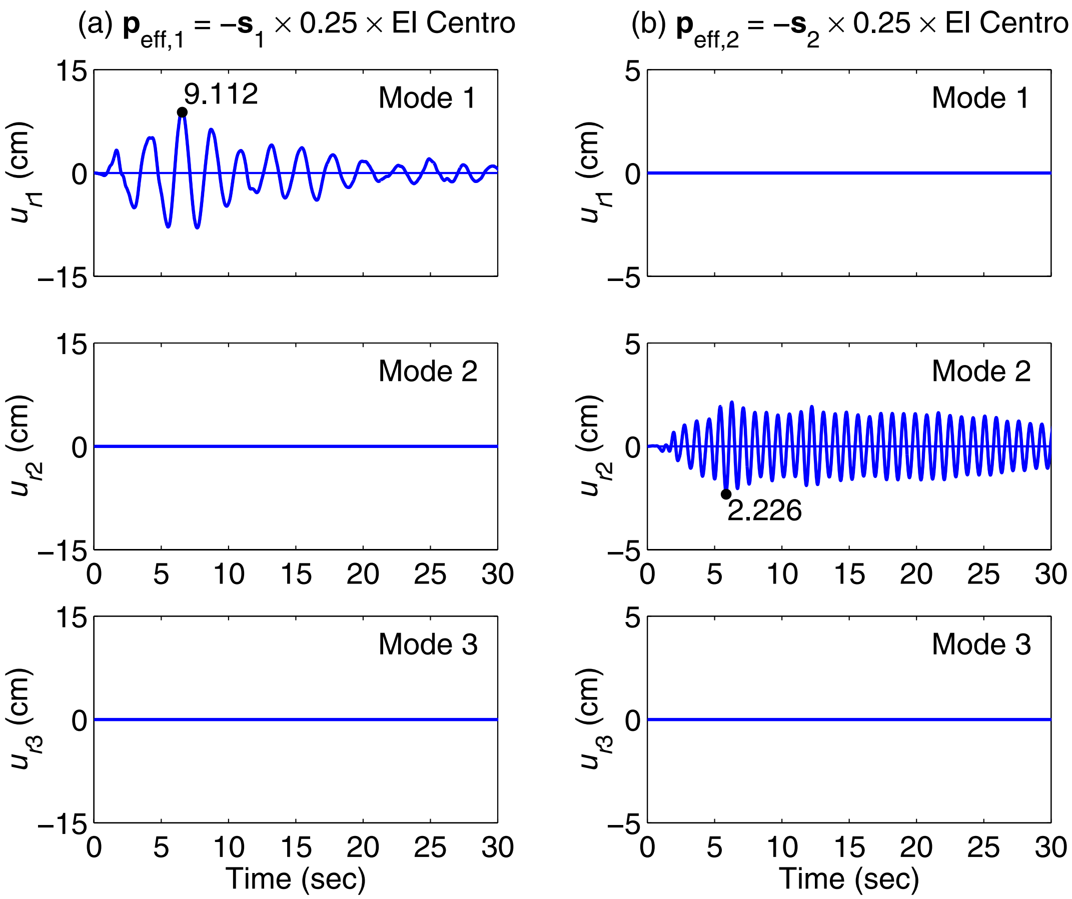

Fig. 4.1. Modal decomposition of the roof displacement due to (a) $\mathbf{p}_{\text{eff},1}(t) = -\mathbf{s}_1 \times 0.25$ x El Centro ground motion; and (b) $\mathbf{p}_{\text{eff},2}(t) = -\mathbf{s}_2 \times 0.25 \times$ El Centro ground motion

modes other than the nth-mode; therefore, it is reasonable to expect that the nth "mode" should be dominant even for inelastic systems.

These assertions are illustrated numerically in Figs. 4.1 and 4.2 for the selected 9-story building. Equation (4.6) was solved by nonlinear RHA, and the resulting roof displacement history was decomposed into its "modal" components. The modal decomposition of the roof displacement for the first three modes due to 0.25 x El Centro ground motion demonstrates that because the building does not yield during this weak ground motion, the response to excitation $\mathbf{p}_{\text{eff},n}(t)$ is all in the nth-mode (Fig. 4.1). The structure yields when subjected to the strong excitation of 1.5 x El Centro ground motion, and the modes other than the nth-mode contribute to the response. The second and third modes start responding to excitation $\mathbf{p}_{\text{eff},1}(t)$ at about

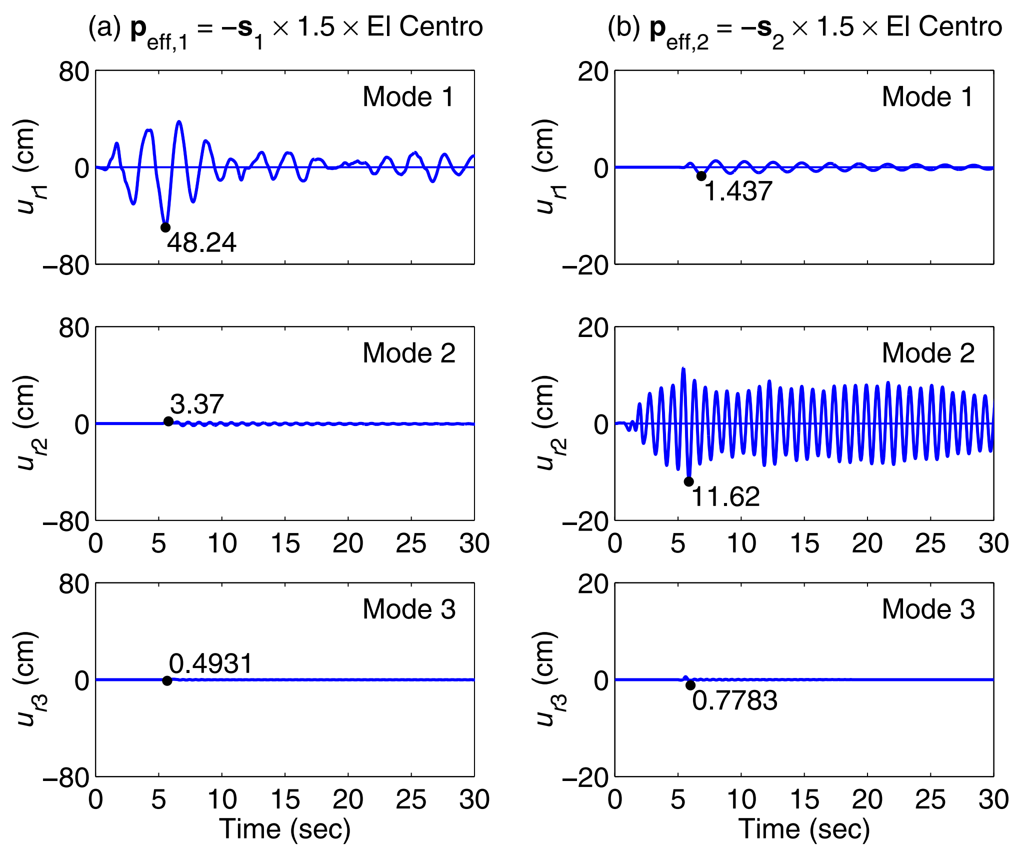

Fig. 4.2. **Modal decomposition of the roof displacement due to: (a)** $\mathbf{p}_{\text{eff},1}(t) = -\mathbf{s}_1 \times 1.5 \times$ **El Centro ground motion; and (b)** $\mathbf{p}_{\text{eff},2}(t) = -\mathbf{s}_2 \times 1.5 \times$ **El Centro ground motion**

5.2 sec, the instant the structure first yields; however, their contributions to the roof displacement are only 7% and 1%, respectively, of the first mode response (Fig. 4.2a). The first and third modes start responding to excitation $\mathbf{p}_{\text{eff},2}(t)$ at about 4.2 sec, the instant the structure first yields; however, their contributions to the roof displacement are 12% and 7%, respectively, of the second mode response (Fig. 4.2b).

Approximating the response of the structure to excitation $\mathbf{p}_{\text{eff},n}(t)$ by Eq. (3.8), substituting Eq. (3.8) in Eq. (4.6) and premultiplying by $\boldsymbol{\phi}_n^T$ gives Eq. (4.4), except for the important approximation that F_{sn} now depends only on one modal coordinate, q_n:

$$F_{sn} = F_{sn}(q_n, \text{sign}\,\dot{q}_n) = \boldsymbol{\phi}_n^T \mathbf{f}_s(q_n, \text{sign}\,\dot{q}_n) \tag{4.7}$$

With this approximation, solution of Eq. (4.4) can be expressed by Eq. (3.11) where $D_n(t)$ is governed by

$$\ddot{D}_n + 2\zeta_n\omega_n\dot{D}_n + \frac{F_{sn}}{L_n} = -\ddot{u}_g(t) \tag{4.8}$$

and

$$F_{sn} = F_{sn}\left(D_n, \operatorname{sign}\dot{D}_n\right) = \boldsymbol{\phi}_n^T \mathbf{f}_s\left(D_n, \operatorname{sign}\dot{D}_n\right) \tag{4.9}$$

is related to $F_{sn}\left(q_n, \operatorname{sign}\dot{q}_n\right)$ because of Eq. (3.11).

Equation (4.8) may be interpreted as the governing equation for the *n*th-"mode" inelastic SDF system, an SDF system with (1) small amplitude vibration properties—natural frequency ω_n and damping ratio ζ_n—of the *n*th-mode of the corresponding linear MDF system; (2) unit mass; and (3) $F_{sn}/L_n - D_n$ relation between resisting force F_{sn}/L_n and modal coordinate D_n defined by Eq. (4.9). Although Eq. (4.4) can be solved in its original form, Eq. (4.8) can be solved conveniently by standard software because it is of the same form as the SDF system [Eq. (2.3)], and the peak value of $D_n(t)$ can be estimated from the inelastic response (or design) spectrum [Chopra, 2001; Sections 7.6 and 7.12.1]. Introducing the *n*th-"mode" inelastic SDF system also permitted extension of the well-established concepts for elastic systems to inelastic systems. Compare Eqs. (4.4) and (4.8) to Eqs. (3.9) and (3.10): note that Eq. (3.11) applies to both systems.[4]

Solution of the nonlinear Eq. (4.8) formulated in this manner provides $D_n(t)$, which substituted into Eq. (3.12) gives the floor displacements of the structure associated with the *n*th-"mode" inelastic SDF system. Any floor displacement, story drift, or another deformation response quantity $r(t)$ is given by Eqs. (3.13) and (3.14), where $A_n(t)$ is now the pseudo-acceleration response of the *n*th-"mode" inelastic SDF system. The two analyses leading to r_n^{st} and $A_n(t)$ are shown schematically in Fig. 4.3. Equations (3.13) and (3.14) represent the response of the inelastic MDF system to $\mathbf{p}_{\text{eff},n}(t)$, the *n*th-mode contribution to $\mathbf{p}_{\text{eff}}(t)$. Therefore the response of the system to the total excitation $\mathbf{p}_{\text{eff}}(t)$ is given by Eqs. (3.15) and (3.16). This is the UMRHA procedure.

[4] Equivalent inelastic SDF systems have been defined differently by other researchers [Villaverde, 1996; Han and Wen, 1997].

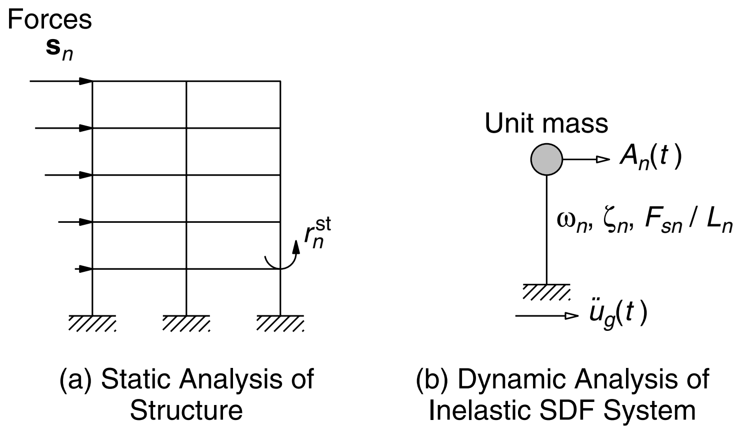

Fig. 4.3. Conceptual explanation of uncoupled modal response history analysis of inelastic MDF systems

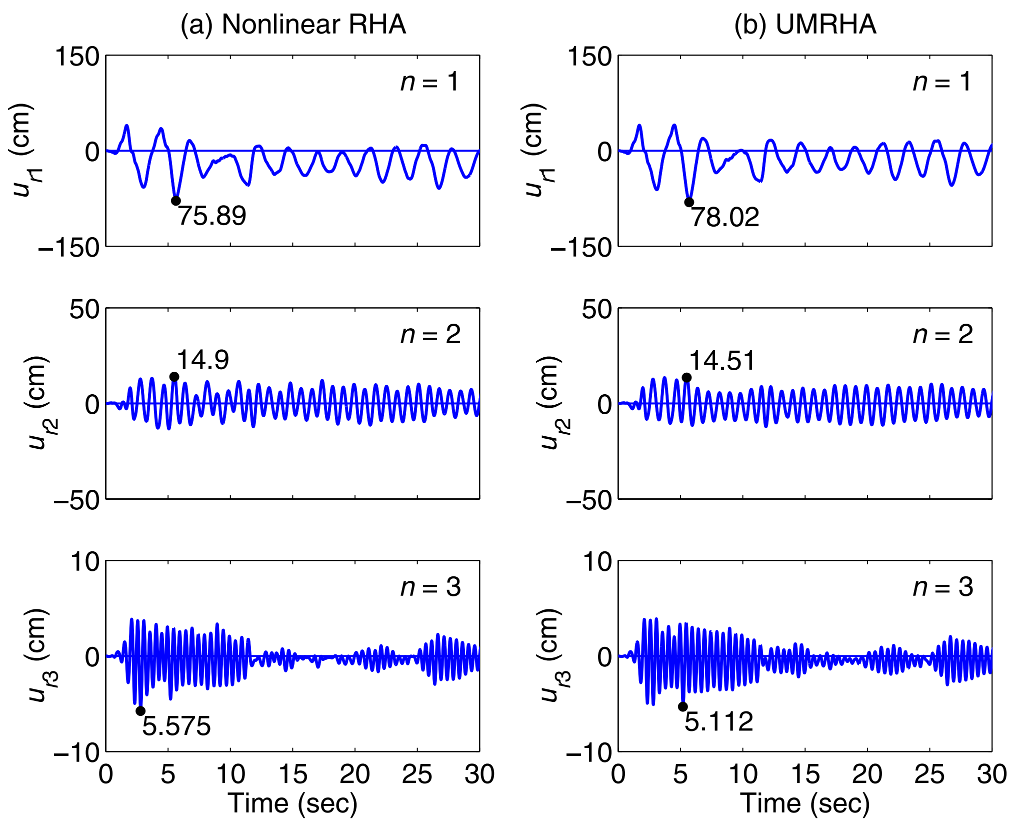

Fig. 4.4. Roof displacement due to $\mathbf{p}_{\text{eff},n}(t) = -\mathbf{s}_n \ddot{u}_g(t)$, $n = 1, 2, \text{and } 3,$ **where** $\ddot{u}_g(t) = 3.0\times$ **El Centro ground motion: (a) exact solution by NL-RHA; and (b) approximate solution by UMRHA**

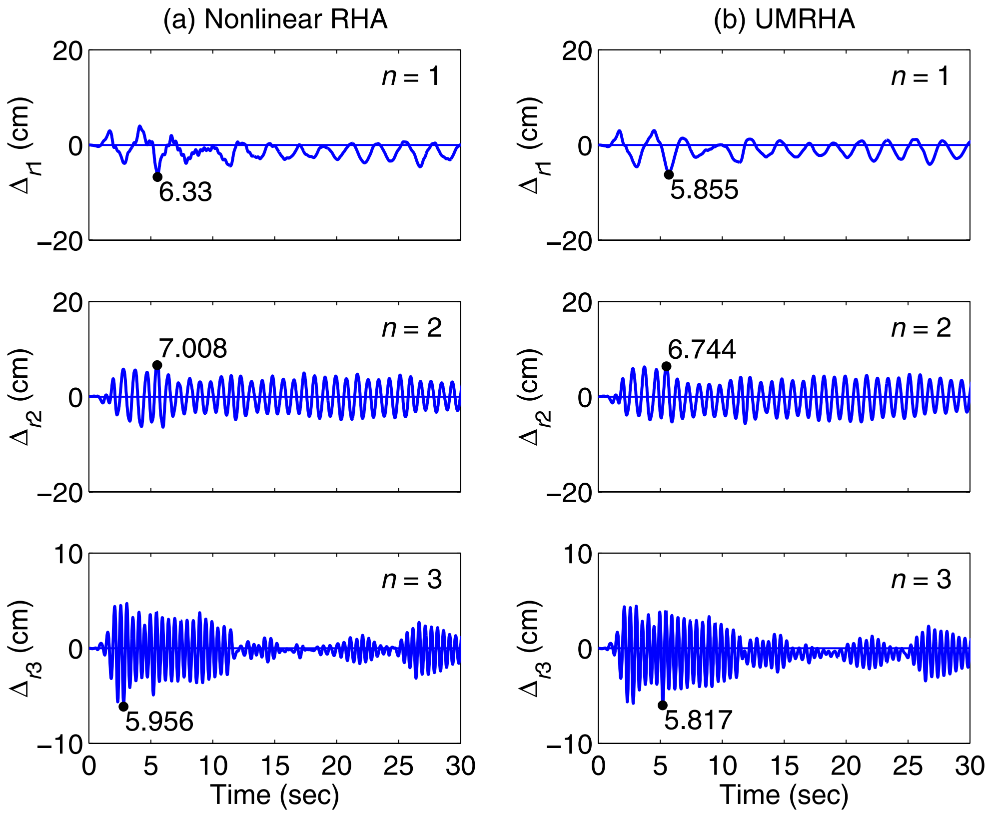

Fig. 4.5. Top story drift due to $\mathbf{p}_{\text{eff},n}(t) = -\mathbf{s}_n \ddot{u}_g(t)$, $n = 1, 2, \text{and } 3,$ **where** $\ddot{u}_g(t) = 3.0\times$ **El Centro ground motion: (a) exact solution by NL-RHA; and (b) approximate solution by UMRHA**

4.2.1 Underlying Assumptions and Accuracy

The approximate solution of Eq. (4.6) by UMRHA is compared with the "exact" solution by nonlinear RHA, both for 3.0 x El Centro ground motion; this intense excitation was chosen to ensure that the structure is excited well beyond its linear elastic limit. Such comparison for roof displacement and top-story drift is presented in Figs. 4.4 and 4.5, respectively. The errors are slightly larger in drift than in displacement, but even for this very intense excitation, the errors in either response quantity are only a few percent.

These errors arise from the following assumptions and approximations: (1) the coupling among modal coordinates $q_n(t)$ arising from yielding of the system [recall Eqs. (4.4) and (4.5)] is neglected; (2) the superposition of responses to $\mathbf{p}_{\text{eff},n}(t)$ $(n = 1, 2 \ldots N)$ according to Eq. (3.15) is strictly valid only for linearly elastic systems; and (3) the $F_{sn}/L_n - D_n$ relation is approximated by a bilinear curve to facilitate solution of Eq. (4.8) in UMRHA. Although several approximations are inherent in this UMRHA procedure, when specialized for linearly elastic systems it is identical to the RHA procedure of Section 3.1. The overall errors in the UMRHA procedure are documented in the examples presented in Section 4.4.

4.2.2 Properties of the *n*th-"mode" Inelastic SDF System

How is the $F_{sn}/L_n - D_n$ relation to be determined in Eq. (4.8) before it can be solved? Because Eq. (4.8) governing $D_n(t)$ is based on Eq. (3.12) for floor displacements, the relationship between lateral forces $\mathbf{f}_s$ and D_n in Eq. (4.9) should be determined by nonlinear static analysis of the structure as the structure undergoes displacements $\mathbf{u} = D_n \boldsymbol{\phi}_n$ with increasing D_n. Although most commercially available software cannot implement such displacement-controlled analysis, it can conduct a force-controlled nonlinear static analysis with an invariant distribution of lateral forces. Therefore we impose this constraint in developing the UMRHA procedure in this section and modal pushover analysis in the next section.

What is an appropriate invariant distribution of lateral forces to determine F_{sn}? For an inelastic system no invariant distribution of forces can produce displacements proportional to ϕ_n at all displacements or force levels. However, within the linearly elastic range of the structure, the only force distribution that produces displacements proportional to ϕ_n is given by Eq. (3.20). Therefore, this distribution seems to be a rational choice—even for inelastic systems—to determine F_{sn} in Eq. (4.9). When implemented by commercially available software, such nonlinear static analysis provides the so-called pushover curve, which is different than the $F_{sn}/L_n - D_n$ curve. The structure is pushed using the force distribution of Eq. (3.20) to some pre-determined roof displacement, and the base shear V_{bn}, is plotted against roof displacement u_{rn}. A bilinear idealization of this pushover curve for the *n*th-"mode" is shown in Fig. 4.6a. At the yield point, the base shear is V_{bny} and roof displacement is u_{rny}.

How to convert this $V_{bn} - u_{rn}$ pushover curve to the $F_{sn}/L_n - D_n$ relation? The two sets of forces and displacements are related as follows:

$$F_{sn} = \frac{V_{bn}}{\Gamma_n} \qquad\qquad D_n = \frac{u_{rn}}{\Gamma_n \phi_{rn}} \tag{4.10}$$

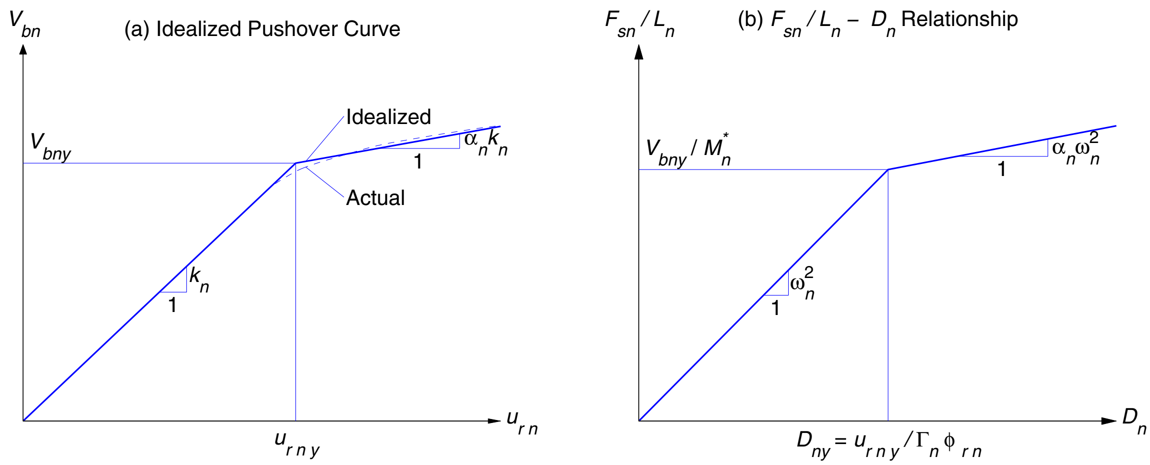

Fig. 4.6. Properties of the *n*th-"mode" inelastic SDF system from the pushover curve

Equation 4.10 enables conversion of the pushover curve to the desired $F_{sn}/L_n - D_n$ relation shown in Fig. 4.6b, where the yield values of F_{sn}/L_n and D_n are

$$\frac{F_{sny}}{L_n} = \frac{V_{bny}}{M_n^*} \qquad D_{ny} = \frac{u_{rny}}{\Gamma_n \phi_{rn}} \tag{4.11}$$

in which $M_n^* = L_n \Gamma_n$ is the effective modal mass [Chopra, 2001, Section 13.2.5]. The two are related through

$$\frac{F_{sny}}{L_n} = \omega_n^2 D_{ny} \tag{4.12}$$

implying that the initial slope of the curve in Fig. 4.6b is ω_n^2. Knowing F_{sny}/L_n and D_{ny} from Eq. (4.11), the elastic vibration period T_n of the *n*th-mode SDF system is computed from

$$T_n = 2\pi \left(\frac{L_n D_{ny}}{F_{sny}} \right)^{1/2} \tag{4.13}$$

This value of T_n, which may differ from the period of the corresponding linear system, should be used in Eq. (4.8). In contrast, the initial slope of the pushover curve in Fig. 4.6a is $k_n = \omega_n^2 L_n$, which is not a meaningful quantity.

4.2.3 Summary

The inelastic response of an *N*-story building with plan symmetric about two orthogonal axes to earthquake ground motion along an axis of symmetry can be estimated as a function of time by the UMRHA procedure just developed, which is summarized next as a sequence of steps; details are available in Appendix A:

1. Compute the natural frequencies, ω_n, and modes, ϕ_n, for linearly-elastic vibration of the building.
2. For the *n*th-mode, develop the base-shear – roof-displacement ($V_{bn} - u_{rn}$) pushover curve for the force distribution $\mathbf{s}_n^*$ [Eq. (3.20)].
3. Idealize the pushover curve as a bilinear curve (Fig. 4.6a).
4. Convert the idealized pushover curve to the $F_{sn}/L_n - D_n$ relation (Fig. 4.6b) by utilizing Eq. (4.11).
5. Compute the deformation history, $D_n(t)$, and pseudo-acceleration history, $A_n(t)$, of the *n*th-"mode" inelastic SDF system (Fig. 4.3b) with force-deformation relation of Fig. 4.6b.
6. Calculate histories of various responses by Eqs. (3.12) and (3.13).
7. Repeat Steps 2 to 6 for as many modes as required for sufficient accuracy. Typically, the first two or three modes will suffice.
8. Combine the "modal" responses using Eqs. (3.15) and (3.16) to determine the total response.
9. Calculate the peak value, r_o, of the total response $r(t)$ obtained in Step 8.

4.3 MODAL PUSHOVER ANALYSIS

A pushover analysis procedure is presented next to estimate the peak response r_{no} of the inelastic MDF system to effective earthquake forces $\mathbf{p}_{\text{eff},n}(t)$. Consider a nonlinear static analysis of the structure subjected to lateral forces distributed over the building height according to $\mathbf{s}_n^*$ [Eq. (3.20)], with the structure is pushed to the roof displacement u_{rno}. This value of the roof displacement is given by Eq. (3.21) where D_n, the peak value of $D_n(t)$, is now determined by solving Eq. (4.8), as described in Section 4.2; alternatively, it can be determined from the inelastic response (or design) spectrum [Chopra, 2001; Sections 7.6 and 7.12]. At this roof displacement, the pushover analysis provides an estimate of the peak value r_{no} of any response $r_n(t)$: floor displacements, story drifts, joint rotations, plastic hinge rotations, etc.

This pushover analysis, although somewhat intuitive for inelastic buildings, seems reasonable. It provides results for elastic buildings that are identical to the well-known RSA procedure (Section 3.4.3) because, as mentioned earlier, the lateral force distribution used possesses two properties: (1) it appears to be the most rational choice among all invariant distribution of forces; and (2) it provides the exact modal response for elastic systems.

The response value r_{no} is an estimate of the peak value of the response of the inelastic system to $\mathbf{p}_{\text{eff},n}(t)$, governed by Eq. (4.6). As shown in Sections 3.2 and 3.3, for elastic systems, r_{no} also represents the exact peak value of the *n*th-mode contribution $r_n(t)$ to response $r(t)$. Thus, we will refer to r_{no} as the peak "modal" response even in the case of inelastic systems.

The peak "modal" responses r_{no}, each determined by one pushover analysis, are combined using an appropriate modal combination rule, e.g., Eq. (3.18), to obtain an estimate of the peak value r_o of the total response. This application of modal combination rules to inelastic systems obviously lacks a theoretical basis. However, it seems reasonable because it provides results for elastic buildings that are identical to the well-known RSA procedure described in Section 3.2.

4.3.1 Summary

The peak inelastic response of a building to earthquake excitation can be estimated by the MPA procedure just developed, which is summarized next as a sequence of steps; details are available in Appendix B.

Steps 1 to 4 of the MPA are same as those for UMRHA.

5. Compute the peak deformation, D_n, of the nth-"mode" inelastic SDF system (Fig. 4.3b) with force-deformation relation of Fig. 4.6b by solving Eq. (4.8), or from the inelastic response (or design) spectrum.
6. Calculate the peak roof displacement u_{rno} associated with the *n*th-"mode" inelastic SDF system from Eq. (3.21).
7. At u_{rno}, extract from the pushover database values of other desired responses, r_{no}.

8. Repeat Steps 3 to 8 for as many "modes" as required for sufficient accuracy. Typically, the first two or three "modes" will suffice.
9. Determine the total response by combining the peak "modal" responses using the SRSS combination rule of Eq. (3.18). From the total rotation of a plastic hinge, subtract the yield value of hinge rotation to determine the hinge plastic rotation.

4.4 COMPARATIVE EVALUATION OF ANALYSIS PROCEDURES

The response of the 9-story building described earlier is determined by the two approximate methods: UMRHA and MPA, and compared with the results of a rigorous nonlinear RHA using the DRAIN-2DX computer program. To ensure that this structure responds well into the inelastic range the El Centro ground motion is scaled up by a factor varying from 1.0 to 3.0.

4.4.1 Uncoupled Modal Response History Analysis

The structural response to 1.5 x the El Centro ground motion including the response contributions associated with three "modal" inelastic SDF systems, determined by the UMRHA procedure, is presented next. Figure 4.7 shows the individual "modal" responses, the combined response due to three "modes", and the "exact" response from nonlinear RHA for the roof displacement and top-story drift. The peak values of response are as noted; in particular, the peak roof displacement due to each of the three "modes" is $u_{r1o} = 48.3\,\text{cm}$, $u_{r2o} = 11.7\,\text{cm}$, and $u_{r3o} = 2.53\,\text{cm}$. The peak values of displacements of all floors and drifts in all stories are presented in Tables 4.1 and 4.2, respectively; also included are the combined responses due to one, two, and three "modes," the "exact" results, and the percentage errors in the approximate results. The peak values of floor displacements and story drifts including one, two, and three modes are compared with the "exact" values in Fig. 4.8, and the errors in the approximate results are shown in Fig. 4.9.

Observe that errors tend to decrease as response contributions of more "modes" are included, although the trends are not systematic as when the system remained elastic (Section 3.4.2). This is to be expected; in contrast to modal analysis (Section 3.1), the UMRHA procedure lacks a rigorous theory. This deficiency also implies that, with, say, three "modes" included, the response is much less accurate (Tables 4.1 and 4.2) if the system yields significantly versus if the system remains within the elastic range (Tables 3.1 and 3.2). However, for a fixed number of "modes" included, the errors in story drifts are larger compared to floor displacements, just as for elastic systems.

Next, we investigate how the errors in the UMRHA vary with the deformation demands imposed by the ground motion, in particular, the degree to which the system deforms beyond its elastic limit. For this purpose the UMRHA and exact analyses were repeated for ground motions of varying intensity, defined as the El Centro ground motion multiplied by 0.25, 0.5, 0.75, 0.85, 1.0, 1.5, 2.0, and 3.0. For each excitation, the errors in responses computed by UMRHA including three "modes" relative to the "exact" response were determined; recall that the computed errors have been presented earlier for ground motion multipliers 0.25 (Tables 3.1 and 3.2) and 1.5 (Tables 4.1 and 4.2).

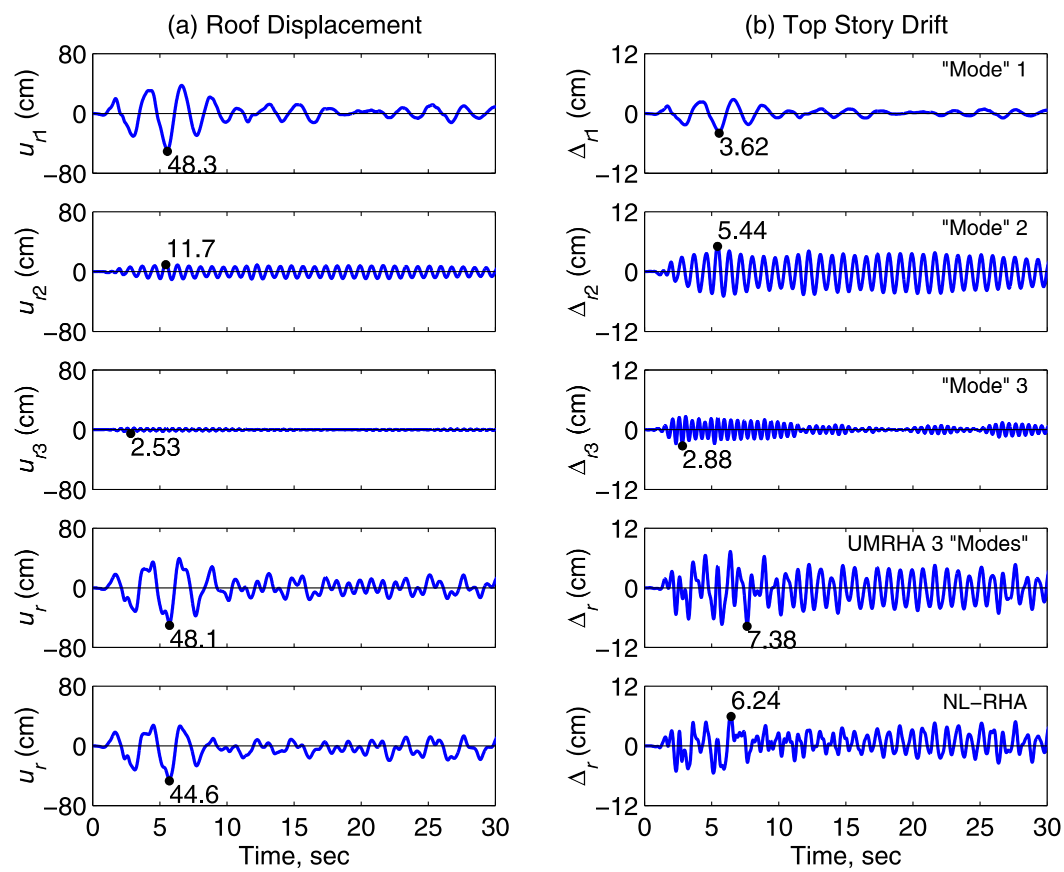

Fig. 4.7. Response histories of roof displacement and top-story drift due to 1.5 × El Centro ground motion: individual "modal" responses and combined response from UMRHA, and total response from NL-RHA

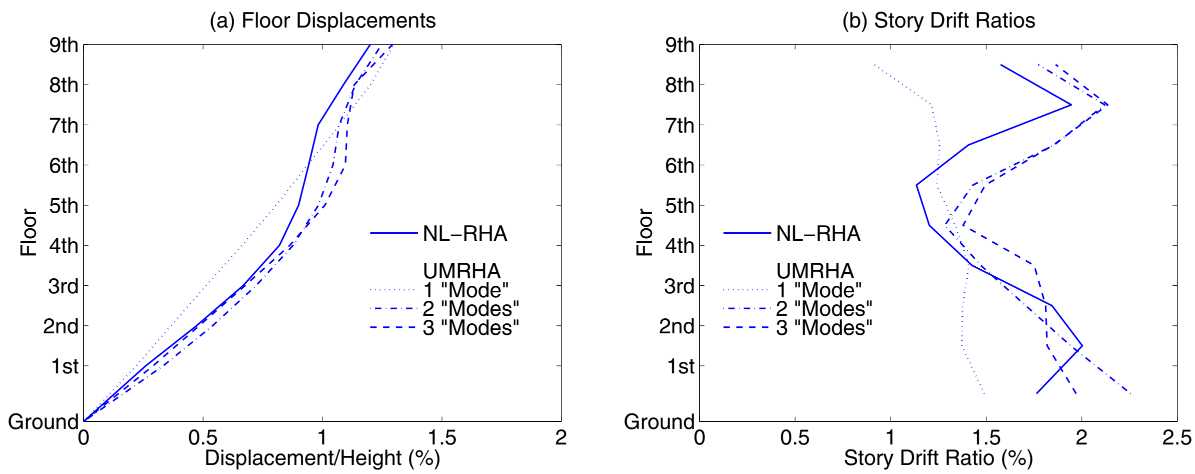

Fig. 4.8. Height-wise variation of floor displacements and story drift ratios from UMRHA and NL-RHA for 1.5 × El Centro ground motion

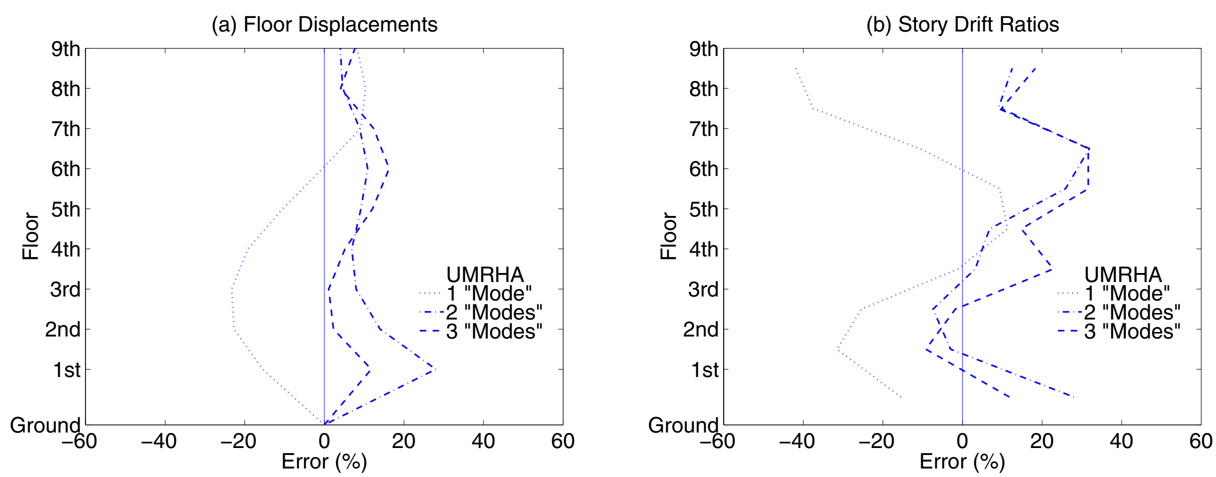

Fig. 4.9. Height-wise variation of error in floor displacements and story drifts estimated by UMRHA including one, two, or three "modes" for 1.5 x El Centro ground motion

Figure 4.10 summarizes the error in UMRHA as a function of ground motion intensity, indicated by a ground motion multiplier. Shown is the error in each floor displacement (Fig. 4.10a), in each story drift (Fig. 4.10b), and the error envelope for each case. To interpret these results, it will be useful to know the deformation of the system relative to its yield deformation. For this purpose, the pushover curves using force distributions $\mathbf{s}_n^*$ [Eq. (3.20)] for the first three modes of the system are shown in Fig. 4.11, with the peak displacement of each "modal" SDF system noted for each ground motion multiplier. Two versions of the pushover curve are included: the actual curve and its idealized bilinear version. The location of plastic hinges and their rotations, determined from "exact" analyses, were noted but are not shown here.

Figure 4.10 permits the following observations regarding the accuracy of the UMRHA procedure: the errors (1) are small (less than 5%) for ground motion multipliers up to 0.75; (2) increase rapidly as the ground motion multiplier increases to 1.0; (3) maintain roughly similar values for more intense ground motions; and (4) are larger in story drift compared to floor displacements. The system remains elastic up to ground motion multiplier 0.75, and, as mentioned in Section 3.4.2, the errors in truncating the higher mode contributions are negligible. Additional errors are introduced in UMRHA of systems responding beyond the linearly elastic limit for at least two reasons. First, as mentioned in Section 4.2, UMRHA lacks a rigorous theory and is based on several approximations. Second, the pushover curve for each "mode" is idealized by a bilinear curve in solving Eq. (4.10) for each "modal" inelastic SDF system (Figs 4.6 and 4.1). The idealized curve for the first "mode" deviates most from the actual curve near the peak displacement corresponding to ground motion multiplier 1.0. Perhaps this explains why the errors are large at this excitation intensity, even though the system remains essentially elastic; the ductility factor for the first mode system is only 1.01 (Fig. 4.11a). For more intense excitations, the first reason mentioned above seems to be the primary source for the errors.

4.4.2 Modal Pushover Analysis

The results of modal pushover analysis procedure considering the response due to the first three "modes" was implemented for the selected building subjected to 1.5 x the El Centro ground motion. The structure is pushed using the force distribution of Eq. (3.20) with n = 1, 2, and 3 (Fig. 3.4) to roof displacements u_{rno} = 48.3 cm, 11.7 cm, and 2.53 cm, respectively, the values determined by RHA of the nth-mode inelastic SDF system (Fig. 4.7). Each of these three pushover analyses provides the pushover curve (Fig. 4.11), the peak values of displacements at all floors (Table 4.3), drifts in all stories (Table 4.4), and plastic hinge rotations at the external beam end at each floor level (Table 4.5).

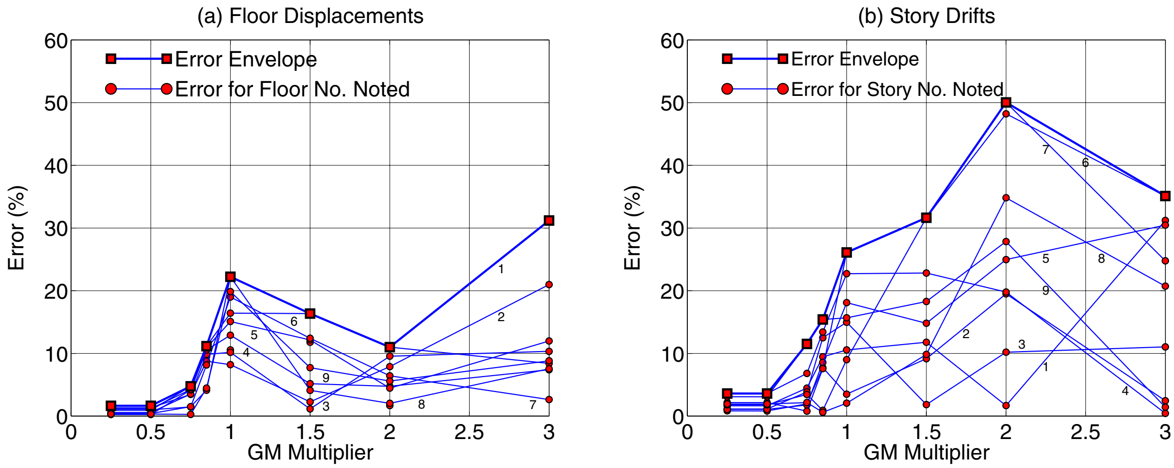

Fig. 4.10. Errors in UMRHA as a function of ground motion intensity: (a) floor displacements; and (b) story drifts

Table 4.1. Peak values of floor displacements (as % of building height = 37.14 m) from UMRHA for 1.5 × El Centro ground motion

Floor	Displacement /Height (%)							Error (%)		
	"Modal" Response			Combined (UMRHA)			NL RHA			
	"Mode" 1	"Mode" 2	"Mode" 3	1 "Mode"	2 "Modes"	3 "Modes"		1 "Mode"	2 "Modes"	3 "Modes"
1st	-0.220	-0.121	-0.055	0.220	0.333	0.291	0.260	-15.5	28.0	11.8
2nd	-0.366	-0.187	-0.071	0.366	0.540	0.484	0.473	-22.7	14.0	2.3
3rd	-0.513	-0.226	-0.057	0.513	0.722	0.676	0.668	-23.3	8.0	1.1
4th	-0.663	-0.235	-0.018	0.663	0.877	0.863	0.820	-19.2	6.9	5.2
5th	-0.806	-0.201	0.033	0.806	0.983	1.010	0.900	-10.5	9.2	12.1
6th	-0.938	-0.126	0.071	0.938	1.044	1.096	0.942	-0.5	10.9	16.3
7th	-1.072	0.003	0.065	1.072	1.070	1.104	0.982	9.1	8.9	12.4
8th	-1.201	0.169	0.009	1.201	1.138	1.133	1.088	10.4	4.6	4.1
9th	-1.298	0.315	-0.068	1.298	1.248	1.293	1.200	8.2	4.0	7.7

Table 4.2. Peak values of story drift ratios (as % of story height) from UMRHA for 1.5 × El Centro ground motion

Story	Drift Ratio (%)							Error (%)		
	Modal Response			Combined (UMRHA)			NL RHA			
	"Mode" 1	"Mode" 2	"Mode" 3	1 "Mode"	2 "Modes"	3 "Modes"		1 "Mode"	2 "Modes"	3 "Modes"
1st	-1.490	-0.820	-0.370	1.490	2.256	1.971	1.763	-15.5	28.0	11.8
2nd	-1.372	-0.616	-0.154	1.372	1.942	1.819	2.003	-31.5	-3.0	-9.2
3rd	-1.376	-0.371	0.130	1.376	1.707	1.811	1.844	-25.4	-7.4	-1.8
4th	-1.410	-0.079	0.371	1.410	1.472	1.751	1.426	-1.1	3.2	22.8
5th	-1.338	0.317	0.478	1.338	1.283	1.379	1.202	11.3	6.8	14.8
6th	-1.241	0.698	0.350	1.241	1.430	1.495	1.135	9.3	25.9	31.6
7th	-1.256	1.216	-0.049	1.256	1.856	1.852	1.407	-10.7	31.9	31.6
8th	-1.214	1.554	-0.526	1.214	2.120	2.136	1.945	-37.5	9.0	9.8
9th	-0.914	1.373	-0.727	0.914	1.772	1.863	1.575	-41.9	12.5	18.3

Figures 4.12 and 4.13 and Tables 4.3 through 4.5 present estimates of the combined response according to Eq. (3.18), considering one, two, and three "modes," respectively, and the errors in these estimates relative to the exact response from nonlinear RHA. Fortuitously, for two or three modes included, the errors in the modal pushover results are, in general, significantly smaller than in UMRHA (compare Fig. 4.13 with Fig. 4.9 and Tables 4.3 and 4.4 with Tables 4.1 and 4.2). Obviously, the additional errors due to the approximation inherent in modal combination rules tend to cancel out the errors due to the various approximation contained in the UMRHA. The first "mode" alone is inadequate, especially in estimating the story drifts (Fig. 4.12 and Tables 4.3 and 4.4). However, significant improvement is achieved by including response contributions due to the second "mode," but the third "mode" contributions do not seem especially important (Fig. 4.12 and Tables 4.3 and 4.4). As shown in Figs. 4.13 and Tables 4.3 and 4.4, MPA including three "modes" underestimates the displacements of the lower floors by up to 8% and overestimates the upper floor displacements by up to 14%. The drifts are underestimated by up to 13% in the lower stories, overestimated by up to 18% in the middle stories, and are within a few percent of the exact values for the upper stories.

The errors are especially large in the hinge plastic rotations estimated by the MPA procedure, even if three "modes" are included (Fig. 4.13 and Table 4.5); although the error is recorded as 100% if MPA estimates zero rotation when the nonlinear RHA computes a non-zero value, this error is not especially significant because the hinge plastic rotation is very small. Observe that the primary contributor to plastic hinge rotations in the lower stories is the first "mode" and the second "mode" in the upper stories; the third "mode" does not contribute because this SDF system remains elastic (Fig. 4.11c). Pushover analysis seems to be inherently limited in computing accurately hinge plastic rotations.

The locations of plastic hinges shown in Fig. 4.14, were determined by four analyses: MPA considering one "mode," two "modes," and three "modes;" and nonlinear RHA. One "mode" pushover analysis was unable to identify the plastic hinges in the upper stories where higher mode contributions to response are known to be more significant. The second "mode" was necessary to identify hinges in the upper stories; however, the results were not always accurate. For example, the hinges identified in beams at the 6th floor were at variance with the "exact" results. Furthermore, MPA failed to identify the plastic hinges at the column bases in

Fig. 4.14; but was more successful when the excitation was more intense (results are not included).

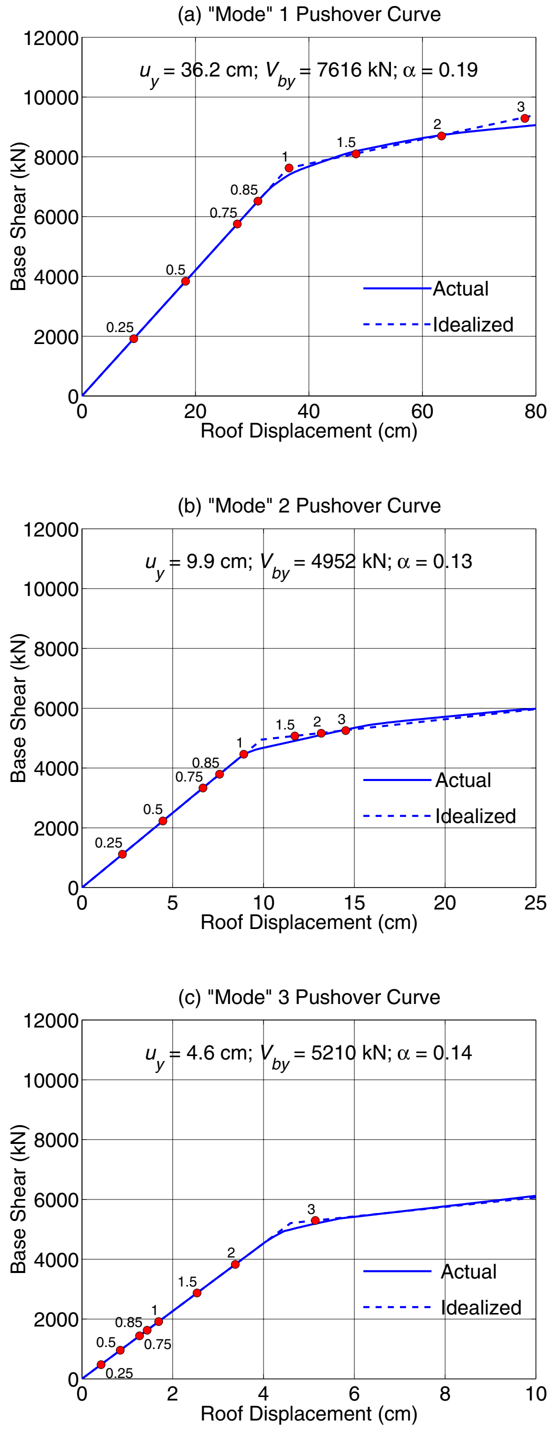

Fig. 4.11. "Modal" pushover curves with peak roof displacements identified for 0.25, 0.5, 0.75, 1.0, 1.5, 2.0, and 3.0 × El Centro ground motion

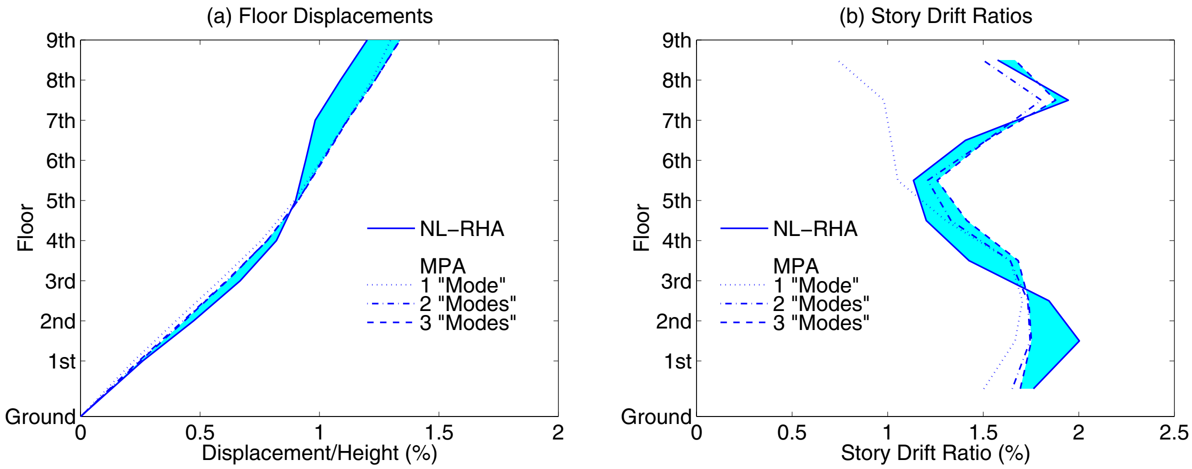

Fig. 4.12. Height-wise variation of floor displacements and story drift ratios from MPA and NL-RHA for 1.5 × El Centro ground motion; shading indicates errors in MPA including three "modes"

Figure 4.15 summarizes the error in MPA considering three "modes" as a function of ground motion intensity, indicated by a ground motion multiplier. Shown is the error in each floor displacement (Fig. 4.15a), each story drift (Fig. 4.15b), and the error envelope for each case. While various sources of errors in UMRHA, identified in Section 3.4 also apply to MPA, the errors in MPA were fortuitously smaller than in UMRHA (compare Figs. 4.10 and 4.15) for ground multipliers larger than 1.0, implying excitations intense enough to cause significant yielding of the structure. However, the errors in MPA were larger for ground motion multipliers less than 0.75, implying excitations weak enough to limit the response in the elastic range of the structure. In this case, as discussed in Sections 3.4.2 and 3.4.3, UMRHA is essentially exact, whereas MPA contains errors inherent in modal combination rules.

The errors are only weakly dependent on ground motion intensity (Fig. 4.15), an observation with practical implications. As mentioned in Section 3.3 for elastic systems (or weak ground motions), the MPA procedure is equivalent to the RSA procedure, now standard in engineering practice, implying that the modal combination errors contained in these procedures are acceptable. The fact that MPA is able to estimate the response of buildings responding well into the inelastic range to a similar degree of accuracy indicates that this procedure is accurate enough for practical application in building retrofit and design.

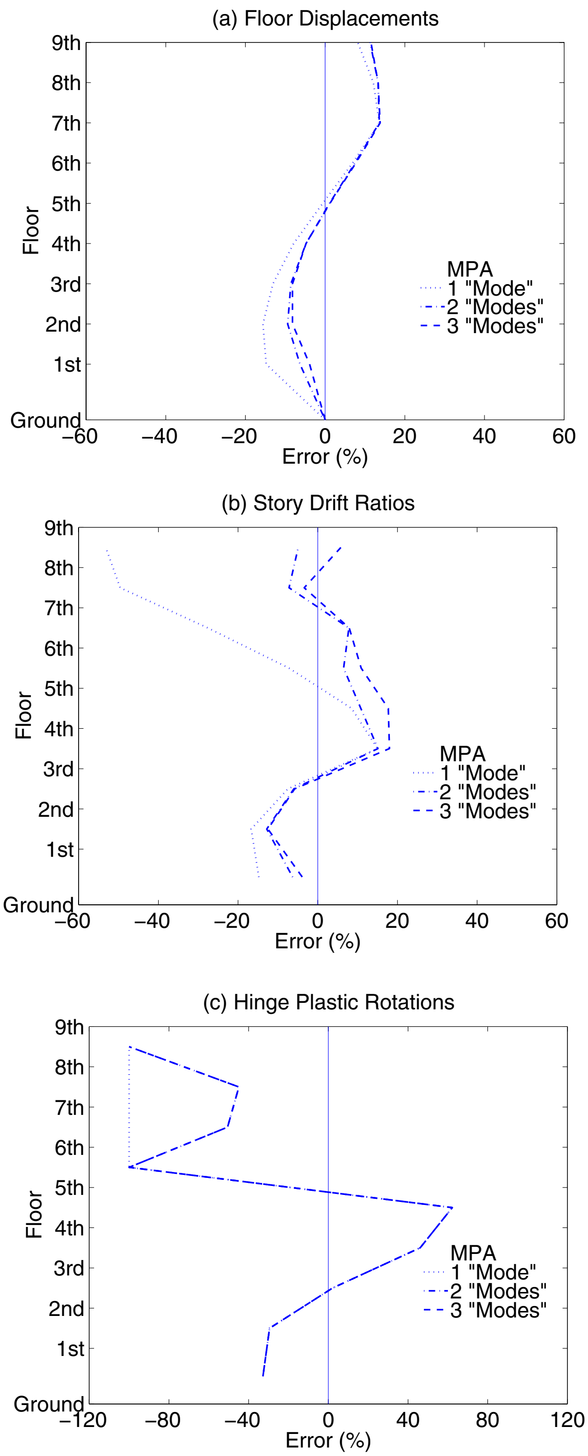

Fig. 4.13. Errors in floor displacements, story drifts, and hinge plastic rotations estimated by MPA including one, two, and three "modes" for 1.5 x El Centro ground motion.

Table 4.3. Peak values of floor displacements (as % of building height = 37.14 m) from MPA for 1.5 × El Centro ground motion

Floor	Displacement /Height (%)							Error (%)		
	"Modal" Response			Combined (MPA)			NL RHA			
	"Mode" 1	"Mode" 2	"Mode" 3	1 "Mode"	2 "Modes"	3 "Modes"		1 "Mode"	2 "Modes"	3 "Modes"
1st	0.222	-0.101	0.055	0.222	0.244	0.250	0.260	-14.8	-6.3	-3.9
2nd	0.399	-0.156	0.071	0.399	0.429	0.435	0.473	-15.6	-9.4	-8.2
3rd	0.581	-0.190	0.057	0.581	0.611	0.614	0.668	-13.1	-8.6	-8.2
4th	0.756	-0.197	0.018	0.756	0.781	0.781	0.820	-7.9	-4.8	-4.8
5th	0.895	-0.168	-0.033	0.895	0.910	0.911	0.900	-0.6	1.1	1.2
6th	1.007	-0.105	-0.071	1.007	1.012	1.015	0.942	6.9	7.5	7.7
7th	1.116	0.015	-0.066	1.116	1.116	1.118	0.982	13.6	13.6	13.8
8th	1.220	0.176	-0.009	1.220	1.233	1.233	1.088	12.1	13.3	13.3
9th	1.298	0.315	0.068	1.298	1.336	1.338	1.200	8.2	11.3	11.5

Table 4.4. Peak values of story drift ratios (as % of story height) from MPA for 1.5 × El Centro ground motion

Story	Drift Ratio (%)							Error (%)		
	"Modal" Response			Combined (MPA)			NL RHA			
	"Mode" 1	"Mode" 2	"Mode" 3	1 "Mode"	2 "Modes"	3 "Modes"		1 "Mode"	2 "Modes"	3 "Modes"
1st	-1.503	0.687	-0.371	1.503	1.652	1.694	1.763	-14.8	-6.3	-3.9
2nd	-1.667	0.516	-0.154	1.667	1.745	1.752	2.003	-16.7	-12.8	-12.5
3rd	-1.705	0.311	0.130	1.705	1.733	1.738	1.844	-7.5	-6.0	-5.8
4th	-1.640	0.066	0.372	1.640	1.641	1.683	1.426	15.0	15.1	18.0
5th	-1.304	-0.266	0.478	1.304	1.331	1.414	1.202	8.5	10.8	17.7
6th	-1.053	-0.594	0.351	1.053	1.209	1.259	1.135	-7.2	6.5	10.9
7th	-1.018	-1.125	-0.049	1.018	1.517	1.518	1.407	-27.6	7.8	7.9
8th	-0.980	-1.514	-0.527	0.980	1.804	1.879	1.945	-49.6	-7.2	-3.4
9th	-0.737	-1.305	-0.728	0.737	1.498	1.666	1.575	-53.2	-4.9	5.8

Table 4.5. Peak values of hinge plastic rotations (radians) from MPA for 1.5 × El Centro ground motion

Floor	Hinge Plastic Rotation (rad)							Error (%) "Modal" Response		
	"Modal" Response			Combined (MPA)			NL RHA			
	"Mode" 1	"Mode" 2	"Mode" 3	1 "Mode"	2 "Modes"	3 "Modes"		1 "Mode"	2 "Modes"	3 "Modes"
1st	7.36E-03	0.00E+00	0.00E+00	7.36E-03	7.36E-03	7.36E-03	1.10E-02	-32.8	-32.8	-32.8
2nd	6.72E-03	0.00E+00	0.00E+00	6.72E-03	6.72E-03	6.72E-03	9.53E-03	-29.5	-29.5	-29.5
3rd	7.76E-03	0.00E+00	0.00E+00	7.76E-03	7.76E-03	7.76E-03	7.60E-03	2.1	2.1	2.1
4th	4.37E-03	0.00E+00	0.00E+00	4.37E-03	4.37E-03	4.37E-03	2.99E-03	46.1	46.1	46.1
5th	1.02E-03	0.00E+00	0.00E+00	1.02E-03	1.02E-03	1.02E-03	6.26E-04	62.2	62.2	62.2
6th	0.00E+00	0.00E+00	0.00E+00	0.00E+00	3.19E-10	3.50E-10	9.60E-04	-100.0	-100.0	-100.0
7th	0.00E+00	3.55E-03	0.00E+00	0.00E+00	3.55E-03	3.55E-03	7.18E-03	-100.0	-50.6	-50.6
8th	0.00E+00	3.88E-03	0.00E+00	0.00E+00	3.88E-03	3.88E-03	7.05E-03	-100.0	-44.9	-44.9
9th	0.00E+00	0.00E+00	0.00E+00	0.00E+00	0.00E+00	1.22E-10	2.37E-04	-100.0	-100.0	-100.0

4.4.3 Modal Pushover Analysis with Gravity Loads

To evaluate the accuracy of the dynamic response of the system, the results presented so far did not include gravity load effects. They are now included in the pushover analysis of the structure for the first "mode" only. Static analysis of the structure for gravity loads provides the initial state—forces and deformations—of the structure, and the structure is pushed using the force distribution of Eq. (3.20) with $n = 1$ to a target roof displacement. Obviously gravity load effects will influence the seismic demands due to the first "mode," but not the contributions of higher "modes"; these effects will modify the combined modal response as well as the results of nonlinear RHA.

Results of such analyses for the selected building subject to 1.5 × El Centro ground motion are presented below. Starting with its initial state under gravity loads, the structure is pushed using the force distribution of Eq. (3.20) with $n=1$ (Fig. 3.4) to roof displacement $u_{r1o} = 52.0$ cm, resulting in the pushover curve shown in Fig. 4.16a—which is slightly different than the one excluding gravity loads (Fig. 4.11a). The pushover curves for the second and third modes included in Fig. 4.16 are unchanged, as are the roof displacements $u_{r2o} = 11.7$ cm and $u_{r3o} = 2.53$ cm. Also presented at these roof displacements are the displacements at all floors (Table 4.6), drifts in all stories (Table 4.7), and plastic hinge rotations at selected external beam end at each floor level (Table 4.8). The response contributions of the second and third modes are the same as before (Tables 4.3 - 4.5).

Figures 4.17 and 4.18 and Tables 4.6 through 4.8 present estimates of the combined response according to Eq. (3.18) considering one, two, and three "modes," and the errors in these estimates relative to the exact response from nonlinear RHA. The first "mode" alone provides adequate estimates of floor displacements, but it is inadequate in estimating the story drifts (Fig. 4.17 and Tables 4.6 and 4.7). Significant improvement is achieved by including response contributions due to the second "mode," however, the third "mode" contributions do not seem especially important (Fig. 4.17 and Tables 4.6 and 4.7). As shown in Fig. 4.18 and Tables 4.6 and 4.7, MPA including two "modes" underestimates the displacements of lower floors by up to 6% and overestimates the upper floor displacements by up to 22%. The story drifts are underestimated by up to 7% in the lower stories, and overestimated by up to 29% in the middle stories and by up to 13% in the upper stories. The errors are especially large in the plastic hinge rotations estimated by the MPA procedure even if three “modes” are included (Fig. 4.18 and Table 4.8). Most pushover analysis procedures do not seem to compute to acceptable accuracy plastic hinge rotations.

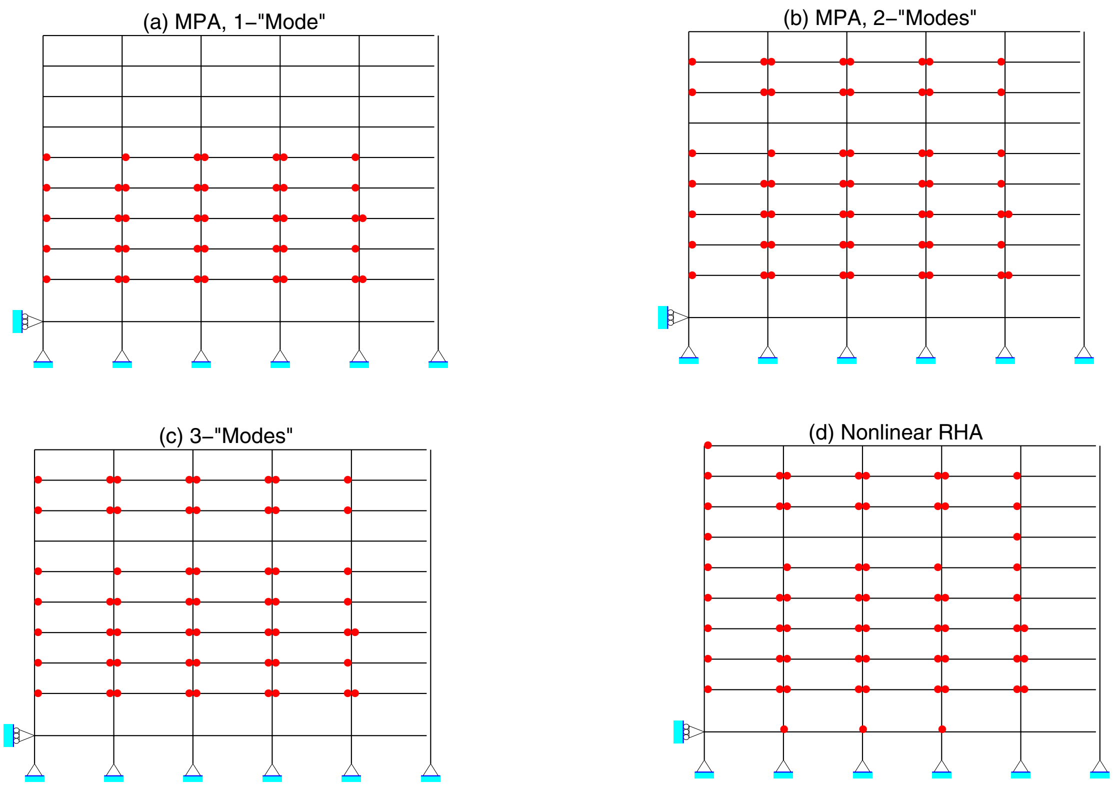

Fig. 4.14. Locations of plastic hinges determined by MPA considering one, two, and three “modes” and by NL-RHA for 1.5 × El Centro ground motion

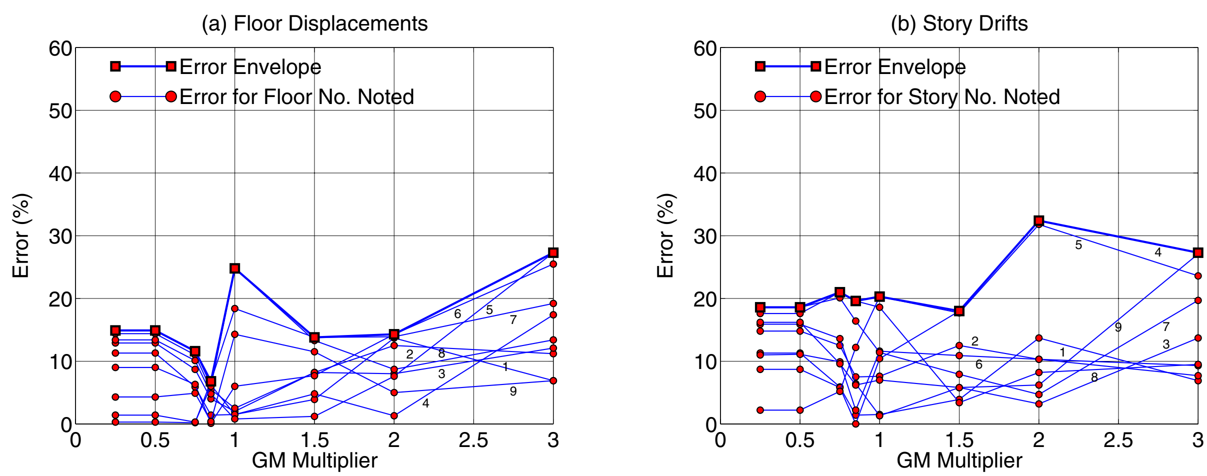

Fig. 4.15. Errors in MPA as a function of ground motion intensity: (a) floor displacements; and (b) story drifts

The locations of plastic hinges shown in Fig. 4.19 were determined by four analyses: MPA considering one "mode," two "modes," and nonlinear RHA. One "mode" pushover analysis is unable to identify the plastic hinges in the upper stories where higher mode contributions to response are known to be more significant. The second "mode" is necessary to identify hinges in the upper stories. With two modes included in MPA, this procedure is able to predict plastic hinge locations essentially consistent with nonlinear RHA.

Figure 4.20 summarizes the error in MPA considering three "modes" as a function of ground motion intensity, indicated by a ground motion multiplier. Shown is the error in each floor displacement (Fig. 4.20a), each story drift (Fig. 4.20b), and the error envelope for each case. MPA provides response values accurate enough for practical application in building retrofit or design; and the errors are only weakly dependent on ground motion intensity. These errors are only slightly larger than those in Fig. 4.15, excluding gravity load effects.

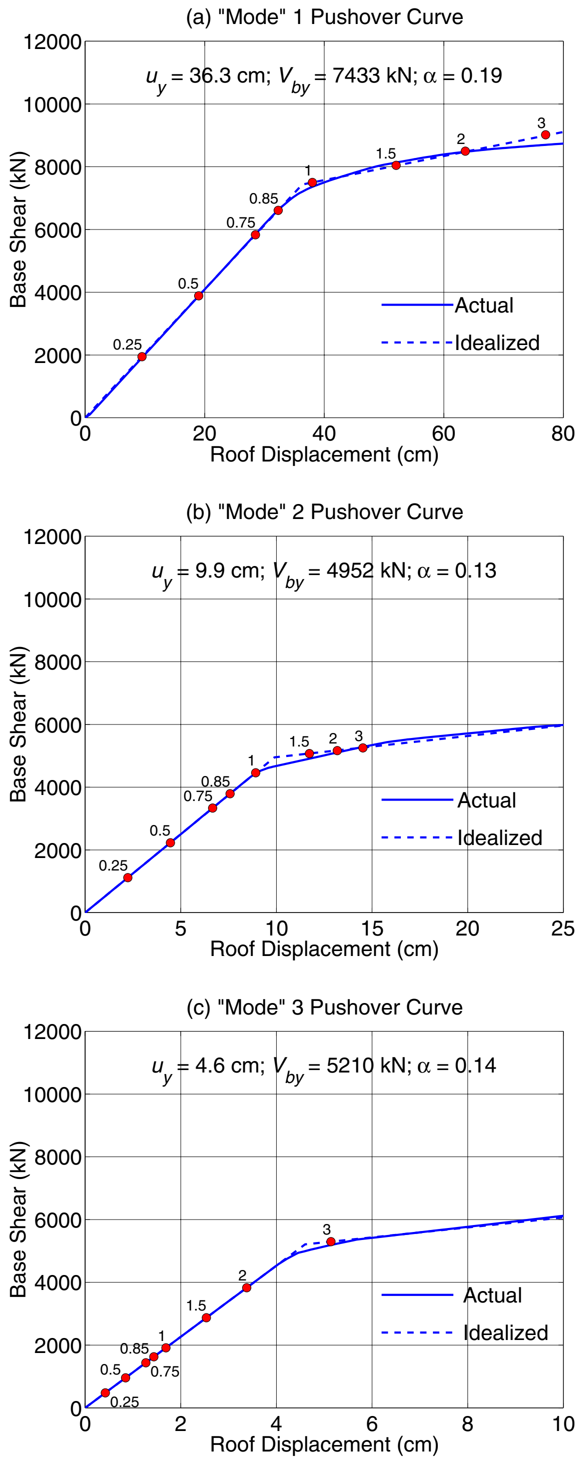

Fig. 4.16. "Modal" pushover curves with gravity loads included; noted are peak values of roof displacement for 0.25, 0.50, 0.75, 0.85, 1.0, 2.0, and 3.0 × El Centro ground motion

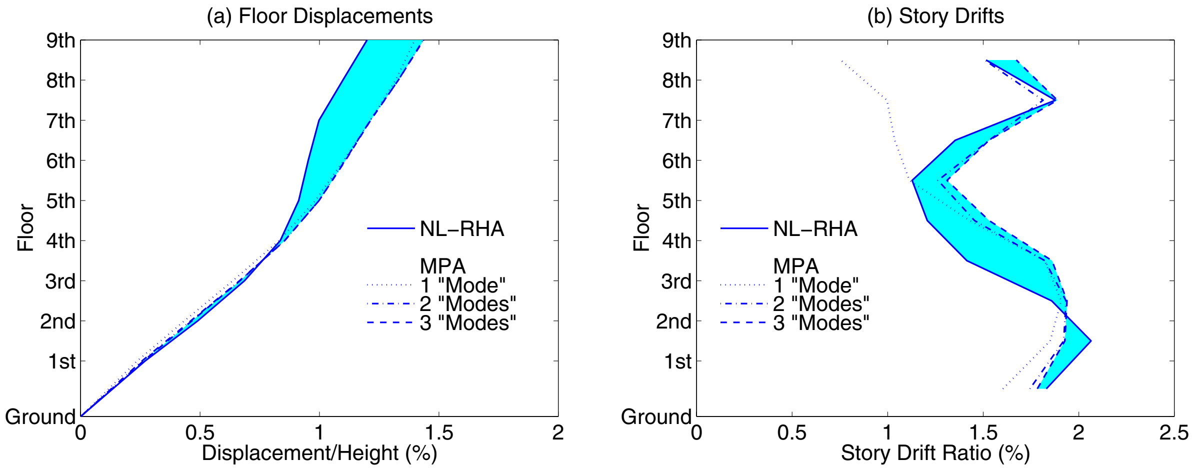

Fig. 4.17. Heightwise variation of floor displacements and story drift ratios from MPA and NL-RHA for 1.5 × El Centro ground motion; gravity loads included; shading indicates errors in MPA including three "modes"

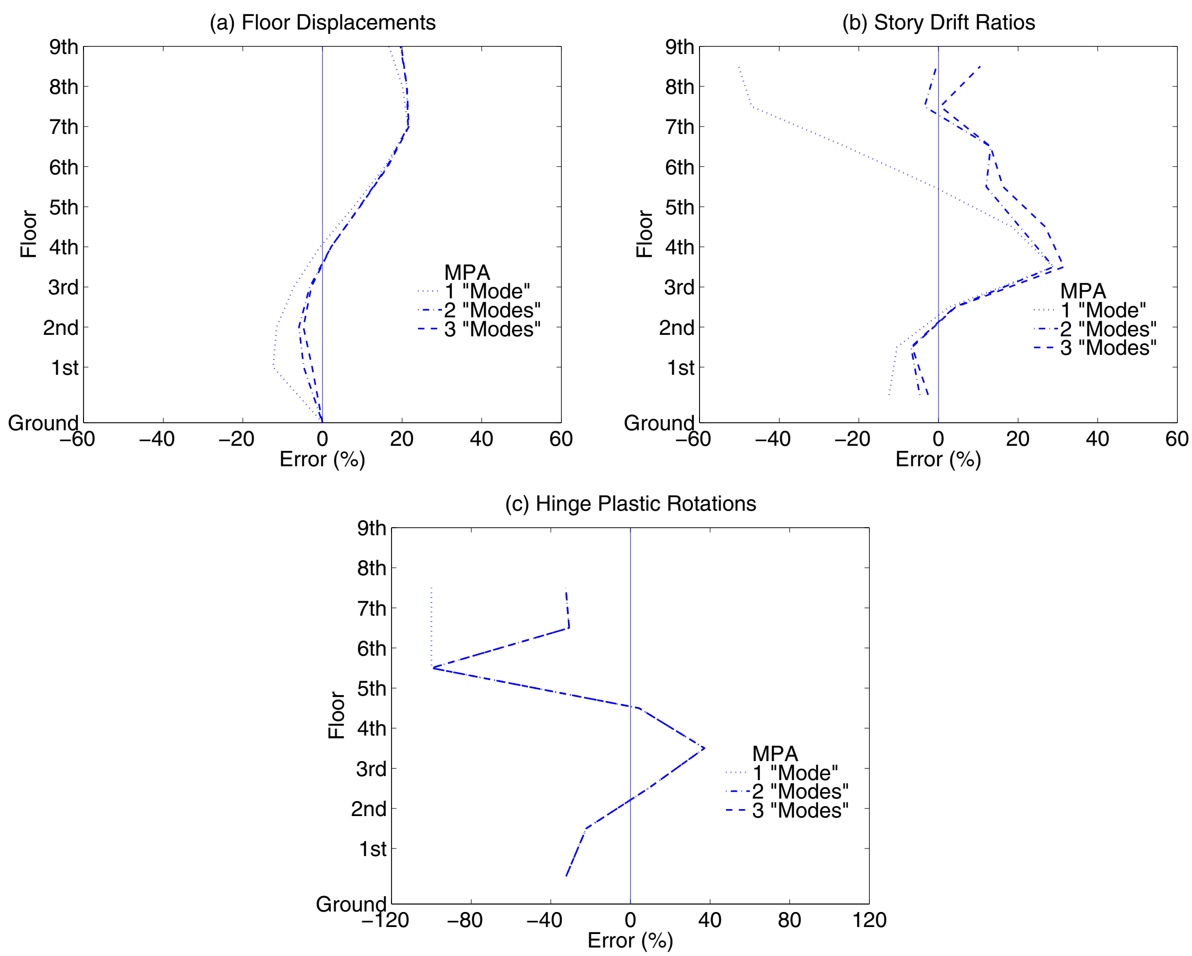

Fig. 4.18. Errors in floor displacements, story drifts, and hinge plastic rotations estimated by MPA including one, two, and three "modes" for 1.5 x El Centro ground motion

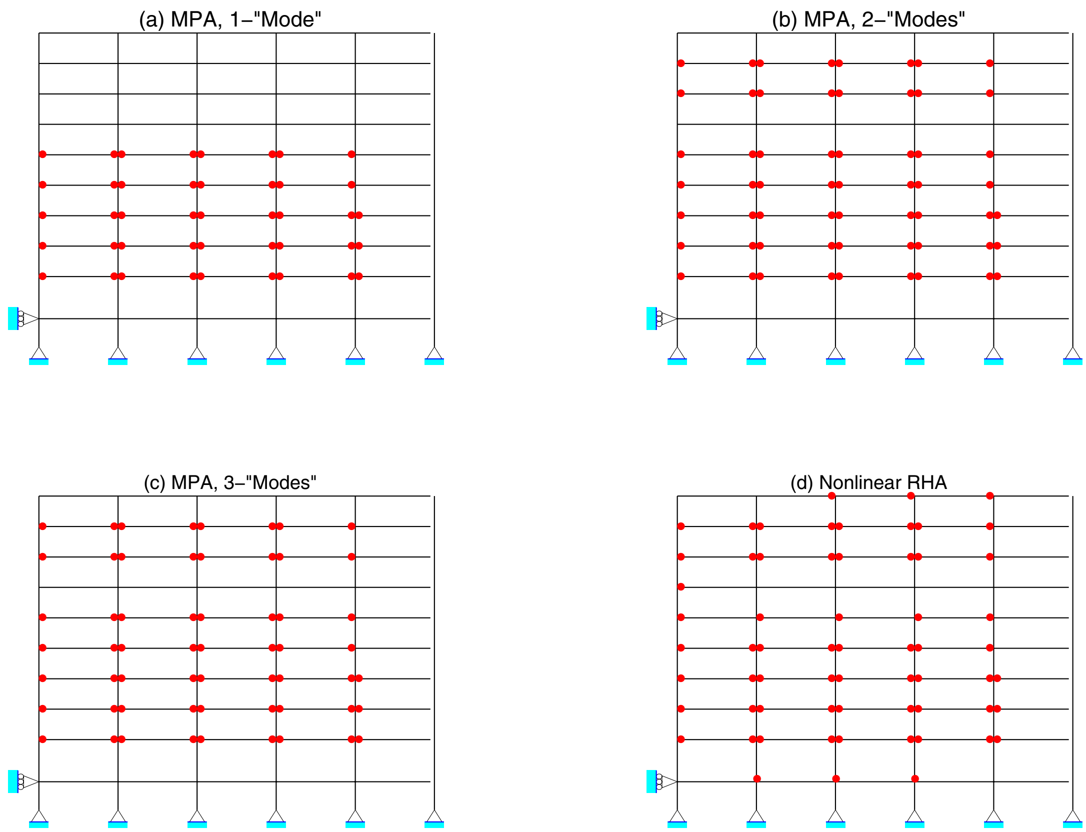

Fig. 4.19. Locations of plastic hinges determined by MPA considering one, two, and three "modes" and by NL-RHA for 1.5 × El Centro ground motion; gravity loads included

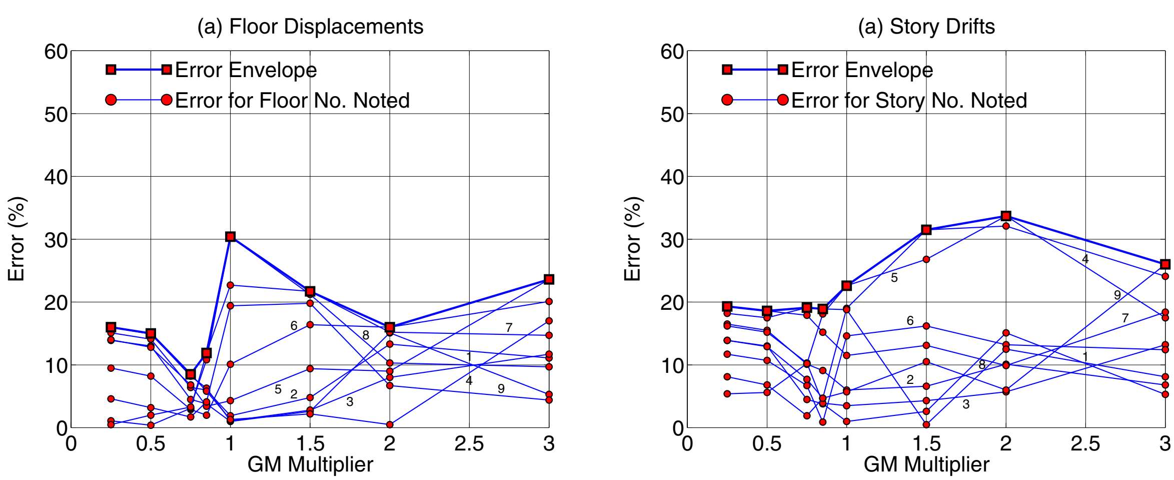

Fig. 4.20. Errors in MPA as a function of ground motion intensity: (a) floor displacements; and (b) story drifts; gravity loads included

Table 4.6. Peak values of floor displacements (as % of building height = 37.14 m) from MPA for 1.5 × El Centro ground motion; gravity loads included

Floor	Displacement /Height (%)							Error (%)		
	"Modal" Response			Combined (MPA)			NL RHA			
	"Mode" 1	"Mode" 2	"Mode" 3	1 "Mode"	2 "Modes"	3 "Modes"		1 "Mode"	2 "Modes"	3 "Modes"
1st	0.237	-0.101	0.055	0.237	0.257	0.263	0.270	-12.4	-4.7	-2.6
2nd	0.434	-0.156	0.071	0.434	0.461	0.466	0.490	-11.5	-5.9	-4.8
3rd	0.637	-0.190	0.057	0.637	0.665	0.667	0.686	-7.2	-3.2	-2.8
4th	0.831	-0.197	0.018	0.831	0.854	0.854	0.836	-0.6	2.2	2.2
5th	0.983	-0.168	-0.033	0.983	0.998	0.998	0.913	7.8	9.3	9.4
6th	1.102	-0.105	-0.071	1.102	1.107	1.109	0.953	15.7	16.2	16.4
7th	1.213	0.015	-0.066	1.213	1.213	1.214	0.998	21.5	21.5	21.7
8th	1.319	0.176	-0.009	1.319	1.330	1.330	1.098	20.1	21.2	21.2
9th	1.399	0.315	0.068	1.399	1.434	1.436	1.199	16.7	19.6	19.8

Table 4.7 Peak values of story drift ratios (as % of story height) from MPA for 1.5 × El Centro ground motion; gravity loads included

Story	Drift Ratio (%)							Error (%)		
	"Modal" Response			Combined (MPA)			NL RHA			
	"Mode" 1	"Mode" 2	"Mode" 3	1 "Mode"	2 "Modes"	3 "Modes"		1 "Mode"	2 "Modes"	3 "Modes"
1st	-1.603	0.687	-0.371	1.603	1.744	1.783	1.830	-12.4	-4.7	-2.6
2nd	-1.850	0.516	-0.154	1.850	1.921	1.927	2.064	-10.4	-6.9	-6.6
3rd	-1.908	0.311	0.130	1.908	1.933	1.938	1.858	2.7	4.1	4.3
4th	-1.821	0.066	0.372	1.821	1.822	1.860	1.414	28.8	28.9	31.5
5th	-1.429	-0.266	0.478	1.429	1.454	1.530	1.207	18.4	20.4	26.8
6th	-1.114	-0.594	0.351	1.114	1.263	1.310	1.128	-1.2	12.0	16.2
7th	-1.037	-1.125	-0.049	1.037	1.530	1.530	1.353	-23.3	13.1	13.1
8th	-0.996	-1.514	-0.527	0.996	1.813	1.888	1.877	-46.9	-3.5	0.5
9th	-0.754	-1.305	-0.728	0.754	1.507	1.673	1.515	-50.2	-0.5	10.5

Table 4.8 Peak values of hinge plastic rotations (radians) from MPA for 1.5 × El Centro ground motion; gravity loads included

Floor	Hinge Plastic Rotation (rad)							Error (%) "Modal" Response		
	"Modal" Response			Combined (MPA)			NL RHA			
	"Mode" 1	"Mode" 2	"Mode" 3	1 "Mode"	2 "Mode"	3 "Modes"		1 "Mode"	2 "Modes"	3 "Modes"
1st	8.35E-03	0.00E+00	0.00E+00	8.35E-03	8.35E-03	8.35E-03	1.23E-02	-32.3	-32.3	-32.3
2nd	8.11E-03	0.00E+00	0.00E+00	8.11E-03	8.11E-03	8.11E-03	1.04E-02	-22.2	-22.2	-22.2
3rd	9.00E-03	0.00E+00	0.00E+00	9.00E-03	9.00E-03	9.00E-03	8.26E-03	9.0	9.0	9.0
4th	5.19E-03	0.00E+00	0.00E+00	5.19E-03	5.19E-03	5.19E-03	3.78E-03	37.2	37.2	37.2
5th	1.23E-03	0.00E+00	0.00E+00	1.23E-03	1.23E-03	1.23E-03	1.17E-03	4.3	4.3	4.3
6th	0.00E+00	0.00E+00	0.00E+00	0.00E+00	3.04E-10	3.35E-10	9.19E-04	-100.0	-100.0	-100.0
7th	0.00E+00	3.55E-03	0.00E+00	0.00E+00	3.55E-03	3.55E-03	5.13E-03	-100.0	-30.8	-30.8
8th	0.00E+00	3.88E-03	0.00E+00	0.00E+00	3.88E-03	3.88E-03	5.75E-03	-100.0	-32.5	-32.5
9th	0.00E+00	0.00E+00	0.00E+00	0.00E+00	0.00E+00	1.00E-10	0.00E+00			

5 Comparison of Modal and FEMA Pushover Analyses

5.1 FEMA-273 PUSHOVER ANALYSIS

In this investigation we focus on one step in the nonlinear static procedure in the FEMA-273 document [Building Seismic Safety Council, 1997] The pushover curve, a plot of base shear versus roof displacement, is determined by nonlinear static analysis of the structure subjected to lateral forces with invariant distribution over height but gradually increasing values until a target value of roof displacement is reached. The floor displacements, story drifts, joint rotations, plastic hinge rotations, etc., computed at the target displacement represent the earthquake-induced demands on the structure.

Specified in FEMA-273 are three distributions for lateral forces:

1. "Uniform" distribution: $s_j^* = m_j$ (where the floor number $j = 1, 2 \ldots N$);

2. Equivalent lateral force (ELF) distribution: $s_j^* = m_j h_j^k$ where h_j is the height of the jth floor above the base, and the exponent $k = 1$ for fundamental period $T_1 \leqslant 0.5$ sec, $k = 2$ for $T_1 \geqslant 2.5$ sec; and varies linearly in between; and

3. SRSS distribution: $\mathbf{s}^*$ is defined by the lateral forces back-calculated from the story shears determined by response spectrum analysis of the structure, assumed to be linearly elastic.

5.2 COMPARATIVE EVALUATION

Compared in this section are the earthquake-induced demands for the selected building determined by five analyses: pushover analysis using the three force distributions in FEMA-273, MPA considering three “modes,” and nonlinear RHA; gravity load effects were included in all analyses. The three FEMA force distributions are presented in Fig. 5.1, wherein the first two are obvious and the third is determined from response spectrum analysis of the building (Appendix C). Using each of these force distributions, pushover analyses are implemented for a target roof displacement of 52.0 cm, the value determined from RHA of the first-mode inelastic SDF system for 1.5 times the El Centro ground motion. The pushover curves are given in Fig. 5.2, the floor displacement demands in Fig. 5.3a and Table 5.1, the story drift demands in Fig. 5.3b and Table 5.2, plastic hinge rotation demands in Table 5.3, and the locations of all plastic hinges in Fig. 5.4. Also included in these presentations are the MPA results considering three “modes” and the “exact” demands from nonlinear RHA, both presented in Section 4.4.3. The errors in the FEMA and MPA estimates of seismic demands relative to the “exact” demands are presented in Fig. 5.4 and Tables 5.1 through 5.3.

Figures 5.3a and 5.4a, and Table 5.1 demonstrate that the displacement demands are underestimated by the ELF and SRSS force distributions by 12 to 30 % at the lower six floors of the building, with the errors being larger for the SRSS distribution. The “uniform” distribution overestimates all floor displacements by 17-28%. The MPA procedure is more accurate than all the FEMA force distributions. The first four floor displacements are within 5% of the “exact” value, and the displacements of upper floors are overestimated by 9-22%.

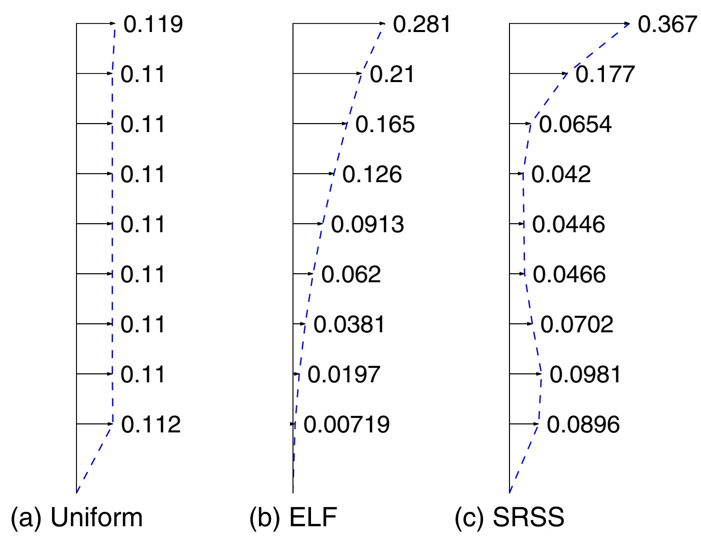

Fig. 5.1. Force distributions in FEMA-273: (a) “uniform”; (b) ELF; and (c) SRSS

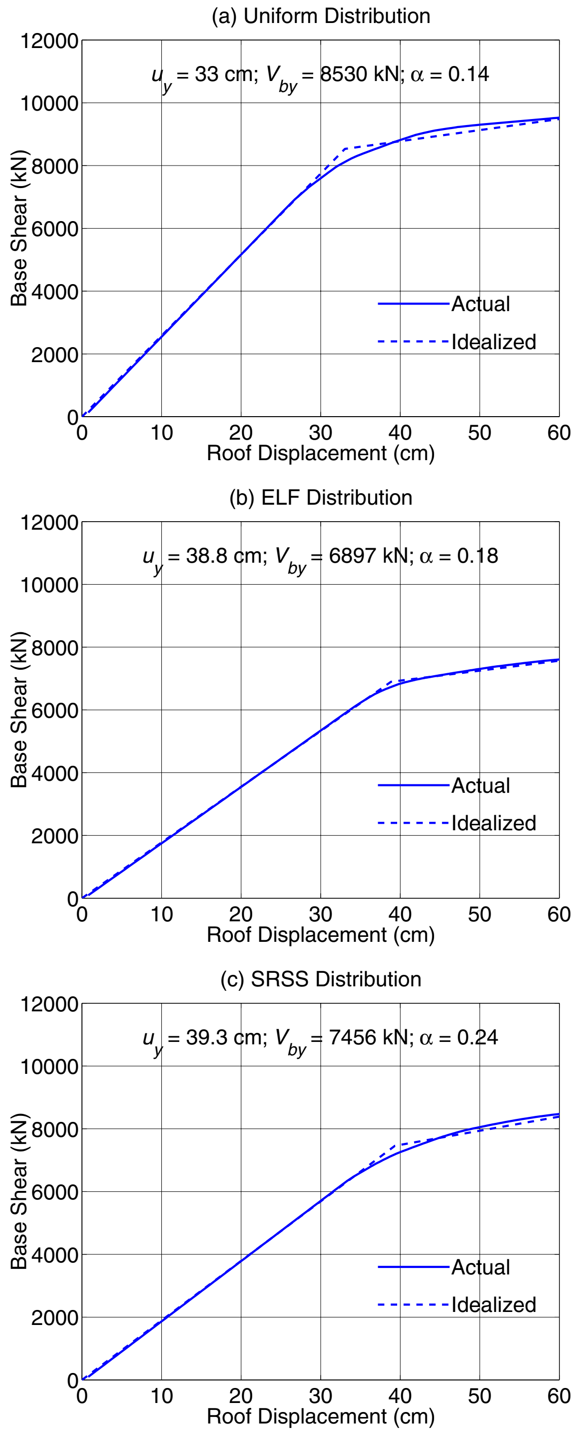

Fig. 5.2. Pushover curves using three force distributions in FEMA-273: (a) "uniform"; (b) ELF; and (c) SRSS; gravity loads are included

Figures 5.3b and 5.4b, and Table 5.2 demonstrate that the story drift demands are greatly underestimated by all the FEMA force distributions. For the uniform distribution, errors are largest in the upper stories, reaching 64%. For the ELF distribution, larger errors are noted in the upper and lower stories, reaching 35%. For the SRSS distribution, the errors are largest in the lower stories, reaching 31%. In contrast, the MPA procedure is more accurate than all the FEMA force distributions, with story drifts under estimated by, at most, 7%, and overestimated by no more than 32%.

Figure 5.4c and Table 5.3 demonstrate that the hinge plastic rotations estimated by all three FEMA force distributions contain unacceptably large errors. Modal pushover analysis procedure gives estimates better than all the FEMA force distributions, but it is still inaccurate, with errors reaching 37% in this example. (The 100% error in a 6^{th} floor hinge is ignored as it simply represents that the MPA estimated zero rotation, whereas nonlinear RHA computed an insignificantly small value.) The pushover analysis procedures considered seem incapable of computing accurately local response quantities, such as hinge plastic rotations. This seems to be an inherent limitation of pushover analysis.

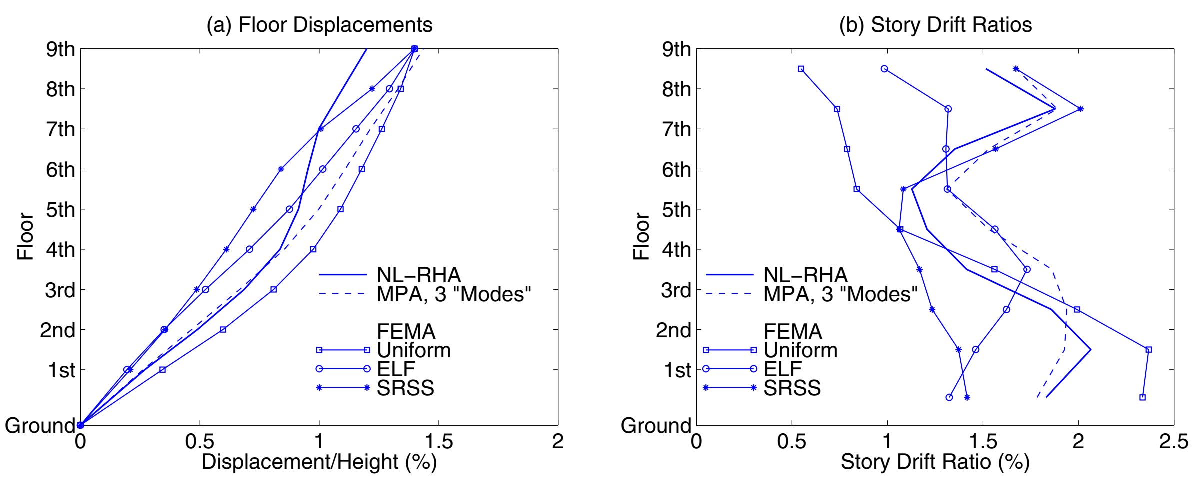

Fig. 5.3. Heightwise variation of floor displacements and story drift ratios estimated using FEMA-273 force distributions, MPA including three “modes,” and NL-RHA; gravity loads included

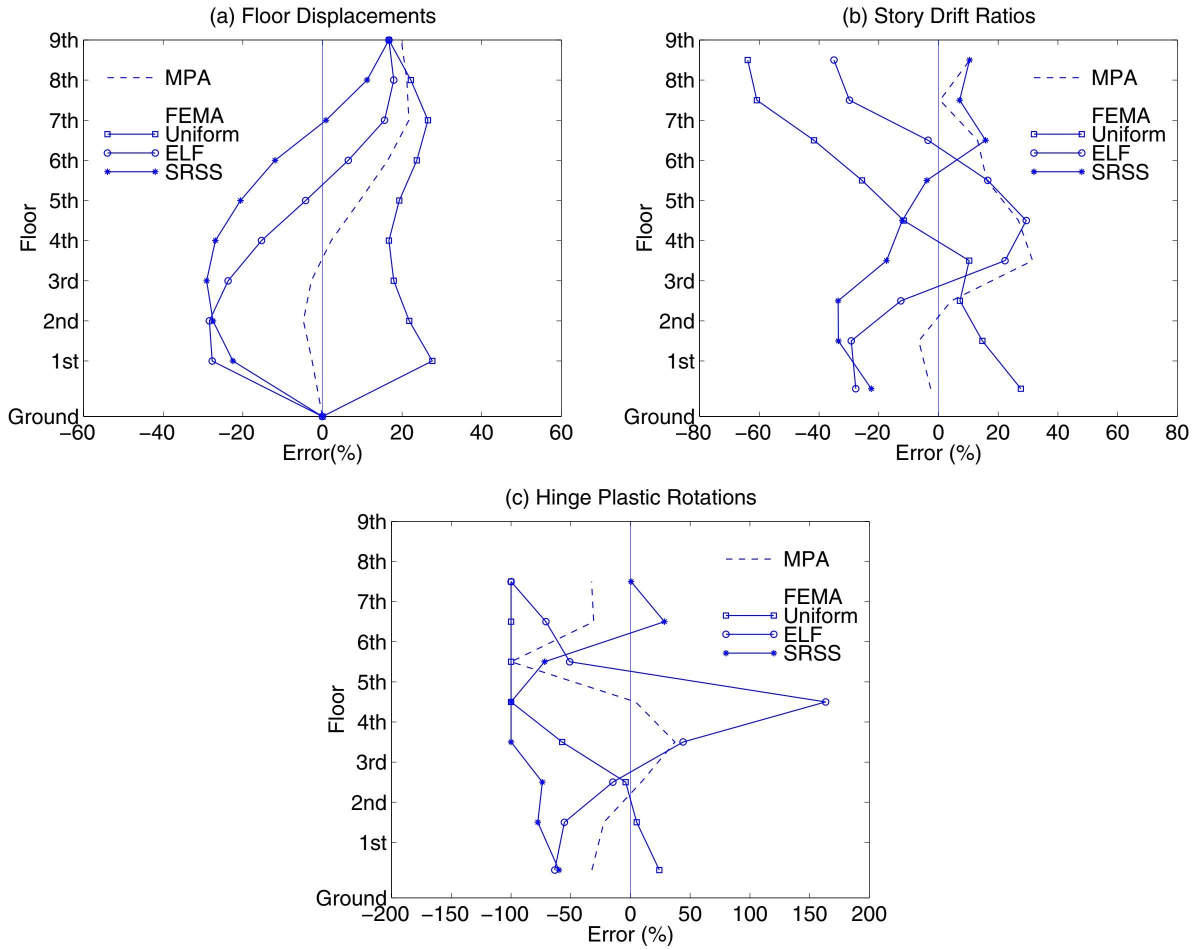

Fig. 5.4. Errors in floor displacements, story drifts, and hinge plastic rotations estimated using FEMA-273 force distributions and MPA (including three "modes"); gravity loads included

The structural engineering profession is now comparing these hinge plastic rotations against rotation limits established in FEMA-273 to judge structural component performance. Based on the results presented here, it appears that structural performance evaluation should be based on story drifts that are known to be closely related to damage and can be estimated to a higher degree of accuracy by pushover analyses. While pushover estimates for floor displacements are more accurate, they are not good indicators of damage.

The locations of plastic hinges shown in Fig. 5.5 were determined by five analyses: MPA considering the three "modes," nonlinear RHA ("exact"), and the three FEMA analyses. The locations of the plastic hinges are not identified correctly by the FEMA force distributions; the "uniform" distribution fails to identify yielding of the beams above the fourth floor; the SRSS distribution fails to identify yielding of beams in the middle floors; and the ELF distribution fails to identify yielding in some locations. The MPA procedure identifies yielding in most locations predicted by “exact” analysis, but fails to predict yielding in a few locations.

Figures 5.6 and 5.7 summarize the error in FEMA analyses relative to the “exact” demands as a function of ground motion intensity indicated by a ground motion multiplier. Shown is the error in each floor displacement and each story drift, and the error envelope for each case. Included for comparison is the error in MPA with three “modes.” The MPA procedure provides estimates of earthquake demands that are significantly more accurate than all FEMA-273 analyses, especially in estimating story drifts. The MPA procedure is superior to FEMA-273 analyses over the entire range of ground motion intensities considered.

Table 5.1. Peak values of floor displacements (as % of building height = 37.14 m) from FEMA force distributions and MPA; gravity loads included

Floor	Displacement /Height (%)					Error (%)			
	FEMA			MPA	NL-RHA	FEMA			MPA
	Uniform	ELF	SRSS			Uniform	ELF	SRSS	
1st	0.344	0.195	0.209	0.263	0.270	27.6	-27.7	-22.5	-2.6
2nd	0.597	0.351	0.355	0.466	0.490	21.8	-28.4	-27.5	-4.8
3rd	0.809	0.524	0.487	0.667	0.686	17.9	-23.7	-29.1	-2.8
4th	0.975	0.708	0.611	0.854	0.836	16.7	-15.3	-26.9	2.2
5th	1.089	0.875	0.724	0.998	0.913	19.3	-4.2	-20.6	9.4
6th	1.178	1.015	0.84	1.109	0.953	23.7	6.5	-11.9	16.4
7th	1.262	1.154	1.007	1.214	0.998	26.5	15.6	0.9	21.7
8th	1.341	1.294	1.221	1.330	1.098	22.2	17.9	11.2	21.2
9th	1.399	1.399	1.399	1.436	1.199	16.7	16.7	16.7	19.8

Table 5.2 Peak values of story drift ratios (as % of story height) from FEMA force distributions and MPA; gravity loads included

Story	Displacement /Height (%)					Error (%)			
	FEMA			MPA	NL-RHA	FEMA			MPA
	Uniform	ELF	SRSS			Uniform	ELF	SRSS	
1st	2.335	1.323	1.417	1.783	1.830	27.6	-27.7	-22.5	-2.6
2nd	2.367	1.462	1.372	1.927	2.064	14.7	-29.2	-33.5	-6.6
3rd	1.992	1.623	1.234	1.938	1.858	7.2	-12.6	-33.6	4.3
4th	1.560	1.730	1.168	1.860	1.414	10.3	22.3	-17.4	31.5
5th	1.067	1.562	1.061	1.530	1.207	-11.6	29.4	-12.1	26.8
6th	0.839	1.314	1.083	1.310	1.128	-25.6	16.5	-3.9	16.2
7th	0.789	1.306	1.566	1.530	1.353	-41.7	-3.5	15.8	13.1
8th	0.736	1.318	2.011	1.888	1.877	-60.8	-29.8	7.1	0.5
9th	0.547	0.984	1.672	1.673	1.515	-63.9	-35.0	10.4	10.5

Table 5.3 Peak values of hinge plastic rotations (radians) from FEMA force distributions and MPA

Floor	Hinge Plastic Rotation (rad)					Error (%)			
	FEMA			MPA	NL-RHA	FEMA			MPA
	Uniform	ELF	SRSS			Uniform	ELF	SRSS	
1st	1.53E-02	4.51E-03	4.94E-03	8.35E-03	1.23E-02	24.2	-63.4	-59.9	-32.3
2nd	1.10E-02	4.65E-03	2.34E-03	8.11E-03	1.04E-02	5.2	-55.3	-77.6	-22.2
3rd	7.93E-03	7.03E-03	2.16E-03	9.00E-03	8.26E-03	-4.0	-14.8	-73.8	9.0
4th	1.62E-03	5.45E-03	0.00E+00	5.19E-03	3.78E-03	-57.2	44.1	-100.0	37.2
5th	0.00E+00	3.09E-03	0.00E+00	1.23E-03	1.17E-03	-100.0	163.4	-100.0	4.3
6th	0.00E+00	4.52E-04	2.58E-04	3.35E-10	9.19E-04	-100.0	-50.9	-71.9	-100.0
7th	0.00E+00	1.50E-03	6.59E-03	3.55E-03	5.13E-03	-100.0	-70.8	28.4	-30.8
8th	0.00E+00	0.00E+00	5.78E-03	3.88E-03	5.75E-03	-100.0	-100.0	0.5	-32.5
9th	0.00E+00	0.00E+00	0.00E+00	1.00E-10	0.00E+00				

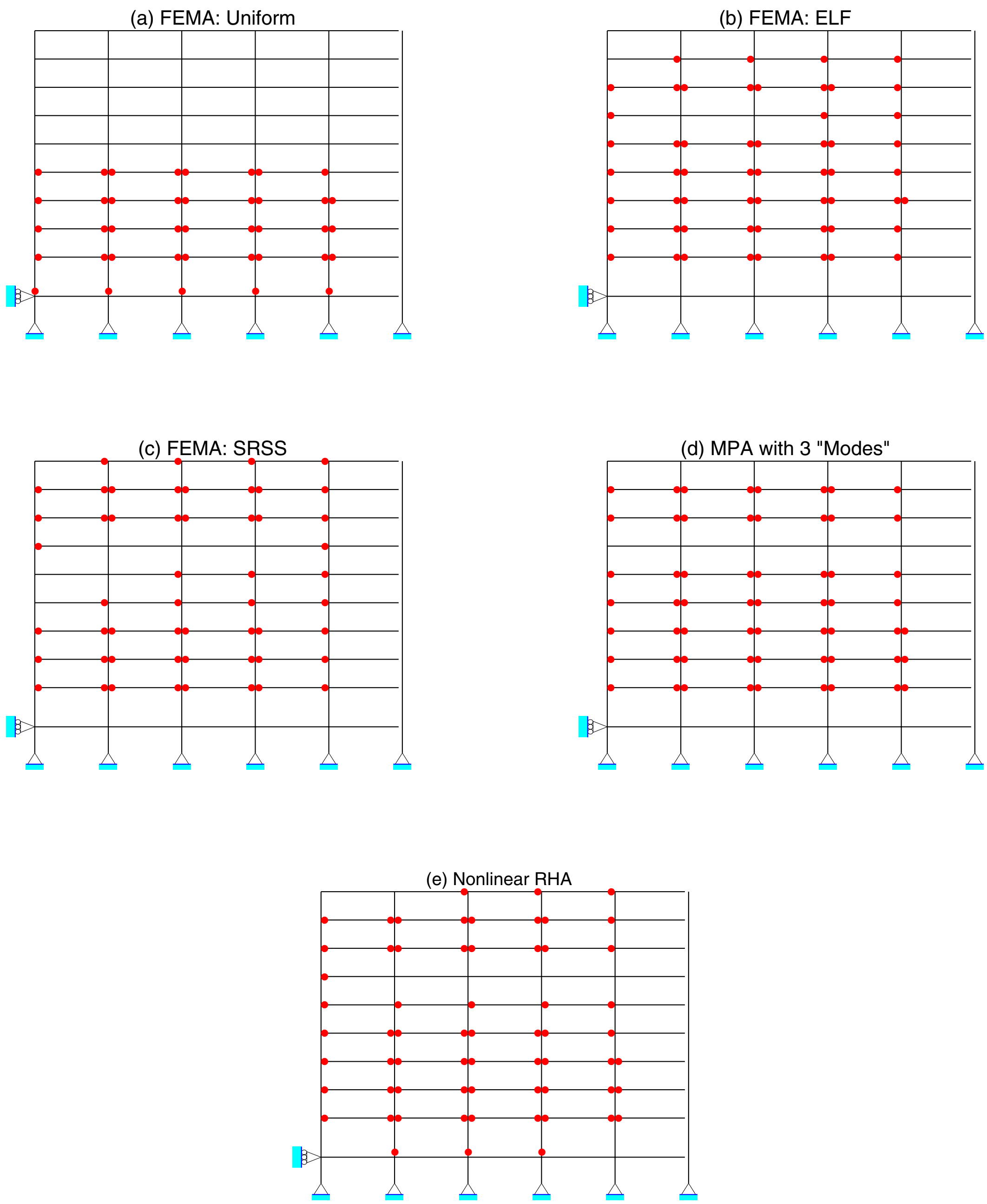

Fig. 5.5. Locations of plastic hinges determined from three force distributions in FEMA-273, MPA including three "modes" and NL-RHA for 1.5 × El Centro ground motion; gravity loads included

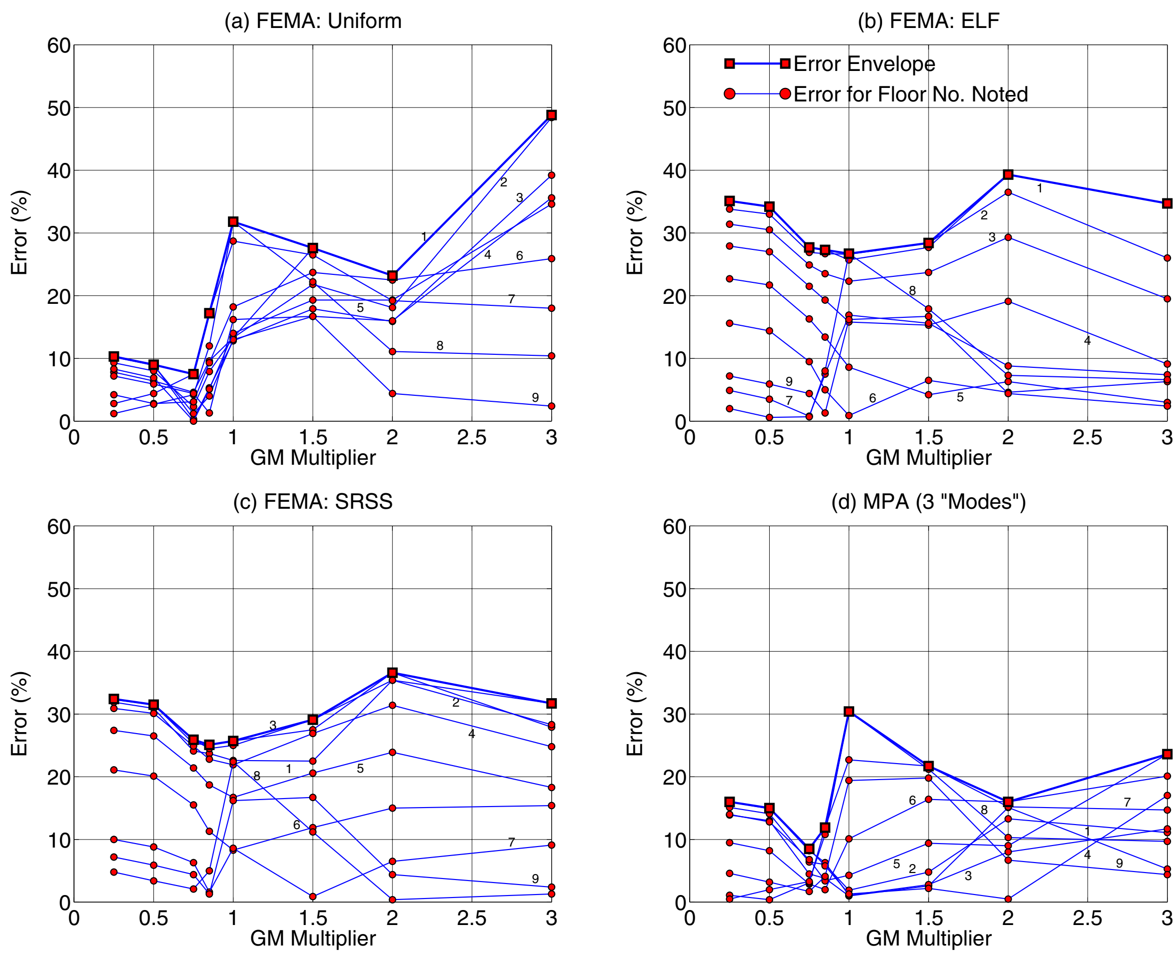

Fig. 5.6. Errors in floor displacements from three force distributions in FEMA-273 and from MPA including three “modes”; gravity loads included

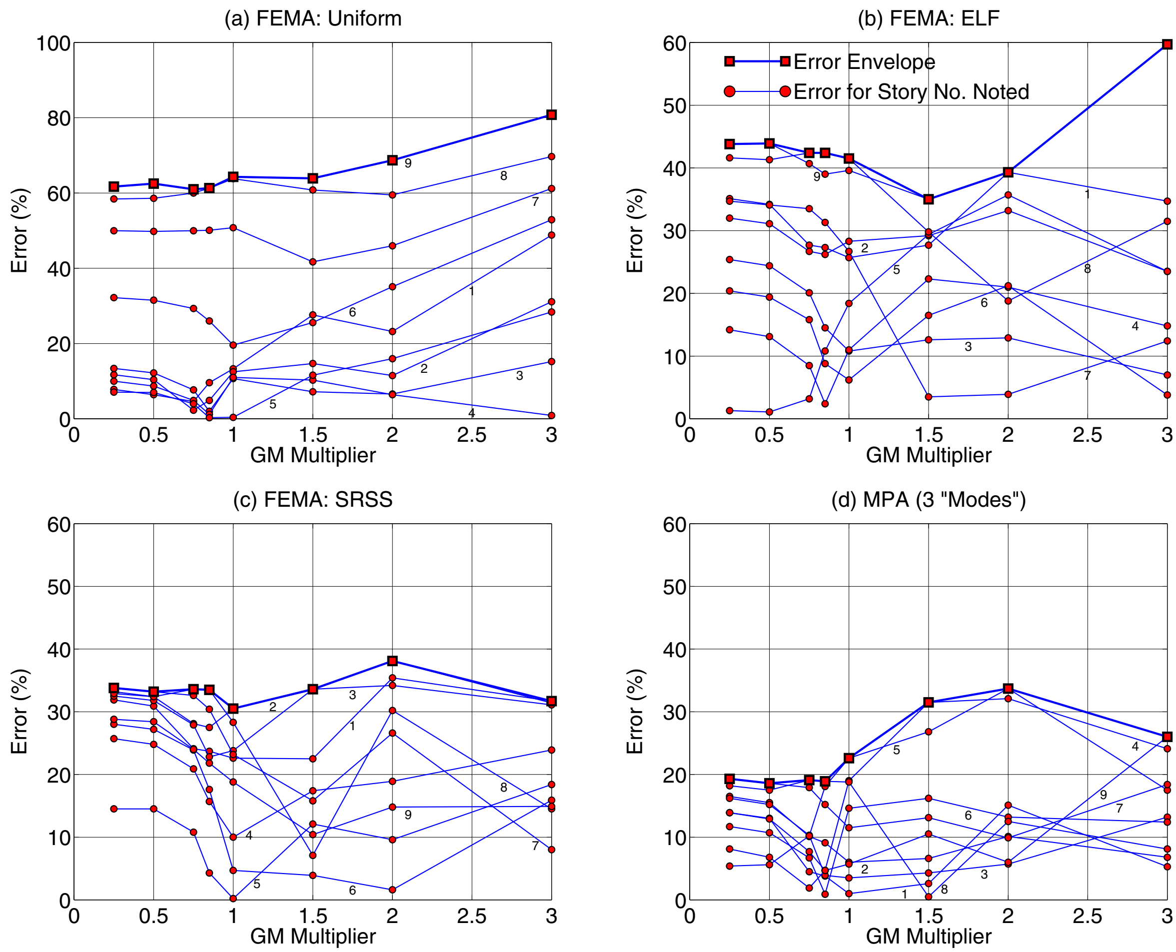

Fig. 5.7. Error in story drifts from three force distributions in FEMA-273 and from MPA including three "modes"; gravity loads included

6 Conclusions

This investigation was aimed toward developing an improved pushover analysis procedure based on structural dynamics theory, which retains the conceptual simplicity and computational attractiveness of the procedure with invariant force distribution, now common in structural engineering practice. It has led to the following conclusions:

1. Pushover analysis of a one-story inelastic system predicts perfectly peak seismic demands: deformation, joint rotations, hinge plastic rotation, etc. However, pushover analysis is inherently limited in the sense that it cannot provide any cumulative measure of response; e.g., the energy dissipated in yielding or the cumulative rotation of a plastic hinge.

2. The peak response of an elastic multistory building due to its *n*th vibration mode can be exactly determined by static analysis of the structure subjected to lateral forces distributed over the building height according to $\mathbf{s}_n^* = \mathbf{m}\boldsymbol{\phi}_n$, where $\mathbf{m}$ is the mass matrix of the building and $\boldsymbol{\phi}_n$ its *n*th mode, and the structure is pushed to the roof displacement determined from the peak deformation D_n of the *n*th-mode elastic SDF system. This system has vibration properties—natural frequency ω_n and damping ratio, ζ_n—of the *n*th-mode of the MDF system. For this system, D_n is available from the elastic response (or design) spectrum. Combining these peak modal responses by an appropriate modal combination rule (e.g., SRSS) leads to the modal pushover analysis (MPA) procedure.

3. This MPA procedure for elastic buildings is shown to be equivalent to the standard response spectrum analysis (RSA) procedure, where the nature and magnitude of errors arising from approximate modal combination rules are well understood.

4. To enable systematic extension of the MPA procedure to inelastic systems, an uncoupled modal response history analysis (UMRHA) is developed by (1) neglecting the coupling among modal coordinates arising from yielding of the system; and (2) superposing responses of the inelastic MDF system to individual terms, $\mathbf{p}_{\text{eff},n}(t) = -\mathbf{s}_n \ddot{u}_g(t)$—$n$ denotes mode number—in the modal expansion of the effective earthquake forces, $\mathbf{p}_{\text{eff}}(t) = -\mathbf{m}\,\boldsymbol{\iota}\,\ddot{u}_g(t)$. These underlying assumptions and approximations are evaluated and the errors in the UMRHA procedure relative to the "exact" nonlinear response history analysis are documented.

5. The MPA procedure developed to estimate the seismic demands for inelastic buildings consists of two phases:

   (i) the peak response r_{no} of the inelastic MDF system to effective earthquake forces $\mathbf{p}_{\text{eff},n}(t)$ is determined by pushover analysis; and

   (ii) the total response r_o is determined by combining the r_{no} $(n = 1, 2, \ldots)$ according to an appropriate combination rule (e.g., the SRSS rule).

6. The response value r_{no} is determined by implementing the following steps:

   (i) Develop the base-shear—roof-displacement $(V_{bn} - u_{rn})$ curve from a pushover analysis of the structure for the force distribution $\mathbf{s}_n^* = \mathbf{m}\boldsymbol{\phi}_n$, where $\boldsymbol{\phi}_n$ is now the nth natural mode for small-amplitude linear vibration.

   (ii) Idealize the pushover curve as a bilinear curve and convert it to the bilinear force-deformation relation for the nth-"mode" inelastic SDF system, with vibration properties in the linear range same as those of the nth-mode elastic SDF system.

   (iii) Compute the peak deformation D_n of this system with unit mass by nonlinear response history analysis or from the inelastic response (or design) spectrum.

(iv) At the roof displacement determined from D_n, the pushover analysis provides the peak value r_{no} of any response quantity: floor displacements, story drifts, joint rotations, plastic hinge rotations, etc.

7. Comparing the peak inelastic response of a 9-story SAC building determined by the approximate MPA procedure—including only the first two or three r_{no} terms—with rigorous nonlinear RHA demonstrates that the approximate procedure while providing good estimates of floor displacements and story drifts, and identifying locations of most plastic hinges, it fails to compute with acceptable accuracy plastic rotations of the hinges. Pushover analyses seem to be inherently limited in computing accurately hinge plastic rotations.

8. Based on results presented for El Centro ground motion scaled by factors varying from 0.25 to 3.0, the errors in the MPA procedure are shown to be only weakly dependent on ground motion intensity. This implies that MPA is able to estimate the response of buildings responding well into the inelastic range to a similar degree of accuracy when compared to standard RSA for estimating the peak response of elastic systems. Thus the MPA procedure is accurate enough for practical application in building evaluation and design.

9. The initial state—forces and deformations—of the structure can be considered in the MPA procedure by including these gravity load effects in pushover analysis of the structure only for the first "mode."

10. Comparing the earthquake-induced demands for the selected 9-story building determined by pushover analysis using three force distributions in FEMA-273, MPA, and nonlinear RHA, demonstrates that the FEMA force distributions greatly underestimate the story drift demands, and lead to unacceptably large errors in the hinge plastic rotations. The MPA procedure is more accurate than all the FEMA force distributions in estimating floor displacements, story drifts, and hinge plastic rotations. However, all pushover analysis procedures do not seem to compute with acceptable accuracy local response quantities, such as hinge plastic rotations.

11. The present trend in the structural engineering profession of comparing computed hinge plastic rotations against rotation limits established in FEMA-273 to judge structural performance does not seem prudent. Instead, structural performance evaluation should be based on story drifts that are known to be closely related to damage and can be estimated to a higher degree of accuracy by pushover analyses. While pushover estimates for floor displacements are even more accurate, they are not good indicators of damage.

This report has focused on development of the MPA procedure and its initial evaluation in estimating the seismic demands on a building imposed by a selected ground motion, with the excitation scaled to cover a wide range of ground motion intensities and building response. This new method for estimating seismic demands at low performance levels, such as life safety and collapse prevention, should obviously be evaluated for a wide range of buildings and ground motion ensembles.

7 References

Allahabadi, R. and Powell, G. H. (1988). DRAIN-2DX user guide, *Report No. UCB/EERC-88/06*, Earthq. Engrg. Res. Cen., Univ. of Calif., Berkeley, Calif.

Bracci, J. M., Kunnath, S. K. and Reinhorn, A. M. (1997). Seismic performance and retrofit evaluation for reinforced concrete structures, *J. Struc. Engrg*., ASCE 123(1):3-10.

Building Seismic Safety Council (1997). *NEHRP Guidelines for the Seismic Rehabilitation of Buildings*, *FEMA-273*, Federal Emergency Management Agency, Washington, D.C.

Chopra, A.K. (2001). *Dynamics of Structures: Theory and Applications to Earthquake Engineering*, Prentice Hall: New Jersey.

Fajfar, P. and Fischinger, M. (1988). N2—a method for nonlinear seismic analysis of regular structures, *Proc*., 9th World Conf. Earthq. Engrg., 5:111-116, Tokyo-Kyoto, Japan..

Gupta, A. and Krawinkler, H. (1999). Seismic demands for performance evaluation of steel moment resisting frame structures (SAC Task 5.4.3), *Report No. 132*, John A. Blume Earthquake Engineering Center, Stanford University, Stanford, Calif.

Gupta, A. and Krawinkler, H. (2000). Estimation of seismic drift demands for frame structures, *Earthq. Engrg. Struc. Dyn*., 29:1287-1305.

Gupta, B. and Kunnath, S. K. (2000). Adaptive spectra-based pushover procedure for seismic evaluation of structures, *Earthq. Spectra*, 16(2):367-392

Han, S. W. and Wen, Y. K. (1997). Method of reliability-based seismic design. I: Equivalent nonlinear system, ASCE, *J. Struc. Engrg*., 123:256-265.

Kim, S. and D'Amore, E. (1999). Pushover analysis procedure in earthquake engineering, *Earthq. Spectra*, 15:417-434.

Krawinkler, H. and Gupta, A. (1998). Story drift demands for steel moment frame structures in different seismic regions, *Proc*., 6th U.S. Nat. Conf. on Earthq. Engrg., Seattle, Washington.

Krawinkler, H. and Seneviratna, G. D. P. K. (1998). Pros and cons of a pushover analysis of seismic performance evaluation, *J. Engrg. Struc.*, 20(4-6):452-464.

Kunnath, S. K. and Gupta, B. (2000). Validity of deformation demand estimates using nonlinear static procedures. In: *Proc.*, U.S. Japan Workshop on Performance-Based Engineering for Reinforced Concrete Building Structures, Sapporo, Hokkaido, Japan.

Lawson, R. S., Vance, V. and Krawinkler, H. (1994). Nonlinear static pushover analysis—why, when and how?. In: *Proc.,* 5th U.S. Conf. Earthq. Engrg. 1:283-292.

Maison, B. and Bonowitz, D. (1999). How safe are pre-Northridge WSMFs? A case study of the SAC Los Angeles Nine-Story Building, *Earthq. Spectra*, 15(4):765-789.

Matsumori, T., Otani, S., Shiohara, H. and Kabeyasawa, T. (1999). Earthquake member deformation demands in reinforced concrete frame structures. In: *Proc.*, U.S.-Japan Workshop on Performance-Based Earthq. Engrg. Methodology for R/C Bldg. Structures, pp. 79-94, Maui, Hawaii

Miranda, E. (1991). Seismic evaluation and upgrading of existing buildings, Ph. D. Dissertation, Dept. of Civil Engrg., Univ. of Calif., Berkeley, Calif.

Naiem, F. and Lobo, R. M. (1998). Common pitfalls in pushover analysis, *Proc.*, SEAOC 1998 Convention, Structural Engineers of California.

Ohtori, Y., Christenson, R. E., Spencer, B. F., Jr., and Dyke, S. J. (2000). Benchmark Control Problems for Seismically Excited Nonlinear Buildings, http://www.nd.edu/~quake/, Notre Dame University, Indiana.

Paret, T. F., Sasaki, K. K., Eilbekc, D. H. and Freeman, S. A. (1996). Approximate inelastic procedures to identify failure mechanisms from higher mode effects. In: *Proc.*, 11th World Conf. Earthq. Engrg., Paper No. 966, Acapulco, Mexico.

Saiidi, M. and Sozen, M. A. (1981). Simple nonlinear seismic analysis of R/C structures, *J. Struc. Div.*, ASCE, 107(ST5):937-951.

Sasaki, K. K., Freeman, S. A. and Paret, T. F. (1998). Multimode pushover procedure (MMP)—A method to identify the effects of higher modes in a pushover analysis. In: *Proc.*, 6th U.S. Nat. Conf. on Earthq. Engrg., Seattle, Washington.

Skokan, M. J. and Hart, G. C. (2000). Reliability of nonlinear static methods for the seismic performance prediction of steel frame buildings. In: *Proc.*, 12th World Conf. Earthq. Engrg., Paper No. 1972, Auckland, New Zealand.

Villaverde, R. (1996). Simplified response spectrum seismic analysis of nonlinear structures, *J. Engrg. Mech.,* ASCE*,* 122:282-285.

Appendix A Uncoupled Modal Response History Analysis

A.1 STEP-BY-STEP PROCEDURE

A detailed step-by-step implementation of the uncoupled modal response history analysis (UMRHA) procedure is presented in this section and illustrated by an example in the next section.

1. Compute natural frequencies, ω_n, and modes, ϕ_n, for linear-elastic vibration of the building.

2. For the *n*th-"mode," develop the base-shear–roof-displacement ($V_{bn} - u_{rn}$) pushover curve for the force distribution $\mathbf{s}_n^*$:

   2.1. Define the force distribution $\mathbf{s}_n^*$ from Eq. (3.20): $\mathbf{s}_n^* = \mathbf{m}\phi_n$

   2.2. Apply force distribution of Step 2.1 incrementally and record the base shears and associated roof displacements. The structure should be pushed just beyond the target (or expected) roof displacement in the selected mode. Since the target roof displacement may not be known at the start of the procedure, iterations may be necessary. This step can be conveniently implemented in any commercially available software, e.g., DRAIN-2DX [Allahabadi and Powell, 1988].

3. Idealize the pushover curve as a bilinear curve (Fig. A.1) using the FEMA-273 procedure (Building Seismic Safety Council, 1977).

   3.1. Define the anchor point, *B*, of the bilinear curve at the target roof displacement. Let the roof displacement and base shear at the anchor point be u_{rno} and V_{bno}, respectively.

   3.2. Calculate the area under the actual pushover curve, A_{pn}, using any numerical integration method, e.g., trapezoidal rule.

3.3. Estimate the yield base shear, V_{bny}^{i}. This value, obtained by judgment, will be refined by an iterative procedure that seeks to equate areas under the actual and the idealized pushover curves.

3.4. Calculate initial slope of the idealized bilinear curve, k_n^i, by connecting a straight line between origin, *O*, and a point on the actual pushover curve with base shear equal to $0.6 \times V_{bny}^{i}$. This step gives the secant stiffness at a base shear equal to 60% of the yield base shear.

3.4.1. From the pushover data, determine the roof displacement, $u_{rn,0.6}^{i}$, at base shear equal to $0.6 \times V_{bny}^{i}$.

3.4.2. Calculate the slope, $k_n^i = \left(0.6 \times V_{bny}^{i}\right) \big/ u_{rn,0.6}^{i}$.

3.5. Calculate the yield displacement, $u_{rny}^{i} = V_{bny}^{i} \big/ k_n^i$, corresponding to the estimated yield base shear, V_{bny}^{i}. Let the point with base shear = V_{bny}^{i} and roof displacement = u_{rny}^{i} be denoted as *A*.

3.6. Draw the curve *OAB* by connecting the three points *O*, *A*, and *B* with straight-line segments to obtain the idealized bilinear curve.

3.7. Calculate the post-yielding strain-hardening ratio,

$$\alpha_n^i = \left[\left(V_{bno} / V_{bny}^{i}\right) - 1\right] \Big/ \left[\left(u_{rno} / u_{rny}^{i}\right) - 1\right]$$

3.8. Calculate area under the bilinear curve *OAB*, A_{bn}^{i}.

3.9. Calculate the error = $100 \times \left(A_{bn}^{i} - A_{pn}\right) \big/ A_{pn}$. If the error exceeds some pre-specified tolerance, iterations are necessary.

3.9.1. Calculate $V_{bny}^{i+1} = V_{bny}^{i} \times \left(A_{pn} \big/ A_{bn}^{i}\right)$. If desired, other appropriate methods can be used.

3.9.2. Replace $i+1$ with i and repeat Steps 3.4 to 3.8.

4. Develop the $F_{sn}/L_n - D_n$ relation (Fig. A.2).

   4.1. Compute the L_n and Γ_n from Eq. (3.4) and effective modal mass from $M_n^* = L_n \Gamma_n$.

   4.2. Scale the horizontal axis by $\Gamma_n \phi_{rn}$ to obtain $D_{no} = u_{rno}/\Gamma_n \phi_{rn}$ and $D_{ny} = u_{rny}/\Gamma_n \phi_{rn}$ (Eqs. 4.10b and 4.11b).

   4.3. Scale the vertical axis with M_n^* to obtain $F_{sno}/L_n = V_{bno}/M_n^*$ and $F_{sny}/L_n = V_{bny}/M_n^*$ [Eqs. (4.10a) and (4.11a)].

5. Compute deformation history, $D_n(t)$, and pseudo-acceleration history, $A_n(t)$, of the nth-"mode" inelastic SDF system (Fig. 4.3b) with unit-mass and force-deformation relation of Fig. A.2.

6. Calculate histories of various responses using Eqs. (3.12) and (3.13).

7. Repeat Steps 3 to 6 for as many modes as required for sufficient accuracy. In general first two or three modes will suffice.

8. Combine the "modal" responses using Eqs. (3.15) and (3.16).

9. Calculate peak values, r_o, of the combined responses obtained in Step 8.

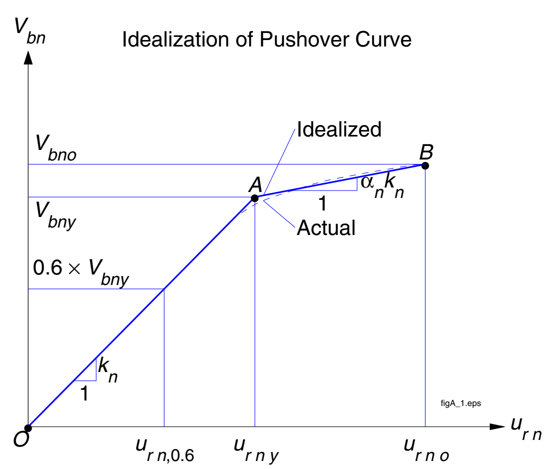

Fig. A.1. Idealization of *n*th-"mode" pushover curve

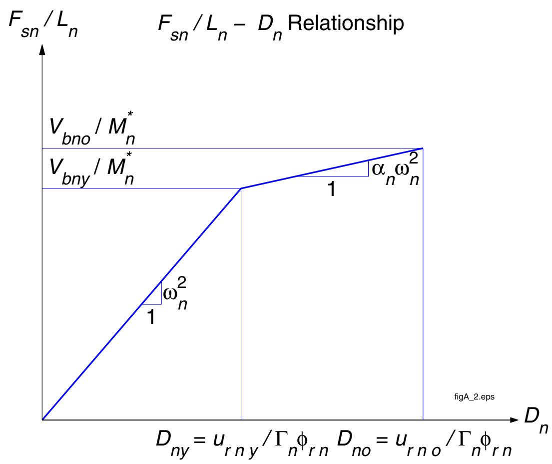

Fig. A.2. Properties of the *n*th-"mode" inelastic SDF system

A.2 EXAMPLE

The UMRHA procedure is implemented to calculate the response of the 9-story building described in Section 3.4. to the north-south component of the El Centro (1940) ground motion scaled up by a factor of 1.5. Following is step-by-step implementation of the procedure described in Section A.1.

1. First three mode shapes and frequencies of the selected building were computed and are shown in Fig. 3.3.

2. The base-shear – roof-displacement ($V_{bn} - u_{rn}$) pushover curve for the force distribution $\mathbf{s}_n^*$:

   2.1. The force distributions, $\mathbf{s}_n^*$, computed for the first three modes are shown in Fig. 3.4.

   2.2. The pushover curves for the first three modes, generated using DRAIN-2DX, are shown in Fig. A.3. Target displacements used to generate these pushover curves are 63.5 cm (25 in.), 25.4 cm (10 in.), and 12.7 cm (5 in.), for the first, second, and third mode, respectively.

3. Idealized bilinear curves for each of the three modes are included in Fig. A.3. The following steps illustrate the procedure to develop the idealize curve for the first "mode".

   3.1. The anchor point, B, is defined at the target roof displacement. At this point, $u_{r1o} = 63.5\text{ cm}$ and $V_{b1o} = 8729.6\text{ kN}$.

3.2. Area under the actual pushover curve, $A_{p1} = 360,777$ kN-cm.

3.3. The first estimate of the yield base shear $V_{b1y}^{i} = 8006.4$ kN.

3.4. The initial slope of the idealized bilinear curve, k_1^i, is calculated as follows.

3.4.1. Determined from the pushover database, $u_{r1,0.6}^{i} = 22.86$ cm at $0.6 \times V_{b1y}^{i} = 4803.8$ kN.

3.4.2. $k_1^i = \left(0.6 \times V_{b1y}^{i}\right) \Big/ u_{r1,0.6}^{i} = 4803.8/22.86 = 210.18$ kN/cm.

3.5. The yield displacement, $u_{r1y}^{i} = V_{b1y}^{i} \Big/ k_1^i = 8006.4/210.18 = 38.09$ cm. The point *A* on the bilinear curve is defined by $u_{r1y}^{i} = 38.09$ cm and $V_{b1y}^{i} = 8006.4$ kN.

3.6. The curve *OAB* obtained by connecting the three points *O*, *A*, and *B* with straight-line segments gives the idealized bilinear curve.

3.7. The post-yielding strain-hardening ratio, $\alpha_1^i = \left[\left(V_{b1o} \big/ V_{b1y}^{i}\right) - 1\right] \Big/ \left[\left(u_{r1o} \big/ u_{r1y}^{i}\right) - 1\right]$ = $\left[(8729.6/8006.4) - 1\right] / \left[(63.5/38.09) - 1\right] = 0.135$.

3.8. Area under the bilinear curve *OAB*, $A_{b1}^{i} = 365100$ kN-cm.

3.9. Error = $100 \times (365100 - 360777)/360777 = 1.198\%$. This value exceeds the pre-specified tolerance of 0.01%. Therefore, iterations are necessary.

3.9.1. The next estimate of the yield shear is $V_{bny}^{i+1} = 8006.4 \times (360777/365100)$ = 7911.6 kN.

3.9.2. The results of the iterative procedure are summarized in Table A.1. The procedure converged after nineteen cycles to give $u_{r1y} = 36.23$ cm, $V_{b1y} = 7615.9$ kN, and $\alpha_1 = 0.194$.

4. The $F_{s1}/L_1 - D_1$ relation for the first "mode" is developed as follows. The results for other modes are summarized in Table A.2. Also included are the modal damping ratios and the periods calculated from Eq. (4.13).

   4.1. $L_1 = 2,736,789$ kg, $\Gamma_1 = 1.3666$, and $M_1^* = 27\,36789 \times 1.3666 = 3,740,189$ kg.

   4.2. Scaling the horizontal axis by $\Gamma_1 \phi_{r1}$ gives $D_{1o} = 46.46$ cm and $D_{1y} = 26.51$ cm.

5. Scaling the vertical axis by M_1^* gives $F_{s1o}/L_1 = 233.40 \left(\text{cm}/\text{sec}^2\right)$ and

   $F_{s1y}/L_1 = 203.62 \left(\text{cm}/\text{sec}^2\right)$.

6. Deformation and pseudo-acceleration histories of the inelastic SDF systems for the first "mode" with unit mass and force-deformation relation developed in Step 4 are plotted in Fig. A.4.

7. Histories of roof displacement and top story drifts for the first "mode" are computed and presented in Fig. 4.7.

8. The results were generated for first three "modes' and are included in Fig. 4.7.

9. The combined modal responses are presented in Fig. 4.7.

10. The peak values are computed and are summarized in Tables 4.1 and 4.2. The peak values are also plotted in Fig. 4.8.

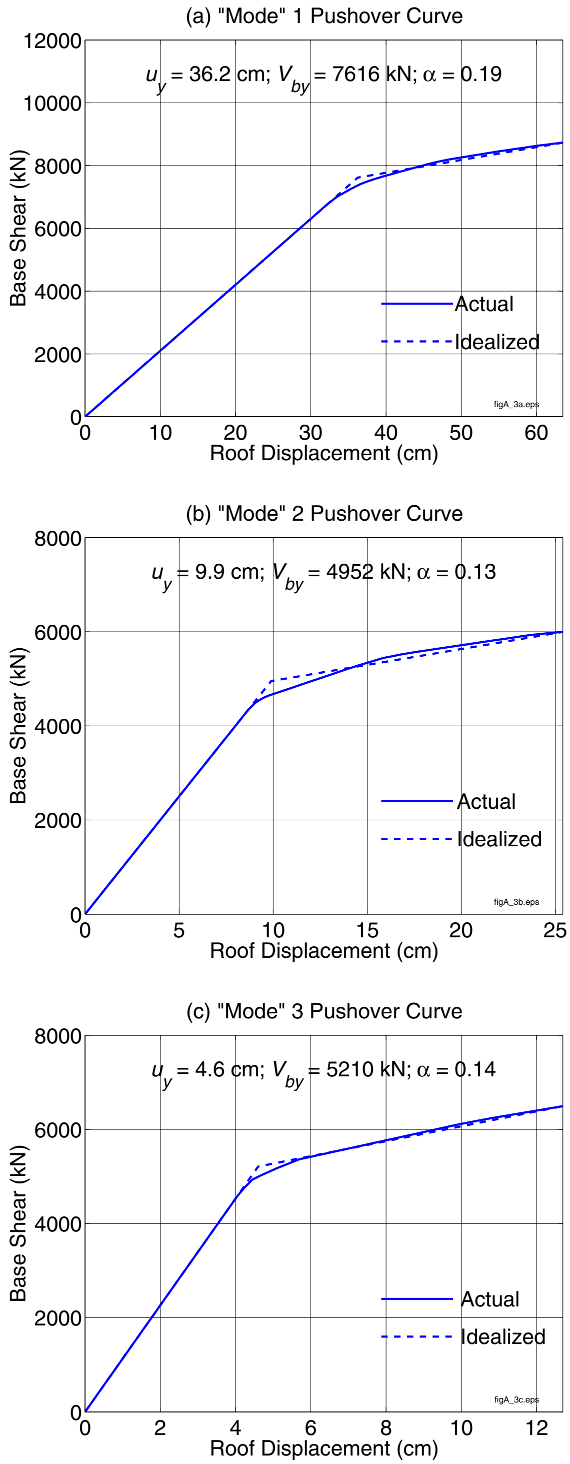

Fig. A.3. "Modal" pushover curves for the example building

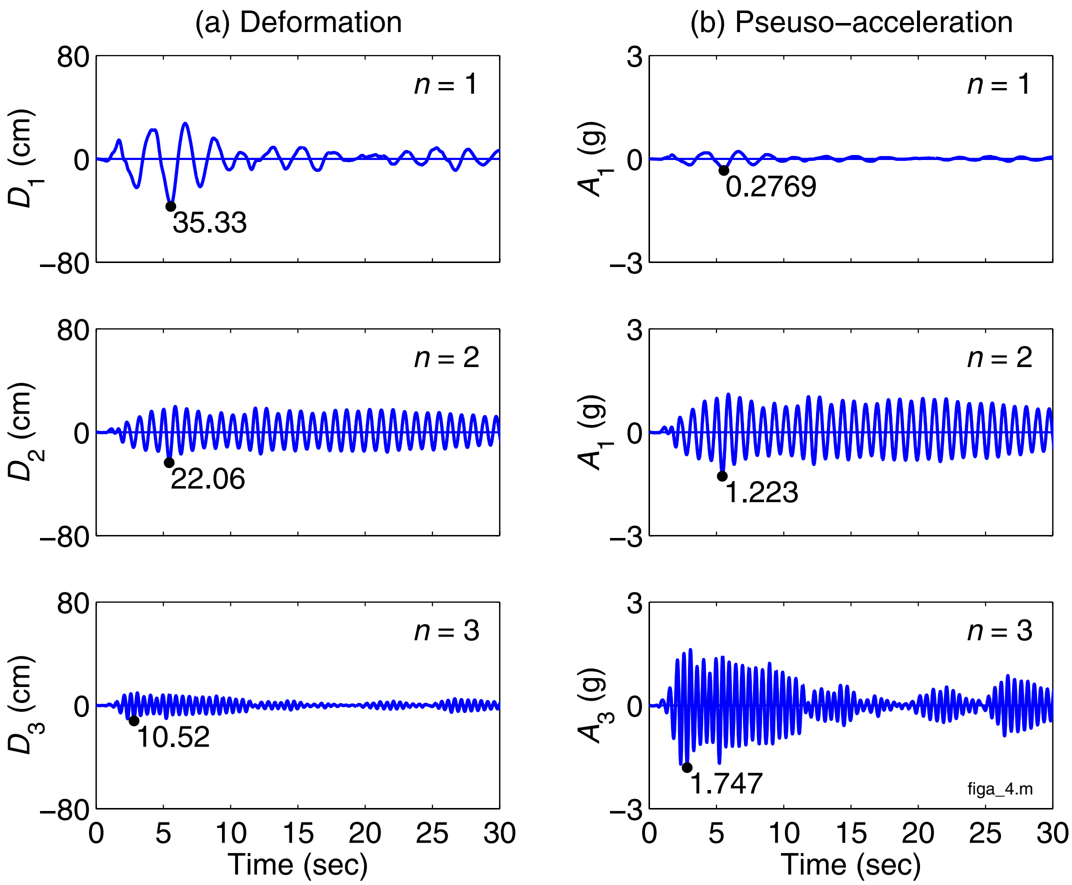

Fig. A.4. **Histories of deformation and pseudo-acceleration due to 1.5 × El Centro ground motion for the first "mode," second "mode," and third "mode" inelastic SDF systems.**

Table A.1. Results of iterative procedure to develop the idealized bilinear curve for the first "mode" inelastic SDF system

Itr. No. i	V_{b1y}^i (kN)	$0.6 \times V_{b1y}^i$ (kN)	$u_{r1,0.6}^i$ (cm)	k_1^i (kN/cm)	u_{r1y}^i (cm)	α_1^i	A_{b1}^i (kN-cm)	Error (%)
1	8006.4	4803.8	22.86	210.18	38.09	0.135	365100	1.198
2	7911.6	4747.0	22.59	210.18	37.64	0.151	364060	0.910
3	7840.3	4704.2	22.38	210.18	37.30	0.162	363276	0.693
4	7786.3	4671.8	22.23	210.18	37.05	0.170	362684	0.529
5	7745.4	4647.2	22.11	210.18	36.85	0.176	362235	0.404
6	7714.2	4628.5	22.02	210.18	36.70	0.180	361892	0.309
7	7690.4	4614.3	21.95	210.18	36.59	0.184	361631	0.237
8	7672.3	4603.4	21.90	210.18	36.50	0.186	361432	0.182
9	7658.4	4595.0	21.86	210.18	36.44	0.188	361279	0.139
10	7647.7	4588.6	21.83	210.18	36.39	0.190	361162	0.107
11	7639.5	4583.7	21.81	210.18	36.35	0.191	361073	0.082
12	7633.3	4580.0	21.79	210.18	36.32	0.192	361004	0.063
13	7628.5	4577.1	21.78	210.18	36.29	0.193	360951	0.048
14	7624.8	4574.9	21.77	210.18	36.28	0.193	360911	0.037
15	7622.0	4573.2	21.76	210.18	36.26	0.193	360880	0.029
16	7619.8	4571.9	21.75	210.18	36.25	0.194	360856	0.022
17	7618.1	4570.9	21.75	210.18	36.25	0.194	360838	0.017
18	7616.9	4570.1	21.74	210.18	36.24	0.194	360824	0.013
19	7615.9	4569.5	21.74	210.18	36.23	0.194	360813	0.010

Table A.2. Properties of "modal" inelastic SDF systems

Properties	"Mode" 1	"Mode" 2	"Mode" 3
L_n (kg)	2736789	-920860	696400
Γ_n	1.3666	-0.5309	0.2406
M_n^* (kg)	3740189	488839.1	167531.5
F_{sny}/L_n (cm/sec^2)	203.62	1013.09	3109.56
D_{ny} (cm)	26.51	18.65	19.12
F_{sno}/L_n (cm/sec^2)	233.40	1226.56	3876.05
D_{no} (cm)	46.46	47.85	52.79
T_n (sec)	2.2671	0.8525	0.4927
ζ_n (%)	1.948	1.103	1.136

Appendix B Modal Pushover Analysis

B.1 STEP-BY-STEP PROCEDURE

A detailed step-by-step implementation of the modal pushover analysis (MPA) procedure is presented in this section and illustrated by an example in the next section. Steps 1 to 4 of the MPA are the same as those for UMRHA presented in Appendix A.

5. Compute the peak deformation, D_n, of the nth-"mode" inelastic SDF system (Fig. 4.3b) with unit mass and force-deformation relation of Fig. 4.6b by solving Eq. (4.8), or from the inelastic response (or design) spectrum.
6. Calculate the peak roof displacement u_{rno} associated with the *n*th-"mode" inelastic SDF system from Eq. (3.21).
7. At u_{rno}, extract from the pushover database values of other desired responses, r_{no}.
8. Repeat Steps 3 to 7 for as many "modes" as required for sufficient accuracy. Typically, the first two or three "modes" will suffice.
9. Determine the total response by combining the peak "modal" responses using the SRSS combination rule of Eq. (3.18). From the total hinge rotation, subtract the yield hinge rotation to determine the plastic hinge rotation.

B.2 EXAMPLE

The MPA procedure is implemented to calculate the response of the 9-story building described in Section 3.4.1 to the north-south component of the El Centro (1940) ground motion scaled up by a factor of 1.5. This is the same example as solved in Appendix A. Following is step-by-step implementation of the procedure described in Section B.1.

5. Solving Eq. (4.8) for the peak deformation of the first-"mode" inelastic SDF system with unit mass and force-deformation relation developed in Step 4 gives $D_1 = 35.33\ \text{cm}$.

6. Peak roof displacement $u_{r1o} = \Gamma_1 \times \phi_{r1} \times D_1 = 1.366 \times 1 \times 35.33 = 48.28$ cm.

7. At $u_{r1o} =$ 48.28 cm, values of floor displacements and story drifts are extracted. The values are summarized in Table 4.3 for the floor displacements normalized by the building.

8. Steps 3 to 7 are repeated for first three "modes," and the results are included in Tables 4.3 and 4.4. Results of Steps 5 and 6 are summarized in Table B.1, where results for other ground motion intensities are also included.

9. The total response computed by combining the peak "modal" responses using the SRSS combination rule of Eq. (3.18) are also included in Tables 4.3 and 4.4. Also included in Table 4.5 are the plastic hinge rotations computed by subtracting the yield hinge rotation from the total hinge rotations.

Table B.1. Calculation of roof displacements u_{rno} from peak deformation of inelastic SDF systems

Ground Motion Multiplier	Quantity	"Mode" 1	"Mode" 2	"Mode" 3
0.25	D_n (cm)	6.678	4.200	1.755
	$\mu = D_n/D_{ny}$	0.252	0.225	0.691
	$u_{rno} = \Gamma_n \phi_{rn} D_n$ (cm)	9.126	2.229	0.4222
0.5	D_n (cm)	13.35	8.395	3.513
	$\mu = D_n/D_{ny}$	0.504	0.450	0.184
	$u_{rno} = \Gamma_n \phi_{rn} D_n$ (cm)	18.25	4.457	0.8451
0.75	D_n (cm)	20.03	12.59	5.268
	$\mu = D_n/D_{ny}$	0.755	0.676	0.275
	$u_{rno} = \Gamma_n \phi_{rn} D_n$ (cm)	27.38	6.660	1.267
0.85	D_n (cm)	22.70	14.27	5.969
	$\mu = D_n/D_{ny}$	0.856	0.766	0.312
	$u_{rno} = \Gamma_n \phi_{rn} D_n$ (cm)	31.03	7.577	1.436
1.0	D_n (cm)	26.71	16.79	7.023
	$\mu = D_n/D_{ny}$	1.007	0.901	0.367
	$u_{rno} = \Gamma_n \phi_{rn} D_n$ (cm)	36.50	8.913	1.690
1.5	D_n (cm)	35.33	22.06	10.52
	$\mu = D_n/D_{ny}$	1.332	1.185	0.551
	$u_{rno} = \Gamma_n \phi_{rn} D_n$ (cm)	48.28	11.73	2.535
2.0	D_n (cm)	46.37	24.82	14.05
	$\mu = D_n/D_{ny}$	1.748	1.332	0.735
	$u_{rno} = \Gamma_n \phi_{rn} D_n$ (cm)	63.37	13.18	3.379
3.0	D_n (cm)	57.13	27.35	21.36
	$\mu = D_n/D_{ny}$	2.154	1.467	1.117
	$u_{rno} = \Gamma_n \phi_{rn} D_n$ (cm)	78.07	14.52	5.139

Appendix C FEMA Force Distribution Calculations

Presented in this appendix are the calculations leading to the FEMA-273 force distributions (Fig. 5.1) used in developing the pushover curves (Fig. 5.2). These distributions were described in Section 5.1

C.1 "UNIFORM" DISTRIBUTION

The lateral force at a floor is equal to the mass at that floor, i.e., $s_j^* = m_j$. For convenience, the floor forces are normalized with the base shear. The results are summarized in Table C.1.

Table C.1. FEMA273 "uniform" lateral force distribution

Floor, j	m_j ($10^{-3}\times$kg)	$s_j^* = \frac{m_j}{\sum_i m_i}$
1	503.5	0.112
2	494.7	0.110
3	494.7	0.110
4	494.7	0.110
5	494.7	0.110
6	494.7	0.110
7	494.7	0.110
8	494.7	0.110
9	534.1	0.119

C.2 EQUIVALENT LATERAL FORCE (ELF) DISTRIBUTION

The lateral force at a floor is computed from $s_j^* = m_j h_j^k$ where m_j is the mass, h_j is the height of the *j*th floor above the base, and the exponent $k = 1$ for fundamental period $T_1 \le 0.5$ sec, $k = 2$ for fundamental period $T_1 > 2.5$ sec; and varies linearly in between. For the selected building, $T_1 = 2.27$ and $k = 1.885$. The resulting lateral forces are summarized in Table C.1. For convenience, the floor forces are normalized with the base shear.

Table C.2. FEMA273 equivalent lateral force (ELF) distribution

Floor j	$m_j h_j^k$ (10^{-3}×kg-m^k)	$s_j^* = \frac{m_j h_j^k}{\sum_i m_i h_i^k}$
1	371.0	0.007
2	1015.0	0.020
3	1963.2	0.038
4	3196.8	0.062
5	4707.4	0.091
6	6488.3	0.126
7	8534.2	0.165
8	10840.6	0.210
9	14471.1	0.281

C.3 SRSS DISTRIBUTION

The calculation of the SRSS distribution is summarized as a series of steps as follows:

1. For the *n*th-mode calculate the lateral forces, $f_{jn} = \Gamma_n m_j \phi_{jn} A_n$ in which *j* denotes the floor number and A_n is the pseudo-acceleration of the *n*th-mode SDF elastic system, leading to columns 2 to 4 of Table C.3.
2. Calculate the story shears, $V_{jn} = \sum_{i=j}^{N} f_{in}$ where *j* is now the story number. Implementing this step gives columns 5 to 7 of Table C.3.

3. Combine the modal story shears using SRSS rule, $V_j = \sqrt{\sum_n \left(V_{jn}\right)^2}$ to get column 8 of Table C.3.
4. Back calculate the lateral forces at the floor levels from the combined story shears V_j to obtain column 9 of Table C.3.

For convenience, the lateral forces are normalized by the base shear to obtain column 10 in Table C.3.

Table C.3. FEMA 273 SRSS force distribution

	Lateral Forces			Story Shears				Lateral Force	
Floor j	f_{j1} (kN)	f_{j2} (kN)	f_{j3} (kN)	V_{j1} (kN)	V_{j2} (kN)	V_{j3} (kN)	V_j (kN)	f_j (kN)	$\tilde{f}_j = \dfrac{f_j}{\sum_i f_i}$
(1)	(2)	(3)	(4)	(5)	(6)	(7)	(8)	(9)	(10)
1	59.7	234.2	277.2	1917.1	1114.9	478.2	2268.7	203.3	0.090
2	97.7	355.0	354.0	1857.4	880.7	200.9	2065.4	222.5	0.098
3	136.8	430.2	285.0	1759.7	525.7	-153.1	1842.9	159.2	0.070
4	176.9	446.1	87.5	1622.9	95.5	-438.1	1683.7	105.7	0.047
5	215.0	381.9	-166.4	1446.0	-350.6	-525.6	1578.0	101.2	0.045
6	250.3	240.6	-352.6	1231.0	-732.5	-359.3	1476.8	95.2	0.042
7	286.0	-5.8	-326.5	980.7	-973.1	-6.6	1381.6	148.4	0.065
8	320.5	-320.7	-46.8	694.7	-967.3	319.9	1233.1	400.9	0.177
9	374.1	-646.6	366.7	374.1	-646.6	366.7	832.2	832.2	0.367